REVIEW

of the

ELECTRICAL COMMUNICATION LABORATORY

NIPPON TELEGRAPH AND TELEPHONE PUBLIC CORPORATION

Former Reports of the Electrical Communication Laboratory
Nippon Telegraph and Telephone Public Corporation
from Vol.1, No.1, Sept. 1953 to Vol. 7, No. 12, Dec. 1959

VOLUME 8
NUMBERS 1-2

Published Bimonthly by

THE ELECTRICAL COMMUNICATION LABORATORY
NIPPON TELEGRAPH AND TELEPHONE PUBLIC CORPORATION
1551, Kitizyôzi, Musasino-si, Tôkyô, Japan

January-February
1960

Review of the Electrical Communication Laboratory

The Review of the Electrical Communication Laboratory is published 6 times a year (bi-monthly) by The Electrical Communication Laboratory, Nippon Telegraph Telephone Public Corporation, 1551, Kitizyôzi, Musasino-si, Tôkyô, Japan. Telephone: Tôkyô (391) 2261 or 2271.

Subscriptions are accepted at ¥1,200 per year. Single copie ¥300 each. Foreign postage is ¥300 per year or ¥50 per copy. Remittance should be made in check payable to the Electrical Communication Laboratory and mail to the Director.

Printed by Aoyama Pinting Co., Tokyo Japan

REVIEW
of the
ELECTRICAL COMMUNICATION LABORATORY

NIPPON TELEGRAPH AND TELEPHONE PUBLIC CORPORATION

Volume 8, Numbers 1-2 January-February 1960

535.54:546:13'33

Coloring of Ionic Crystals by Electron Bombardment*

Yoshitake IGARASHI†

A study has been made of the coloring due to the bombardment of evaporated films and single crystals of NaCl with 600 V elections. A new optical absorption band of nearly 1.1 μ was found, which was connected with the surface structure. Thermal as well as optical bleaching behavior was examined.

Introduction

As a result of the study made by Yoshida[1] on the effects of the electron bombardment of BaO and SrO, using radioactive isotopes Ba^{140} and Sr^{89}, it was found that the evolution of a metallic component occurred. It has also been confirmed by many workers[2] on the oxide cathode that oxygen is also released during electron bombardment. The dissociation mechanism, however, of the oxide has not been made clear because the effect of electron bombardment upon bulk characteristics was not known. Especially, lattice imperfection is considered to have an important effect upon the process of dissociation, but there existed many difficulties in various aspects of the study of alkaline earth oxides.

In this paper experiments made at room temperature on the coloring and subsequent bleaching conditions of evaporated films and single crystals of NaCl, the typical ionic crystal, are reported. The work has been carried out with empasis on the behavior of the lattice defect created by electron bombardment.

* MS received by the Electrical Communication Laboratory May 19, 1959. Originally published in the *Electrical Communication Laboratory Technical Journal*, N.T.T., Vol. 8, No. 6, pp. 976–985, 1959.

† Electronic Components Research Section.

1. Experimental Procedure

Rock salt crystals (Halle Co., Germany) which had been subjected to an annealing treatment in a vacuum at 400° C for about 1 hour were used as the specimen material.

In order to effect electron bombardment, the specimen was mounted in a glass bulb provided with an electron gun. The bulb was thoroughly evacuated, outgassed, and then sealed off.

Cleaved rock salt crystal was used as a single crystal specimen, while an evaporated film was prepared by deposition from the rock salt out of a platinum spiral onto the glass wall. Bombardment voltage was 600 V and current was 10 μA.

The optical transmission spectrum ranging from 320 mμ to 1.2 μ was measured by means of a photoelectric spectro-photometer (Hitachi EPU II). In order to observe the spectral transmission of the specimen sealed in the glass tube, a special chamber constructed for the spectrometer.

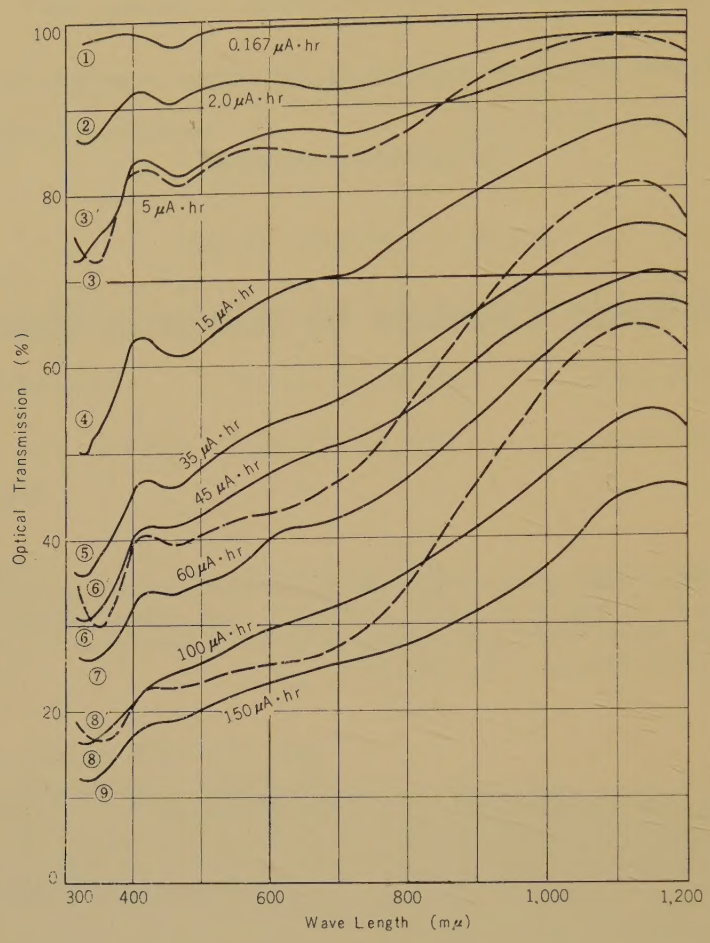

Fig. 1—Optical transmission spectra associated with bombardment quentities of evaporated specimens. (Dashed curves ③′, ⑥′, and ⑧′ show the spectra when the specimen is kept at room temperature for 67 hr 140 hr, and 140 hr after curves ③, ⑥, and ⑧ respectively have been measured.)

2. Results

2.1. Darkening with Electron Bombardment

Figs. 1 and 2 show the spectral transmission during various stages of electron bombardment for evaporated films and single crystals. The numerical values affixed to each curve in these figures indicate the total quantity of incident electrons expressed in $\mu A \times hr$.

(a) *Evaporated film:* In the initial stage of electron bombardment, absorption occurs first in the proximity of 465 mμ (F band), and, in the next stage, absorption occurs in the proximity of 720 mμ (M band) and also under 400 mμ. After that, with the progress of bombardment, darkening deepens and the shape of absorption band becomes more and more moderate for the whole region measured.

(b) *Single crystal:* The F band is formed first in exactly the same way as with the evaporated film. However no peak is to be seen in the region of the M center. Also the spectrum in the proximity of 1.1 μ is quite different from that of the evaporated film, being almost transparent, until the F center is formed to the degree shown by curve ⑤ in Fig. 2. As darkening deepen as, a shift of the peak position as well as

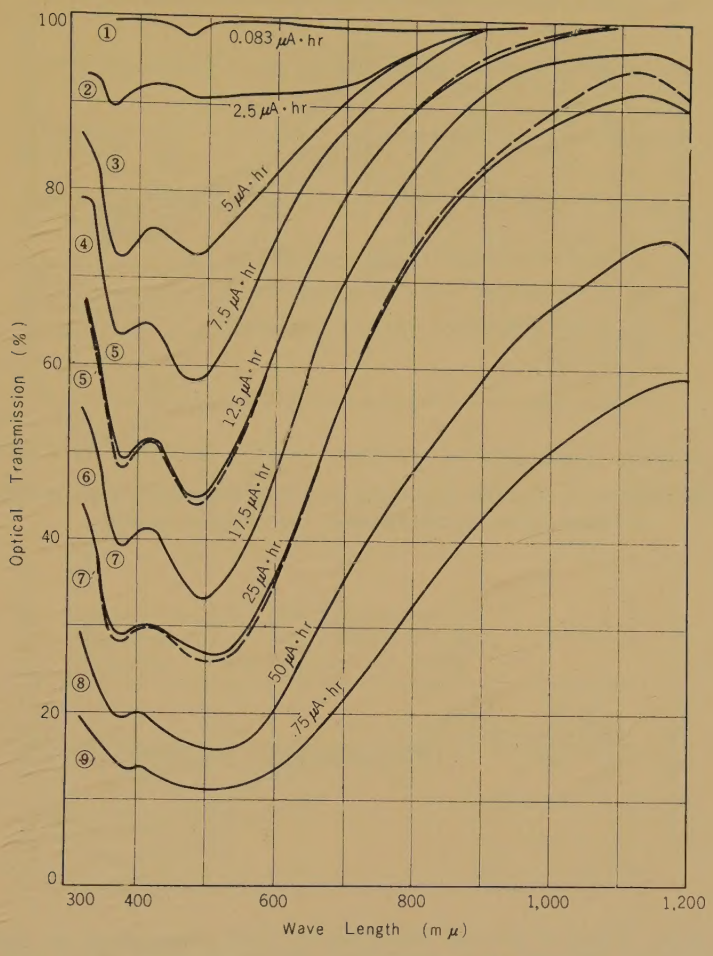

Fig. 2—Optical transmission spectra associated with bombardment quantities of a single crystal specimen. (Dashed Curves ⑤′ and ⑦′ show the spectra when the specimen is kept at room temperature for 16 hr and 19 hr after Curves ⑤ and ⑦ respectively have been measured.)

widening of the band width may be observed.

2.2. 1.1 μ Band

The absorption bands produced by electron bombardment are at least partially unstable at room temperature and their intensities vary when they are kept at room temperature for several hours. This phenomenon is especially remarkable in the case of an evaporated film, as may be clearly seen by comparison of Curves ③ and ③′, ⑥ and ⑥′, ⑧ and ⑧′ of Fig. 1. They show marked bleaching on the longer wavelength side, while they are rather intensified on the shorter wavelength side, with the boundary at 800 mμ, after they have been kept at room temperature for several hours. Further, it was also found that the absorption on the long wavelength side was sensitively intensified due to irradiation by *M*-light and *F*-light (see Paragraph 3 below). From this it may be considered that an absorption band whose peak lies in the proximity of 1.1 μ (to be later referred to as 1.1 μ band) has been produced in NaCl due to electron bombardment.

Fig. 3 (a) and Fig. 3 (b) show the effect of thermal bleaching at room temperature

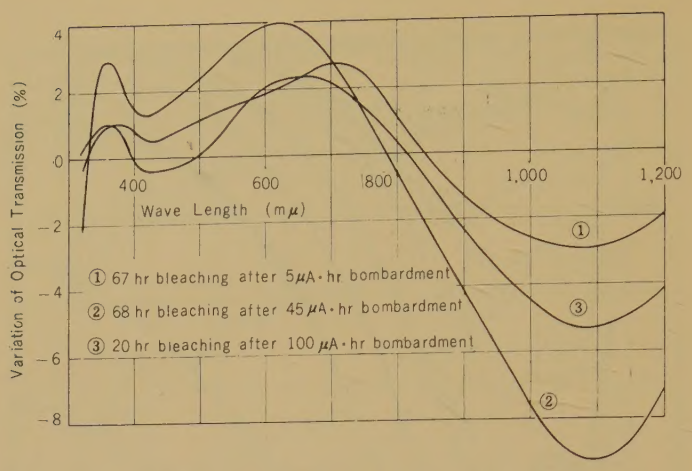

Fig. 3 (a)—Effect of thermal bleaching at room temperature of evaporated specimen (after bombardment) for various stages.

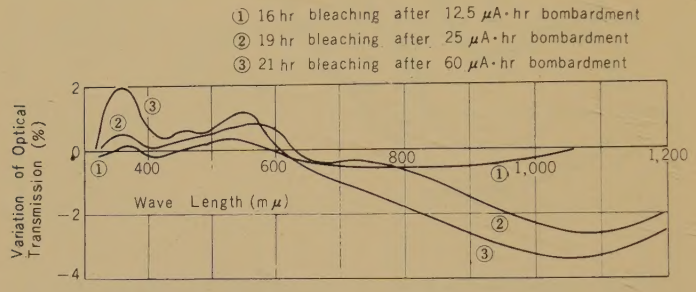

Fig. 3 (b)—Effect of thermal bleaching at room temperature on single crystal specimen during various stages of bombardment.

for the evaporated film and the single crystal, respectively, with the ordinate the difference of transmission before and after thermal bleaching.

2.3. Effect of Light Irradiation

Curves 1 and 2 in Fig. 4 (a) show the change of optical transmission in the case where *M*-light (corresponding to the *M* band) has been focused on the evaporated specimen that had been, after electron bombardment, subjected to thermal bleaching at room temperature for a sufficiently long time (usually several tens of hours). It is confirmed that, as a result of the irradiation by *M*-light, bleaching of the *M* band and increase of the 1.1 μ band occurs. If the specimen is, however, after *M*-light irradiation, again kept at the room temperature, the optical transmission will vary as shown in Curves ①′ and ②′, showing the retardation of the irradiation effect.

An effect of *F*-light irradiation was observed, shown in Fig. 4 (b), whereby transformation between *F* band and 1.1 μ band is performed. To separate the thermal bleaching effect, the optical absorption measurement must be carried out in a short time. Only three wavelengths of 465 mμ, 720 mμ and 1.1 μ were selected as the measuring points to follow up the variation of optical transmission due to electron bombardment, light irradiation and thermal bleaching. The result is shown in Fig. 5. It was found that the rate of such variation became slower with the lapse of time. Investigations were also made of the effect

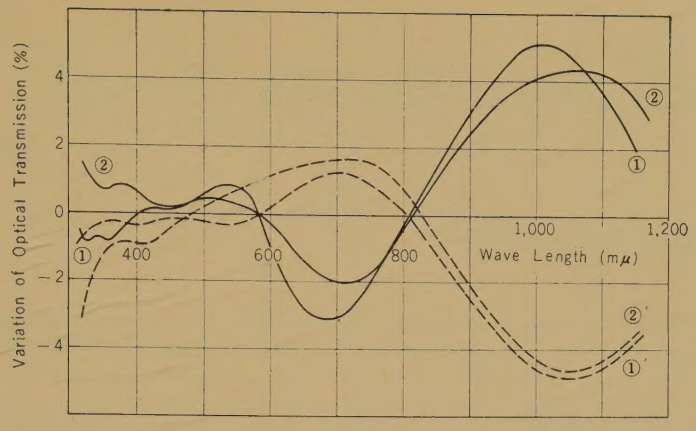

Fig. 4 (a)—Effect of *M*-light irradiation on evaporated specimen.

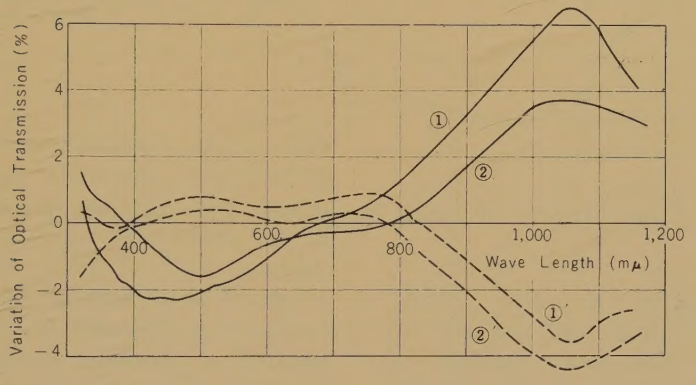

Fig. 4 (b)—Effect of *F*-light irradiation on evaporated specimen.

of light irradiation upon the single crystal, which variation was so small that no result could be obtained to be compared with that for the evaporated specimen.

3. Discussion

Since the bombardment was made with the comparatively low voltage of 600 V, not only the bulk characteristics but also the surface characferistics of NaCl greatly affected the results. The results of the experiment may be outlined as follows:

3.1. Due to electron bombardment, absorption centers such as *F* band, *M* band, and 1.1 μ band are formed in NaCl.

An evaporated specimen and a single crystal differ from each other in their absorption spectra, especially in the formation of 1.1 μ band, so that it may be considered that 1.1 μ band is connected with the surface structure of the evaporated film. It is well known that the evaporated film consists of very small polycrystallites, with wide and incomplete surfaces.

3.2. From the thermal as well as the optical bleaching behavior, it may be considered that the intensities of the absorption bands are governed by the mutual conversion of vacancies (and of trapped electrons) of various types created in the specimen. Owing to the excitation or ionization of color centers due to light irradiation, the vacancies will be caused to aggregate or dissociate, so that the vacancy distribution will change from that before the irradiation. The electrons released by irradiation will partly recombine, and are partly

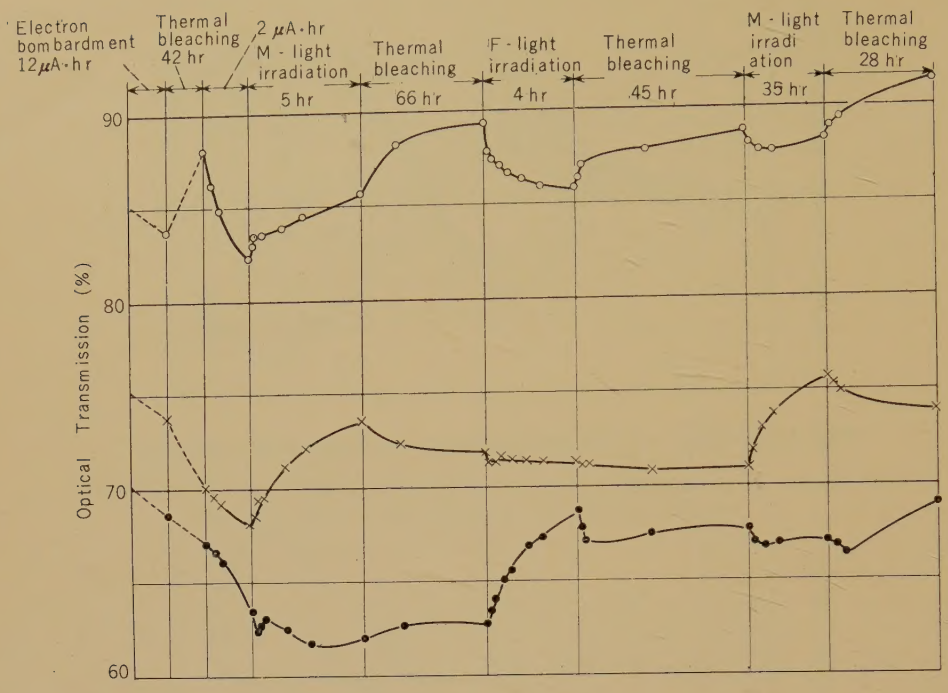

Fig. 5—Time variation of optical transmission with time (not to scale).

trapped into vacancies of other types, thereby changing the shape and intensity of the absorption. If the total number of vacant sites does not change, it is considered that the original, stable and balanced state will gradually be again restored.

3.3. In view of the fact that the absorption of the newly found 1.1 μ band varies inversely with the increase and decrease of F centers or M centers, it may be considered that 1.1 μ band is formed of negative ion vacancies in which electrons are trapped. The rough calculation made with Seitz's model[3] under the assumption that the total number of colored vacancies is conserved throughout the thermal bleaching process, shows that the 1.1 μ center consists of two negative ion vacancies.

3.4. The coloring by electron bombardment is thought to be caused by the creation of vacancies during dissociation of NaCl.[1] Therefore, in order to make argument more quantitative, it would be necessary to take also V-type centers into consideration, though they are unstable at room temperature.

References

(1) Yoshida, Shibata, Igarashi, and Arata, *J. Phys., Soc. Japan*, **9**, p. 640 (1954). Yoshida, Shibata, Igarashi, and Arata, *J. Appl. Phys.*, **27**, p. 497 (1956).
(2) Wood and Wright, *Brit. J. Appl. Phys.*, **4**, p. 56 (1956). Wargo and Shepherd, *Phys. Rev.*, **106**, p. 694 (1957).
(3) F. Seitz, *Rev. Mod. Phys.*, **26**, p. 7 (1954).

* * * *

537.525:537.56

Oscillation Caused by Electron Sheath Breakdown*

Seiji OHARA† and *Kazuo TAKAYAMA*†

Low frequency oscillations in a hot-cathode gas-discharge tube were investigated. By inserting a highly charged positive prove into a dark plasma of the anode glow mode, the breakdown and oscillation of the electron sheath around the probe was observed.

The oscillation was of a relaxation type, whose frequency between 50 c/s and 3,000 c/s was found to be proportional to both the probe current i and the external resistance R of the probe circuit, i.e., $f=\alpha Ri-\beta$, where α and β are constants. In addition, the value ΛR is nearly constant, where Λ is the peak current of the wave.

These relations can be deduced theoretically by considering the breakdown conditions and the diffusion velocity of the plasma.

Introduction

Though noises and oscillation in a discharge tube are very interesting phenomena in themselves, they are, on the other hand, a nuisance which makes experiments in a discharge tube quite difficult. One familiar example of this kind is the noise from a fluorescent lamp in a radio receiver.

The oscillations in a discharge tube can be divided into two types. One is related to plasma itself, and the other is not directly related to plasma but to the external circuit.

The well-known plasma oscillation is of the former type. The mechanism of the latter type is very complicated and has not yet been well understood.

The authors investigated the mechanism of the anode oscillation simplifying the conditions as much as possible; that is, by studying the case when the electron sheath around the probe is broken down because of the high voltage difference between the probe and the sheath edge. The oscillation is regular and amenable to theoretical analysis.

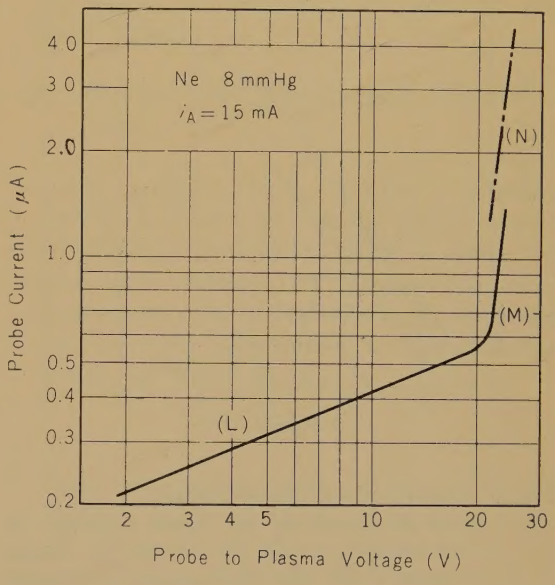

Fig. 1—Volt-ampere characteristic.
(L) is the region of electron saturated probe current as a function of probe voltage, (M) is the region where a glow appears in a thin layer on the probe surface, and (N) is the region where the probe current and voltage are oscillating.

1. Aparatus

The discharge tube used, the heated cathode of which is coated with BaO_2, is shown in Fig. 2. The circuits were simplified by including a lead-acid type storage battery and limiting resistance only. When the

* MS received by the Electrical Communication Laboratory May 19, 1959. Originally published in the *Electrical Communication Laboratory Technical Journal*, N.T.T., Vol. 8, No. 6, pp. 986–993, 1959.

† Shindo's Research Section.

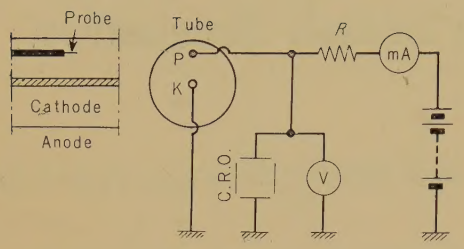

Fig. 2—Schematic diagram of the discharge tube and associated circuit.

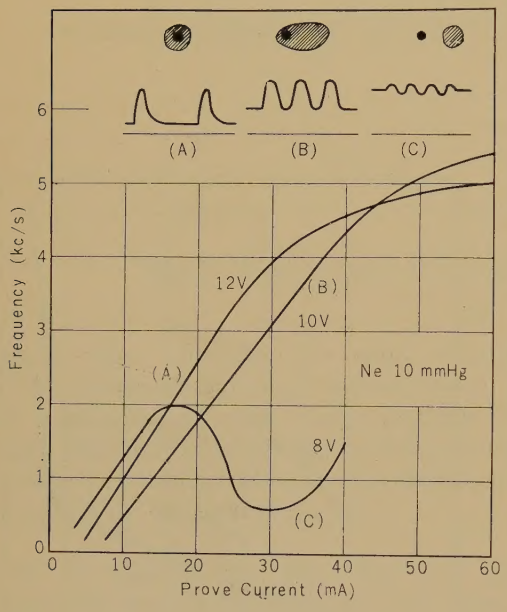

Fig. 3—Frequency vs. probe current. The parameter is the input voltage of the heated cathode. (A) shows the linear region where the frequency is exactly proportional to the probe current. (B) and (C) are the regions where linear relations between the frequency and the probe current do not hold. Oscillograms of the probe current and positions of a glow to the probe are shown on the upper part of the figure.

potential difference between the probe and the sheath edge is made large than a certain value, the electron sheath breaks down suddenly. The probe begins to glow and the oscillation becomes observable at the same time. The features of the current and voltage are observed on a cathode-rays oscilloscope. The gas used is Neon.

2. Experimental Results

The relation between the probe current i and the frequency f is shown in Fig. 3, where the temperature of the cathode is the parameter. The f–i curve is divided into three regions; "A," "B," and "C."

In the "A" region, f is proportional to i. The wave form is of a relaxation type. The glow is axially symmetric about the probe, and the shape of the glow is independent of i.

As the current increases, the wave form changes and the glow shifts to the cathode side in the "B" region.

When the current increases to a point beyond the emission capacity of the cathode, the wave form becomes a sine wave similiar to that of the "Ball of Fire" in the "C" region. At all values of current above this, the oscillation stops and the glow seperates from the probe.

More detailed investigation of the "A" region shows that:

(a) Frequency and Discharge Current

The relation between the frequency f and the discharged current i is shown in Fig. 4, in which external resistance is the parameter.

The empirical equation for f is

$$f=\alpha_1 i-\beta_1$$

where α_1 and β_1 are constants.

(b) Frequency and External Resistance

The relation between the frequency f and the external limiting resistance R is shown in Fig. 5 with i as the parameter. The empirical equation derived is:

$$f=\alpha_2 R-\beta_2$$

where α_2 and β_2 are constants.

(c) Frequency and Probe Voltage

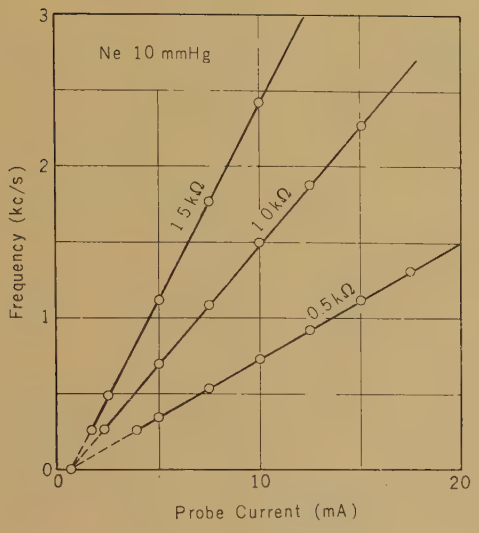

Fig. 4—Relation between the frequency and the probe current. The parameter is the external limiting resistance.

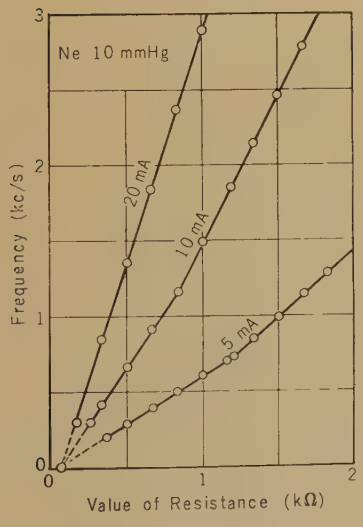

Fig. 5—Relation between the frequency and the limiting resistance. The parameter is the probe current.

We can combine the above two relations and obtain the equation $f=\alpha iR-\beta$, where α, β are constants. As iR is the voltage drop in the external circuit, the frequency should be proportional to the voltage of the external circuit, if the minimum tube voltage is constant.

This relationship is shown in Fig. 6. By experiment, we arrive at the equation

$$f=\alpha(V-V_\beta),$$

where V_B is nearly 3 volts higher than the ionization voltage of the gas; for Ne it is 25.5 volts.

(d) Frequency and Pressure

In case that there is sufficient emission from the cathode, the higher the pressure, the higher the frequency becomes for the same current.

(e) Amplitude of Current and External Resistance

The typical form of the oscillating current is shown in Fig. 7, which shows a oscillating component with a fast rise time super imposed on a constant (d.c.) component. A is independent of frequency and inversely proportional to the external circuit resistance R: that is,

$$RA=\text{const.}$$

These experiments were performed for the oscillations produced about a small positive prove. These are of the same type as the intial oscillation observed for the "ball of fire." In Fig. 8, two types of discharge tubes "P" and "B" are shown. The difference between the two is that in effect the anode and the cathode of the "P" type are in positions opposite to these of the "B" type. Oscillations in the "P" and "B" type tubes are of the same type as those around the probe, but the frequency of the oscillations in the "P" type tube is higher than those of the "B" type tube.

3. Theoritical Considerations

It may be possible to analyze the oscil-

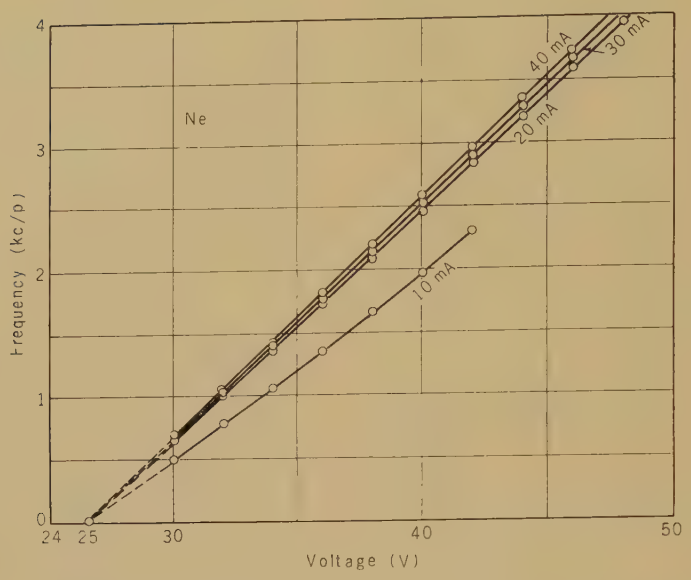

Fig. 6—Frequency vs. voltage of the external circuit.

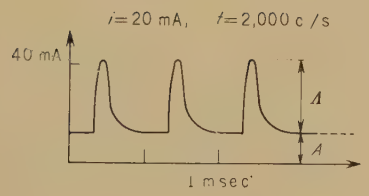

Fig. 7—Wave form of current.

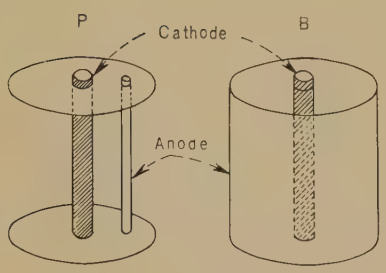

Fig. 8—"P" and "B" type discharge tubes.

lations that have been discussed above in the manner to be described below. When the potential difference between the probe and the plasma exceeds the ionization potential of the gas molecules, ionization processes will occure within the sheath, which results in disintegration of the sheath. Accordingly the currents to the probe grow larger and the probe voltage decreases because of the external limiting resistance, which causes ionization to stop, and the glow disappears. Now, the electron sheath begins to form again. At the very beginning, the electron density around the probe is so high that the sheath is too thin to cause an ionization processes. Within a distance shorter than the mean free path, the probability of ionization will be very small. Meanwhile, the plasma around the probe diverges by diffusion, and a condition of breakdown arises. As we can see, this condition is found to be the same as that of the anode glow mode.[1] The breakdown condition of anode glow mode is a complicated one but can be deduced for our experiment as follows: The depth of electron sheath has an upper critical value a_c.

By using this condition we can derive theoretically the experimental equation.

In a plasma, the flow of current i into

the probe is described by the equation,

$$i=\frac{nl\bar{v}}{4}2\pi\alpha L=kna, \qquad (1)$$

where n is plasma density, $\bar{v}$ mean electron velocity, a sheath radius, L probe length.

Now, let us assume that the initial glow plasma is produced symetrically around the probe with a radius of L.

The diffusion equation of such a plasma is:[2]

$$n(r_1t)=\frac{n_0}{2Dt}\,l^{-\frac{1}{4Dt}}\int_0^l l^{-\frac{r'}{4Dt}}\,I_0\left(\frac{rr'}{2Dt}\right)r'dr', \qquad (2)$$

where D is the diffusion constant, I_0 is the Bessel function of the second kind, and n_0 is initial plasma density.

Near the probe (i.e., $r\fallingdotseq 0$) the above equation be simplified as follows:

$$n(0,t)=n_0(1-l^{\frac{l^2}{4Dt}}). \qquad (3)$$

Now we assume that N_0 is proportional to Λ, the peak current of the wave, then;

$$n_0=\alpha''\Lambda=\beta''(1/R)\,(\alpha'', \beta''\text{const.}), \qquad (4)$$

where $R\Lambda=\text{const.}$

If t_c is the time during which the sheath radius a becomes the critical value a_c, the frequency is the reciprocal of t_c. From (1), (3), and (4) we obtain:

$$R_i=\alpha' f+\beta'$$

where α' and β' are constants.

This is the same equation as the experimental equation

$$f=\alpha iR-\beta.$$

For a true quantitative discussion, however, we must make further experiments.

References

(1) E. O. Johnson, *Studies of External Heated Hot Cathode Arc*, Part III, p. 97.
(2) J. Grank, *The Mathematics of Diffusion.*

* * * *

538.2:546.723:546.66]:538.561

Magnetic Properties and Ferrimagnetic Resonance in Polycrystalline $3Y_2O_3 \cdot (5-x)Fe_2O_3 \cdot xIn_2O_3$*

Yuzo SHICHIJO† and *Tomonao MIYADAI*†

Ferrimagnetic resonance, crystal structure, technical magnetization and the variation of spontaneous magnetization with temperature were studied on polycrystalline indium-substituted yttrium-iron garnet, $3Y_2O_3 \cdot (5-x)Fe_2O_3 \cdot xIn_2O_3$ with x from 0 to 4. The measurement were always made at room temperature except for the case of spontaneous magnetization which was measured in the temperature range from $-196°$ C to $350°$ C.

Ferrimagnetic resonance line width at 20,000 Mc increases rapidly with In content, x ($\Delta H = 130$ Oe at $x=0$–900 Oe at $x=1.3$). g-factor has almost constant values between 2.01 and 2.03 within experimental error. These compounds have a single phase with garnet structure for $0 \leq x \leq 1$, but three phases (garnet$+YFeO_3+In_2O_3$) for $1<x<2$ and two phases ($YFeO_3+In_2O_3$) for $x=2$, respectively. Spontaneous magnetization at $0°$ K, σ_0, initially increases with increasing x, while in the range $0.3<x<1$ it decreases linearly. Curie temperature T_c decreases linearly with increasing x till $x=1$ is reached and then becomes constant. With samples having $x>1$, thermoremanent magnetization was observed and is considered to be due to the $YFeO_3$ phase.

For small x, the initial permeability μ_0 increases with x, accompanied by corresponding decrease in coercive force H_c.

The greater part of the increase in the line width with x (in the single phase region of x), provided that Schlomann's theory holds, appears to be intrinsic.

Introduction

Since the discovery of ferrimagnetic garnets having an isostructure with natural garnets, many investigations have been made on them. Ferrimagnetic garnets have a general formula, $3M_2O_3 \cdot 5Fe_2O_3$, where M stands for an element of Y or rare earths (Sm, Eu, Gd, Tb, Dy, Ho, Er, Tm, Yb, Lu). Bertaut *et al*[1] and Geller *et al*[2] determined their crystal structures, Pauthenet[3] studied their magnetic properties, and Pauthenet[4] and others[5] investigated some substituted garnets. Since Dillon's discovery[6] of an extremely narrow resonance line width in a YIG (yttrium iron garnet) single crystal, many workers[7] investigated it. Among them was Vautier[8] who observed for polycrystalline Cr-substituted YIG that the line width initially decreased slightly and then increased with Cr contents. He attributed this variation in the line width with Cr content mainly to the variation in densities of their specimens used. The data described in the present paper on ferrimagnetic resonance in polycrystalline In-substituted YIG shows tendency somewhat opposite to Vautier's; the line width increases monotonously with In content.

The crystal structure of garnet is a fairly complicated one. An octant of its unit cell is shown in Fig. 1. A unit cell consists of four molecules of $3M_2O_3 \cdot 5Fe_2O_3$. Twenty four Fe^{3+} ions occupy 24(d) or tetrahedral sites, sixteen Fe^{3+} ions 16(a) or octahedral sites, twenty four M^{3+} ions 24(c) sites and ninety six O^{2-} ions 96(h) sites, of which coordinates are determined by three parameters, x, y, z. The 24(d), 16(a) and 24(c) sites are surrounded by four, six and eight O^{2-} ions, respectively. In Fig. 1, only six O^{2-} ions are shown which surround the 16(a) site at the center of the octant, and

* MS received by the Electrical Communication Laboratory Sept. 2, 1959. Originally published in the *Electrical Communication Laboratory Technical Journal*, N.T.T, Vol. 8, No. 11, pp. 1450–1465 (1959).

† Magnetic Materials Research Section.

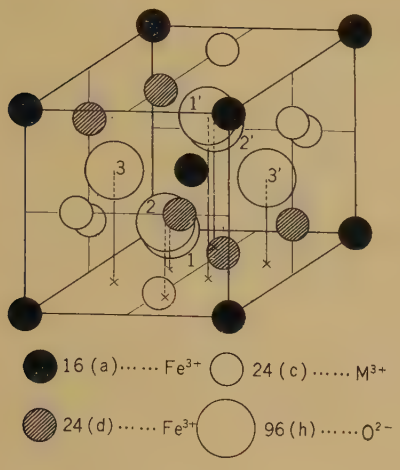

Fig. 1—An octant of the unit cell of garnet structure. Of O^{2-} ion present only six, surrounding the 16(a) site at the center, are shown. Three parameters, x, y, and z are chosen to be equall to -0.03, $+0.06$, and $+0.15$, respectively, corresponding to YIG.

their parameters, x, y, z are chosen to be equal to -0.03, $+0.06$ and $+0.15$, respectively, corresponding to YIG. Ferrimagnetism in ferrimagnetic garnets is interpreted as follows[3]: magnetic moments of Fe^{3+} ions on the 24(d) and 16(a) sites are strongly coupled antiparallel to each other, and their resulting moments are very weakly coupled antiparallelly to the magnetic moments of M^{3+} ions on the 24(c) sites. Therefore, taking into account the numbers of the magnetic ions on the sites of three kinds, the resultant magnetization per molecule at saturation σ_0, is given as, in Bohr magneton,

$$\sigma_0 = 6m_c - (6m_d - 4m_a)\ (\mu_B) \qquad (1)$$

where m_c, m_d and m_a are the magnetic moments of M^{3+}, Fe^{3+} on 24(d) and Fe^{3+} on 16(a) sites, respectively. Here $m_d = m_a = 5(\mu_B)$.

1. Sample Preparation and Experimental Procedures

The samples used were prepared as follows: powders of Y_2O_3 (99.9% pure), Fe_2O_3 (prepared from ferrous oxalate 99.9% pure) and In_2O_3 (commercial) were mixed in desired proportions, pressed into disk-form, sintered at 1,400° C for about six hours in air and cooled slowly in the furnace (presintering was not done). The weights of each sample were equal to about 1.5 g. The compositions of the samples prepared are $x=0$, 0.3, 0.6, 1.0, 1.3, 1.6, 2.0, 3.0 and 4.0 in the formula of $3Y_2O_3 \cdot (5-x)Fe_2O_3 \cdot xIn_2O_3$. The samples with x ranging from 0 to 1.6 were all clearly ferromagnetic, but the ones having larger values of x were not so.

Ferrimagnetic resonance was measured by an usual microwave technique at 20,000 Mc. Microwave power from a 2K25 klystron was frequency-doubled by a crystal, 1N26, and fed into a rectangular cavity of transmission type with an H_{105} mode. The samples used were 0.31 to 0.67 mm in diameter and grounded by Bond's method.[9] The microwave frequency was modulated by applying a saw-teeth wave to the repellor of the klystron. The output power from the detector crystal, which consists of pulses, each representing a Q-curve of the cavity, is amplified, eliminated and finally applied to the X-terminals of an X-Y recorder. To the Y-terminals of the recorder is applied a voltage proportional to the magnet-current. Thus, an absorption curve can be obtained automatically. As an example, a curve thus obtained is shown in Fig. 2. The calibration of magnetic field was done by making use of a free radical DPPH.

X-ray diffraction patterns of powdered samples were taken by an ordinal diffractometer with a Geiger tube, using a radiation of K_α from an iron target. Unfortunately, the quantity of the samples used was not enough to accurately determine lattice constants. Spontaneous magnetization was measured by an automatically recording magnetic balance[10] from -196° C to approximately 350° C. The error in measurement of σ_s is thought to come mainly from that in weighing the sample which had to be chosen less than miligram because of high sensitivity of the magnetic balance. Hysteresis curves in the technical magnetization

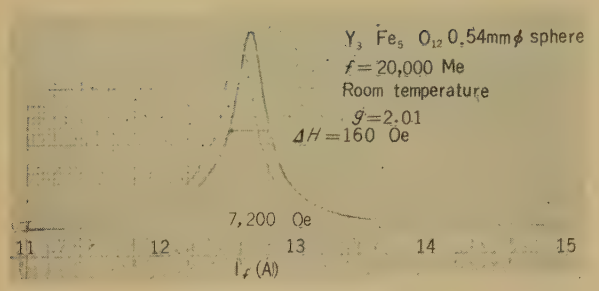

Fig. 2—An example of an absorption curve obtained by an X-Y recorder.

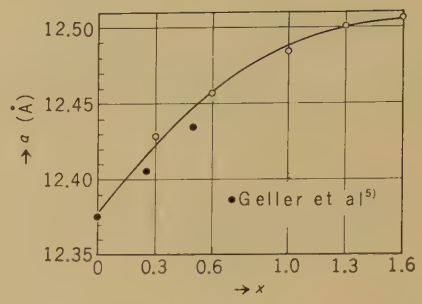

Fig. 3—Variation in lattice constant a with In-content x. (at room temperature)

region were measured, by an automatically recording fluxmeter,[11] on samples in the form of a small toroidal (outer- and inner-diameters being 4 mm and 2 mm, respectively, and height 1 mm). Errors in this measurement were mainly due to the difficulty in accurate measurement of sample-dimensions.

2. Experimental Results

2.1. Crystal Structures

By means of X-ray diffraction technique, it was shown that a) in the region of x, $0 \leqq x \leqq 1$ the samples consist only of a single phase with garnet structure, b) for $x=1.3$ and 1.6, of three phases, which are garnet, perovskite-like ($YFeO_3$) and In_2O_3 structures, and c) at $x=2$, of two phases which are $YFeO_3$ and In_2O_3 structures (containing no garnet phase). For the samples with $x=3$ and 4, only two very broad lines appeared at low diffraction angles. However, as will be shown later, it is concluded from data on σ_s–T curve that the sample with $x=3$ contains a small amount of $YFeO_3$ phase. In any case, no lines corresponding to Y_2O_3 or Fe_2O_3 appeared. The variation in lattice constant a with x is shown in Fig. 3. As shown in the figure, a increases roughly linearly with x (up to 1). The values for the specimens with $x>1$ correspond to a garnet phase.

2.2. Spontaneous Magnetization

For the samples with $x=0$, 0.3, 0.6 and 1.0, the curves of the spontaneous magnetization vs. temperature have forms similar to ordinal ferromagnetics and are shown in Fig. 4. In Fig. 5 is shown the spontaneous magnetization at 0° K, σ_0 (in Bohr magneton per molecule), which was obtained by extrapolating the curves to 0° K, and the Curie temperature T_c. As In content increases, σ_0 increases initially, passes through a maximum near $x=0.3$, and then decreases, roughly speaking, linearly with x, while T_c decreases monotonically up to $x=1$ and remains constant for larger x's. At $x=0$, σ_0 is 8.72 μ_B and T_c is 530° K. These values are, however, a little smaller than Pauthenet's data, 9.44 μ_B and 560° K. Although the reason for this discrepancy is not clear, it might be possible that the difference in σ_0 is due to either the error in the measurement of sample-weight or impurities contained in raw materials.

With samples having $x>1$, a thermal hysteresis and an effect of magnetic annealing were observed. These can be, as will be described later, explained by thermoremanence of $YFeO_3$ phase present in the sample. In Fig. 6 is shown an example in the case of $x=3$: the curves represent susceptibility per gram, χ, plotted against temperature. The curve ① in the figure was obtained by measurements during the first run which was made by magnetic balance while heating the sample, which had been quenched from 1,350° C. It is seen that a peak occurs at about 280° C, this temperature being equal to the Curie temperature of $YFeO_3$. Then, the sample was again cooled

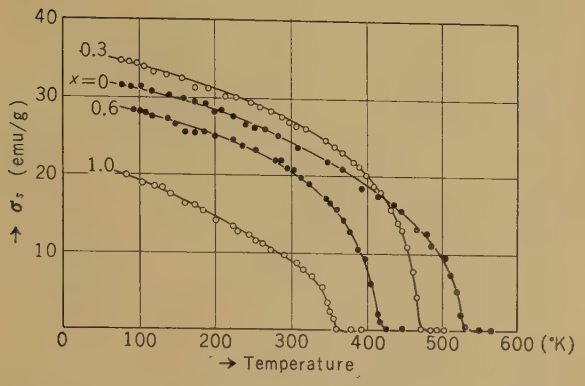

Fig. 4—Temperature dependences of spontaneous magnetization.

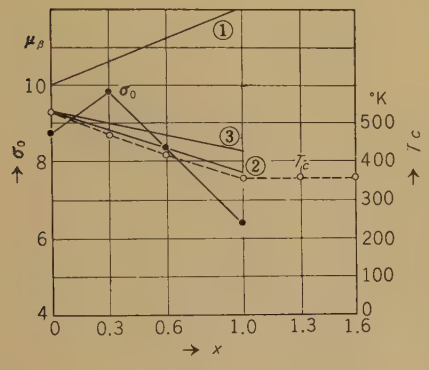

Fig. 5—Variations in σ_0 and T_c with In content, x. σ_0: Spontaneous magnetization at 0° K, T_c: Curie temperature, ①: theoretical curve of σ_0 in the case where In^{3+} ions enter 16(a) sites, ② and ③: theoretical curves of T_c when it is assumed that In^{3+}'s enter 16(a) or 24(d) sites, respectively.

slowly, on continuing the measurement, and the curve ② was obtained, here the sample having become ferromagnetic. And then, as heatings and coolings are repeated, x goes up and down along the curve ②, but not ①. The above "remanent magnetization" still remained even when the sample was cooled without exciting current of the magnet (a remanent field of the magnet exists). The "remanence," however, exists no longer when the sample is cooled after demagnetizing the magnet.

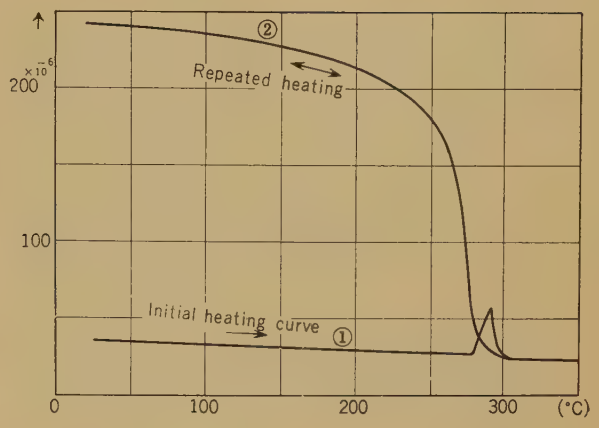

Fig. 6—Susceptibility per gram χ against temperature. ①: initial heating curve, ②: cooling and second heating curves.

2.3. Ferrimagnetic Resonance

In Fig. 7 is shown the variation in the line width ΔH with In content x at room temperature. ΔH at $x=0$ has a value of 130 Oe and it increases rather rapidly with increasing x up to $x=1.3$ where $\Delta H=$ 900 Oe. As for g-factor, although the accuracy of the measurement is not so high, we obtained 2.01 at $x=0$ and 2.03 at $x=1$; it seems that g-factor changes scarcely with x. The absorption intensity varies with x in a similar way to tho magnetization at room temperature M_s which is also shown in Fig. 7. The absorption almost vanishes near $x=2$. The line shape takes a form of Lorentzian at $x=0$, while it seems to be distorted a little for larger values of x.

2.4. Technical Magnetization

The measurement shows that the initial permeability μ_0 and the coercive force H_c take values of about 80 and 1.5 Oe at $x=0$, respectively, and that the former increases and the latter decreases with increasing x for x less than about 0.6.

3. Discussion

If In^{3+} ions enter octahedral 16(a) sites, σ_0 will be given, in the first approximation,

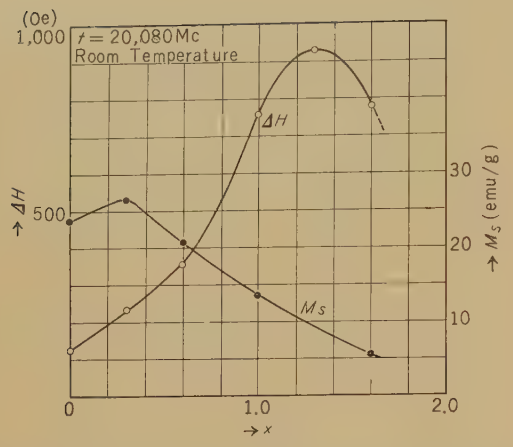

Fig. 7—Variations in line width at 20,000 Mc ΔH and in saturation magnetization at room temperature M_s with In-content x.

as

$$\sigma_0 = 10 + 2x \quad (\mu_B) \qquad (2)$$

since In^{3+} is non magnetic (see Eq. (1)). In Fig. 4 is shown straight line ① representing Eq. (2) and its slope is approximately agreed with the experimental. Since the ionic radius of In^{3+} is greater than Fe^{3+}, it can be expected than In^{3+} enters an octahedral site. Thus, in the region of small x, it seems that In^{3+} ions substitute mainly Fe^{3+} ions on 16(a) sites.

The decrease in the Curie temperature T_c with x can be derived on very simple assumptions that a) T_c equals to the paramagnetic Curie temperature θ_p,[12] b) a–a and d–d interactions are negligible, c) a–d interaction is independent of x:

$$\frac{T_c(x)}{T_c(x=0)} \approx \frac{\theta_p(x)}{\theta_p(x=0)}$$

$$= \begin{cases} \sqrt{1-(x/2)} \ ; In^{3+} \rightarrow 16(a). & (3a) \\ \sqrt{1-(x/3)} \ ; In^{3+} \rightarrow 24(d). & (3b) \end{cases}$$

The curves representing Eqs. (3a) and (3b) are shown in Fig. 4, being designated as ② and ③, respectively. The experimental curve is closer to Curve ② than ③. Although the above approximations are rather crude, the agreement is almost satisfactory. The thermal hysteresis and the magnetic annealing effect can be explained as due to a parasitic ferromagnetism of $YFeO_3$ phase present in the sample. Our measurement was done in the field of nearly 5,000 Oe and even such a field is thought to be smaller than the coercive force of parastic ferromagnetism due to $YFeO_3$ in the sample. Thus, with a thermally demagnetized sample, magnetization can not be observed at low temperatures much lower than the Curie temperature of $YFeO_3$. Just below the Curie temperature, however, since the coercive force will become very small, magnetization appears and at the Curie point it vanishes again. This is the case of Curve ① in Fig. 6. On cooling the sample again a thermal remanence appears and Curve ② is obtained. The fact that the location of the peak on Curve ① is in agreement with the Curie temperature of $YFeO_3$[13], supports the above explanation.

The greater part of the increase in the ferrimagnetic resonance line width with x seems to be intrinsic. For, if the increase is an apparent behavior because of polycrystallinity of the samples used, the amount of increase should be much smaller than observed, as will be shown below, provided that Schlömann's theory[14] holds. With polycrystalline sample, the line width is broadened by the fact that local fields in the sample deviate from the mean value from one crystallite to another because of random orientations of each crystallite and because of demagnetizing fields by pores. The amount by which the line width is broadened, is given according to Schlömann, as

$$\frac{|K_1}{M_s} + 1.5(4\pi M_s)\frac{\Delta V}{V},$$

where K_1 is the first order cubic anisotropy constant of the sample, M_s the magnetization at the temperature during measurement, and $\Delta V/V$ the ratio of total pore volume to sample volume. With the samples used, $|K_1|/M_s$ will not increase with increasing x since Curie temperature decreases with x. The samples used have densities not less than 95% and the increment in M_s

is, at most, ca. 15% at $x=0.3$. The second term, therefore, will not increase beyond 120% of the value at $x=0$, even if it does with x. One can, now, regard greater part of the increase in the single phase ragion of x to be intrinsic and it seems possible that the increase is attributed to some kind of irregularities, e.g. randomness in distribution of Fe^{3+} and In^{3+}.[15]

Conclusion

1) Compounds having a formula, $3Y_2O_3 \cdot (5-x)\,Fe_2O_3 \cdot x In_2O_3$ consist of only a single phase with garnet structure for $0 \leqq x \leqq 1$, three phases (garnet + $YFeO_3$ + In_2O_3) for $1 < x < 2$, and two phases ($YFeO_3$ + In_2O_3) for $x=2$. For $x=3$, an appreciable amount of $YFeO_3$ is contained.

2) For small x, In^{3+} ions substitute Fe^{3+} ions on 16(a) sites.

3) As In substitution proceeds, σ_0 at first increases, passes through a maximum near $x=0.3$ and then decreases linearly with x, as far as $x=1$ is reached. The Curie temperature T_c decrease monotonically with x for $x \leqq 1$ and is constant for $x > 1$.

4) Substitution of a small amount of In has such an effect that it increases the initial permeability and decreases the coercive force.

5) Ferrimagnetic resonance line width ΔH increases rapidly with increasing x. ΔH is about 130 Oe at $x=0$, while it reaches even 900 Oe at $x=1.3$. In the single phase region ($0 \leqq x \leqq 1$), the most of the increase in line width seems to be intrinsic provided Schlömann's theory holds.

Acknowledgement

The authors wish to express their hearty thanks to Prof. N. Tsuya of Tohoku Univ. for general guidance and to Mr. I. Tsubokawa of Tohoku Univ. for measurement of spontaneous magnetization. They also express their many thanks to Dr. Y. Ishikawa of Tokyo Univ. for instructive discussions on thermoremanence.

References

(1) F. Bertaut and F. Forract, *Compt. rend.*, **242** (1956) 382; *ibid.*, **244**, 96 (1957).
(2) M. A. Geller and S. Gilleo, *J. Phys. Chem. Solids*, **3**, 30 (1957).
(3) R. Pauthenet, *Ann. de Phys.*, **3**, 424 (1958).
(4) R. Pauthenet, *J. Appl. Phys.*, **29**, 253 (1958).
(5) M. A. Geller and S. Gilleo, *Phys. Rev.*, **110**, 73 (1958).
(6) J. F. Dillon, Jr., *Phys. Rev.*, **105**, 759 (1957).
(7) e.g. R. C. LeCraw, E. G. Spencer, and C. S. Porter, *Phys. Rev.*, **110**, 1311 (1958).
(8) W. P. Wolf and G. P. Rodrigue, *J. Appl. Phys.*, **29**, 105 (1958).
(9) W. L. Bond, *Rev. Sci. Inst.* **22**, 344 (1951).
(10) T. Hirone, S. Maeda, and N. Tsuya, *Rev. Sci. Inst.*, **25**, 516 (1954).
(11) Y. Odani, Y. Shichijo, M. Mikagi, and Y. Gomi, *Rep. of the E.C.L.*, N.T.T., **5**, 22 (1957).
(12) L. Neel, *Ann. de Phys.*, **3**, 137 (1948).
(13) H. Forestier and G. Guiot-Guillain, *Compt. rend.*, **230**, 1844 (1950).
(14) E. Schlömann, *Conf. on Magnetism and Magnetic Materials*, Boston, p. 600, Oct. 1956 (AIEE).
(15) A. M. Clogston, H. Suhl, L. R. Walker, and P. W. Anderson, *J. Phys. Chem. Solids*, **1**, 129 (1956).
(16) R. Vautier and A. J. Berteaud, *Compt. rend.*, **247**, 1974 (1958).

* * * *

621.318.56:621.394.6]:620.178

Deterioration of Contacts of a Polar Relay with a Rigid Tongue*

Sanae AMADA,† *Kôsaku MUKAI,*† and *Yukichi KANEKO*†

Deterioration of contacts of a polar relay with a rigid tongue is observed under various conditions changing contact materials and associated circuit constants.

Process of contact deterioration is observed. Deteroiration is intimately related to contact welding.

Molybdenum contacts is the least prone to weld. Percentage of contact time to total time fluctuates continuously throughout the operation period.

As long as it does not deviate over a few percent from preset value, transmission quality of a telegraph circuit is not greatly deteriorated.

Introduction

The maintenance of polar relays, which are widely used in telegraph circuits, is of great concern to telegraph engineers. Causes of the fluctuation of the percentage of the time the relay contacts are closed to total time (percentage of contact time, hereafter abbreviated PCT) and caused of the fluctuation of bias distortion are not yet known.

In telegraph circuit troubles, considerable numbers of those of unknown origin are included. The authors attribute a considerable percentage of these troubles to the deterioration of the contacts of the polar relays used, and therefore conducted deterioration tests in an attempt to learn the causes of these troubles.

1. Purposes of These Tests

1.1. To examine the frequently observed fluctuations in the values of PCT and in the values of bias distortion.

1.2. To observe when and how a weld or an unsatisfactory connection occurs.

1.3. To determine if the faults mentioned in Categories 1 and 2 above are functions of the relay contact surface condition and or of the circuit connected to the relay contacts. Also, methods of preventing these phenomena were sought.

1.4. To determine if the faults mentioned in Categories 1 and 2 above are functions of the contact alloy.

2. Methods of Tests

2.1. Selection of Relay

The NTT Type 21 Relay was chosen for these tests. Factors which led to its selection include:

a. Associated circuit is of a type known to cause severe relay contact deterioration (Contact current is 70 mA, applied voltage is 100 V, and load is inductive.).

b. Tongue is rigid, and chatters during operation.

c. No sliding occurs between the contacts.

It was assumed that the contact deterioration is quite severe, but more simple in its phenomenon than that of other types of relays.

2.2. Test Conditions

a. Voltage across opened relay contacts
100 V dc

* MS received by the Electrical Communication Laboratory Oct. 22, 1959. Originally published in the *Electrical Communication Laboratory Technical Journal*, N.T.T., Vol. 9, No. 1, pp. 64–82, 1960.

† Telegraph Section.

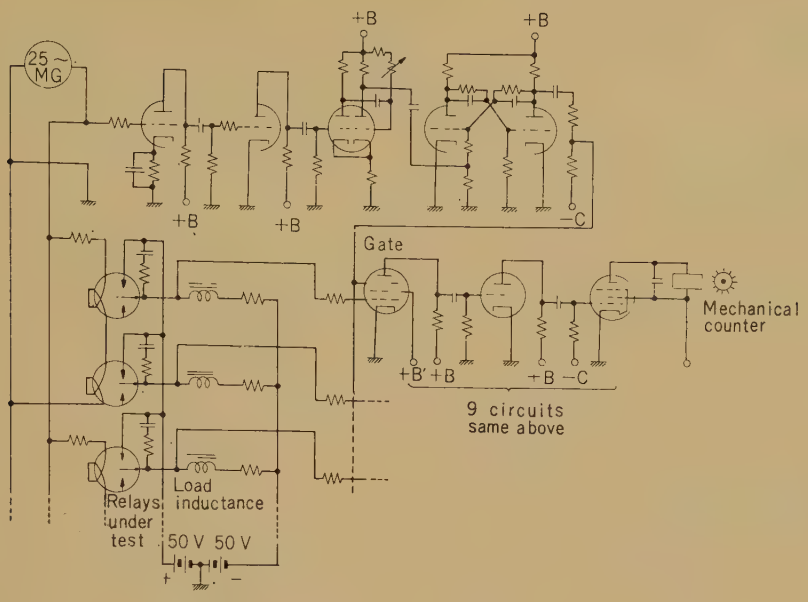

Fig. 1—Welding counter circuit.

b. Current opened by relay contacts
70 mA
c. Operating speed 50 Baud
d. Spark quench circuit series RC circuit
(1) Capacitance 0.5 μF
(2) Resistance 0.3, 1, 3 kΩ
e. Load inductance 2, 4, 6 H
f. Number of relays tested 63
g. Contact materials tested
Pt-Au-Ag (PGS), Au-Ag (GS), Pt, Pt-Ir, Ag-Pd, Cu-Pd, Mo
h. Period of test
30 hours (90,000 operations per hour)

2.3. Items Measured or Observed

During these tests PCT, bias distortion, and contact resistance were measured; and the contact surfaces were carefully observed. The number of times the contacts welded together and the number of times the contacts failed to make a satisfactory connection were counted with the electronic circuit shown in Fig. 1. The test setup is shown in Fig. 2.

3. Test Results

3.1. General

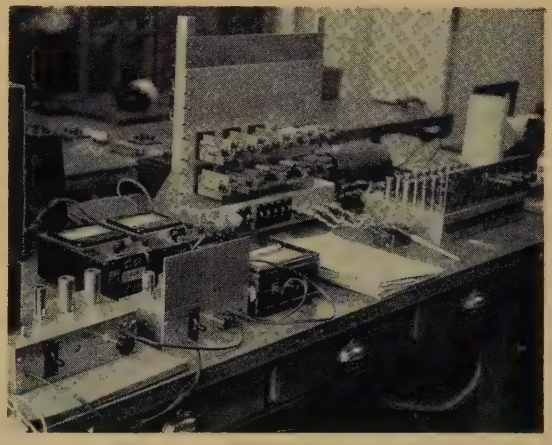

Fig. 2—Test apparatus.

Contact deterioration depended on the material of which the contact was made. The number of times the contacts welded together was directly related to both the condition of the contact surfaces and to the circuit in which the contact were connected.

Bias distortion, PCT, and contact resistance fluctuated continuously during the test period. No interdependence was found between these values or between any of them and the deterioation of the contact.

3.2. Fluctuation of PCT and Bias Distortion

Measured values of PCT, which fluctuated continuously during the tests, are shown in Fig. 3. Bias distortion fluctuated in the same manner as PCT, but the two were not always proportional.

3.3. Fluctuation of Constant Resistance

Measured values of contact resistance are shown in Fig. 4. Five to ten hours after the beginning of the test, contact resistance reached a metastable state. For some contact materials, the values of contact resistance measured bunched into two or three groups. The reason for this phenomenon is not understood.

3.4. Contact Deterioration

Test circuit conditions prevented an arc discharge. However, considerable contact deterioration was observed for some of the contact materials. On the negative contact a conical protrusion was built up, while on the opposite contact a small depression was formed. This protrusion did not grow at a constant speed. At first it was build up rapidly, but after reaching a certain length its length began to decrease. However, before long this build-up process was repeated, as is shown in Fig. 5.

In the case of Cu-Pd contacts, erosion occurred on the opposite (negative) contact. The deterioration of Mo contacts, which are shown in Fig. 6, was too small to be recognized.

3.5. Welding

For some combinations of external circuit conditions and contact materials, a large number of contact welds occurred. A graph of the total number of contact welds is shown in Fig. 7, with up to 10 welds expressed as a bar of unit length, up to 100 welds expressed as a bar of two units length, up to 1,000 welds as a bar of three units length, etc.

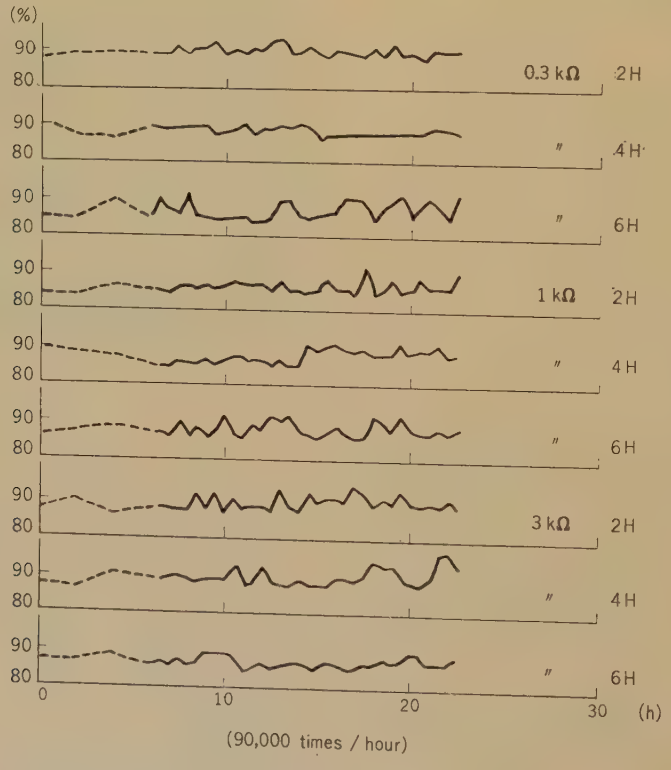

Fig. 3 (a)—Fluctuation of PCT of Pt contact.

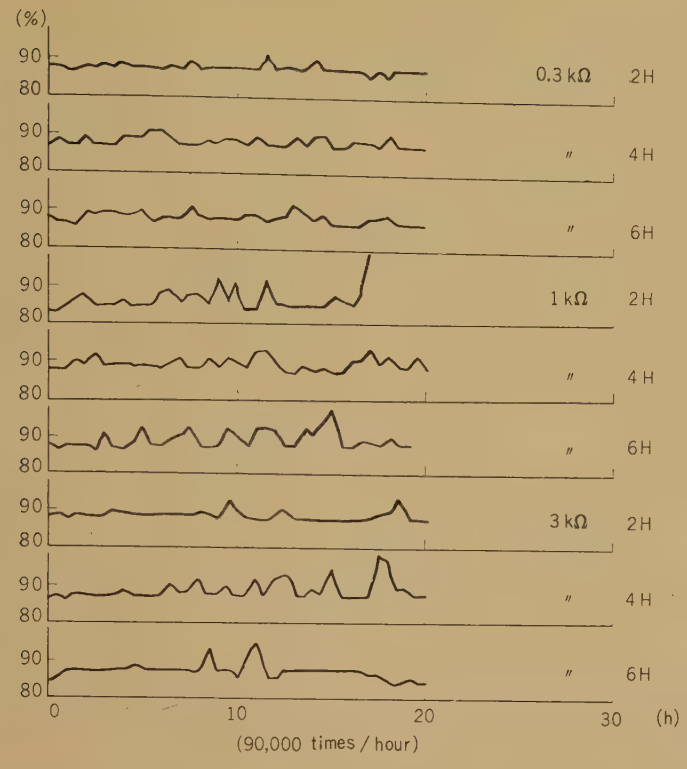

Fig. 3 (b)—Fluctuation of PCT of PGS contact.

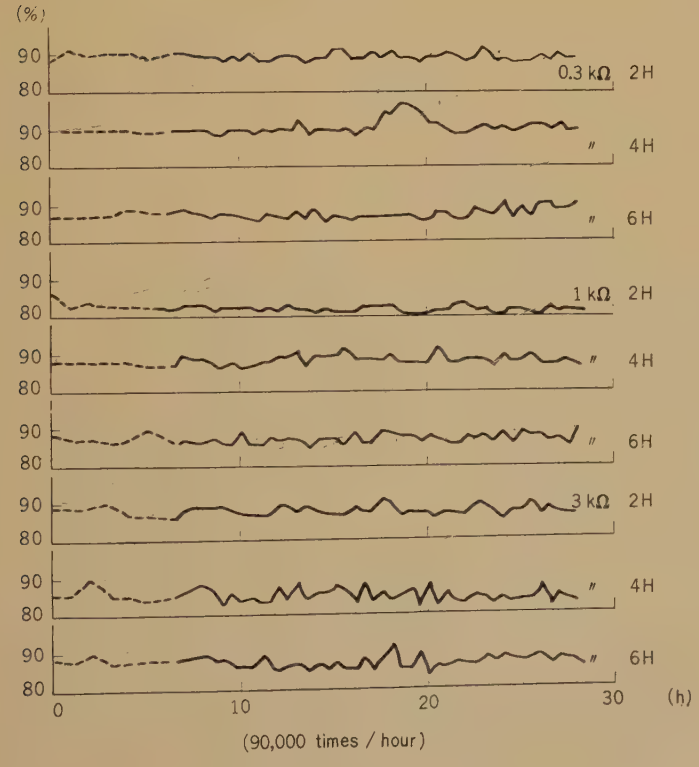

Fig. 3 (c)—Fluctuation of PCT of GS contact.

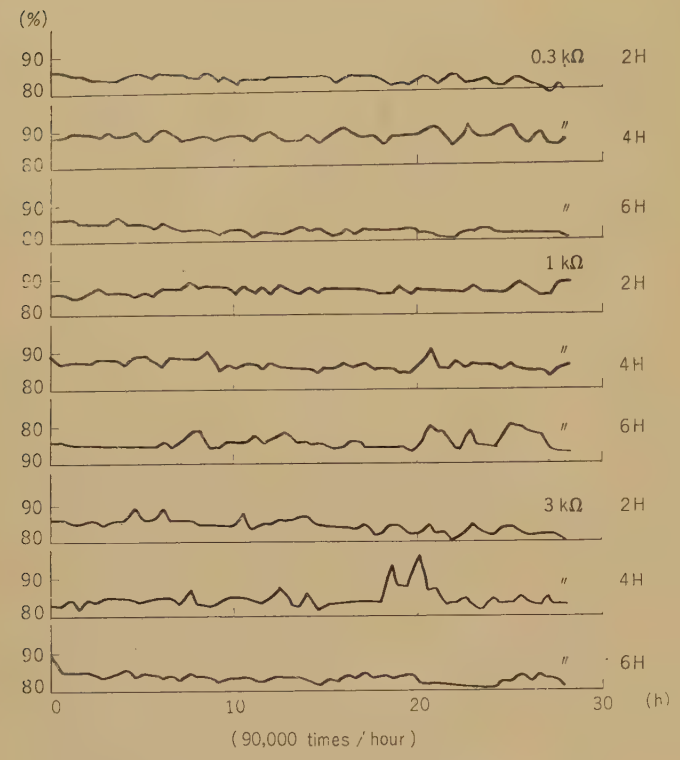

Fig. 3 (d)—Fluctuation of PCT of Ag-Pd contact.

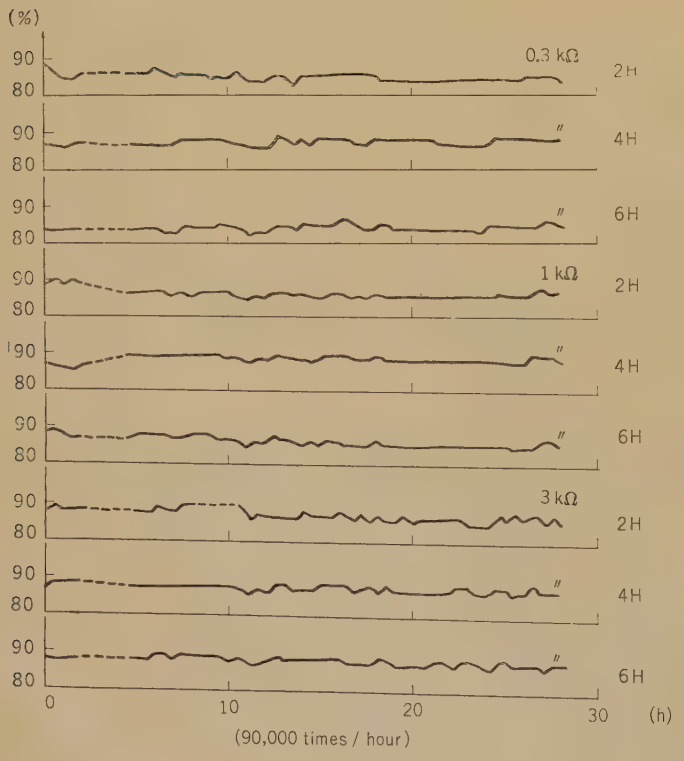

Fig. 3 (e)—Fluctuation of PCT of Cu-Pd contact.

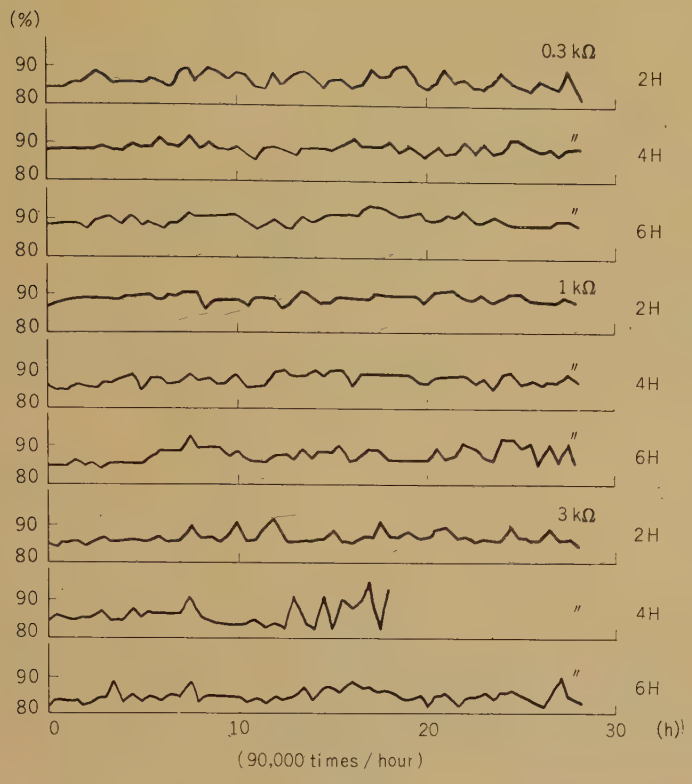

Fig. 3 (f)—Fluctuation of PCT of Pt-Ir contact.

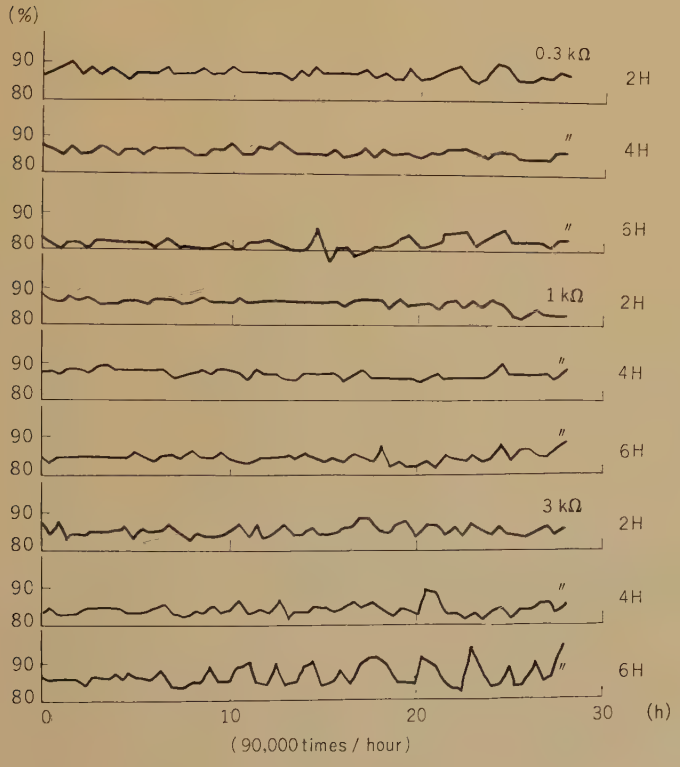

Fig. 3 (g)—Fluctuation of PCT of Mo contact.

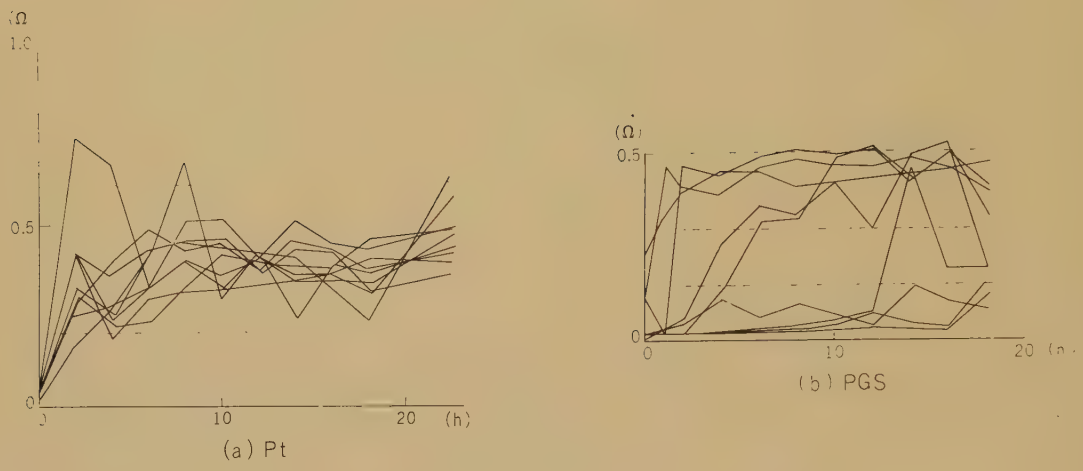

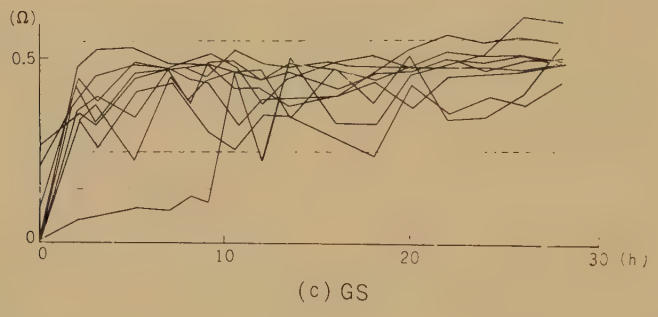

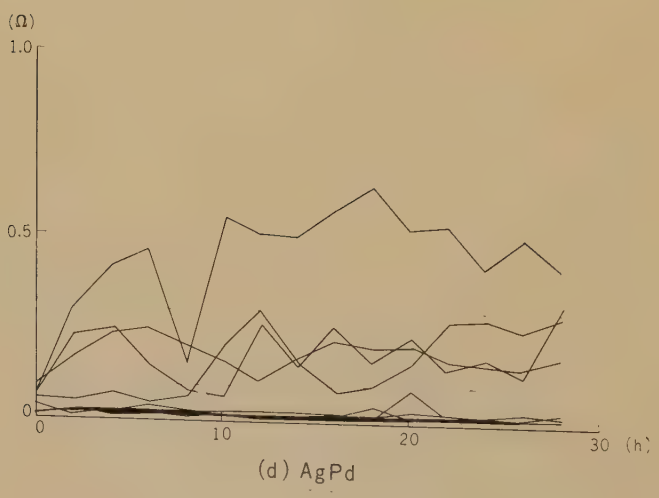

Fig. 4 (a), (b), (c), and (d)—Fluctuation of contact resistance.

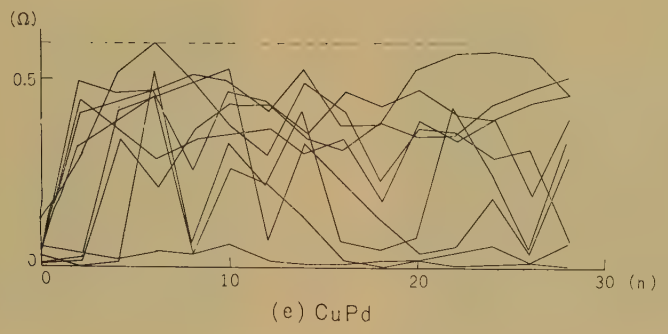

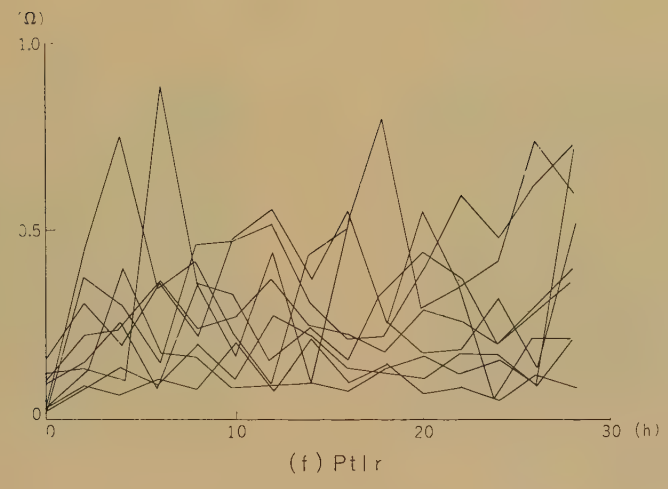

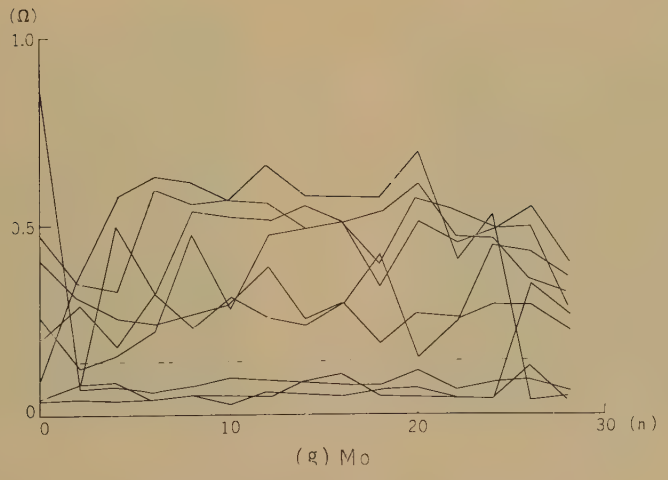

Fig. 4 (e), (f), and (g)—Fluctuation of contact resistance.

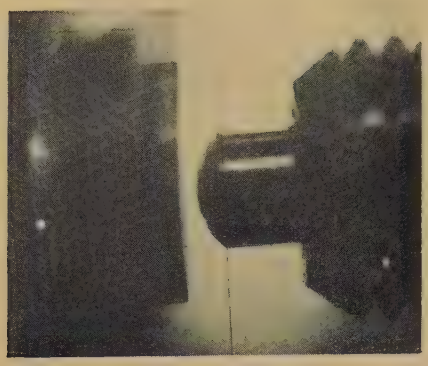

(a) Before Test

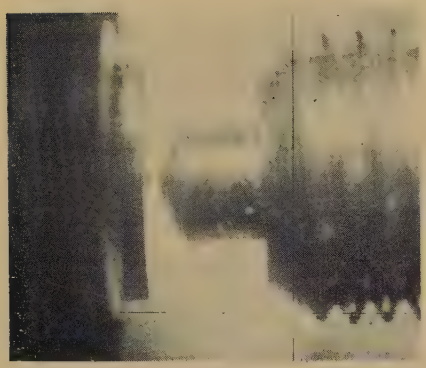

(b) After 1 Hour Operation

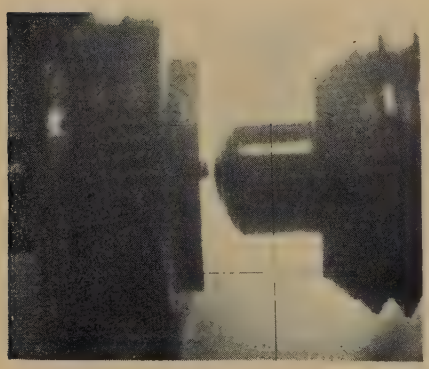

(c) After 2 Hours Operation

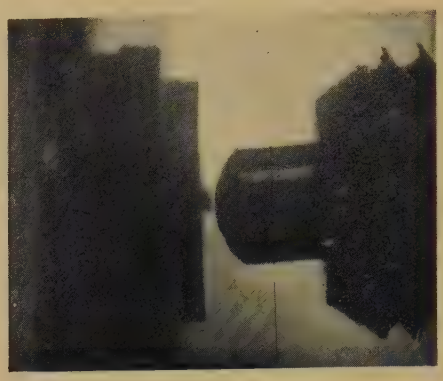

(d) After 4 Hours Operation

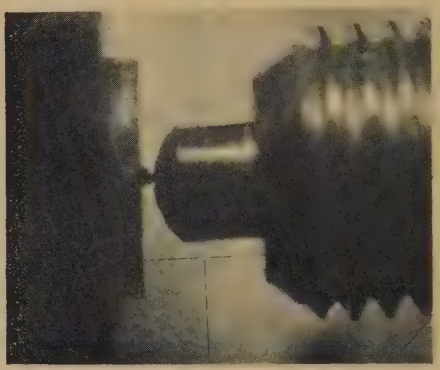

(e) After 6 Hours Operation

(f) After 8 Hours Operation

Fig. 5 (a), (b), (c), (d), (e), and (f)—Wear of PGS contact.

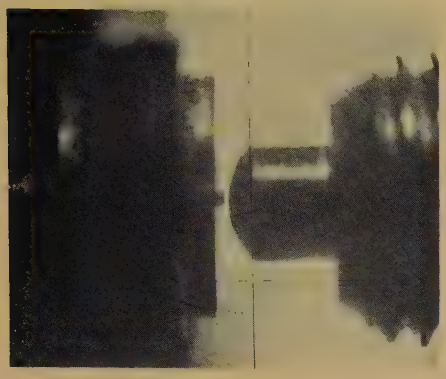

(g) After 12 Hours Operation

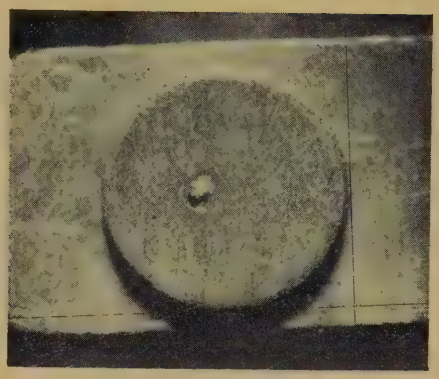

(i) Surface of Negative Contact after Test

(h) After 20 Hours Operation

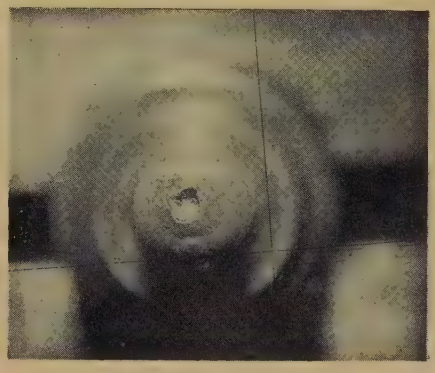

(j) Surface of Positive Contact after Test

Fig. 5 (g), (h), (i), and (j)—Wear of PGS contact.

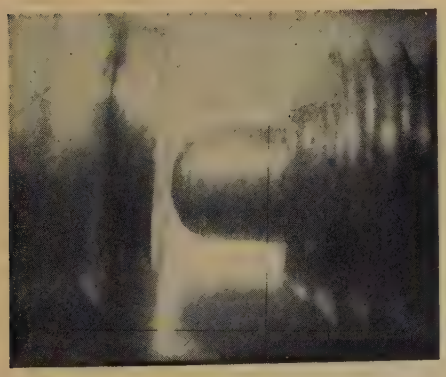

(a) Before Test

(b) After 8 Fours Operation

Fig. 6 (a) and (b)—Wear of Mo contact.

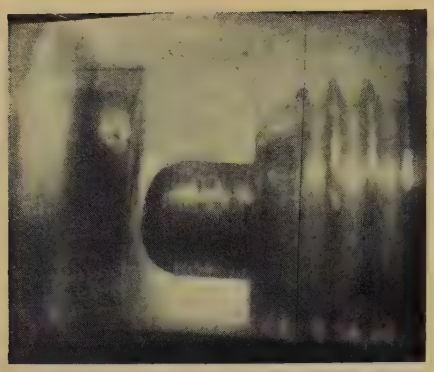

(c) After 20 Hours Operation

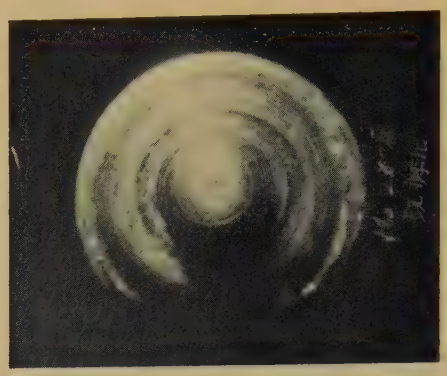

(e) Surface of Possitive Contact after Test

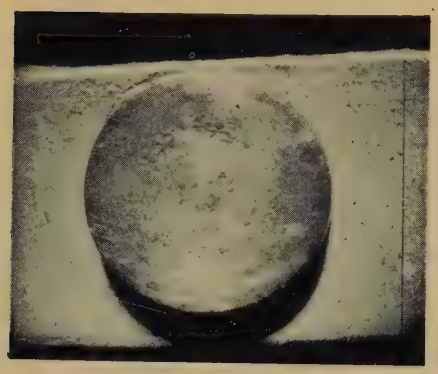

(d) Surface of Negative Contact after Test

Fig. 6 (c) (d), and (e)—Wear of Mo contact.

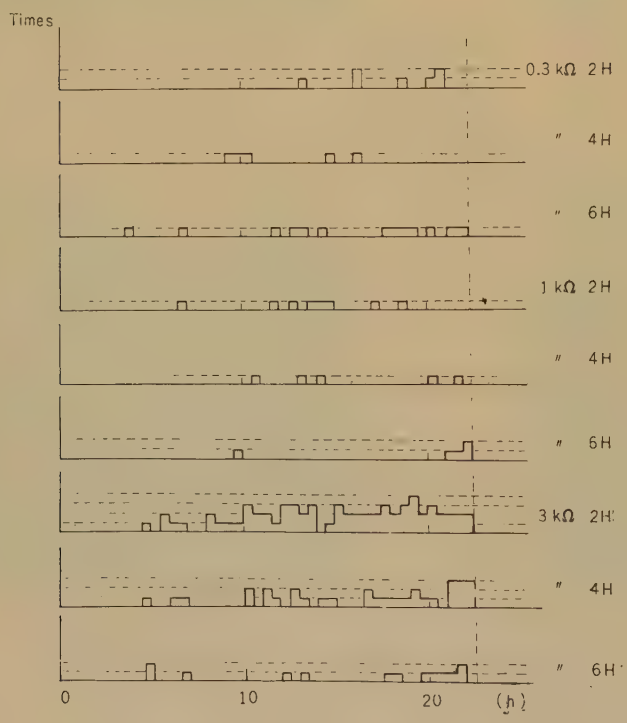

(a) Pt

Fig. 7 (a)—Times of welding.

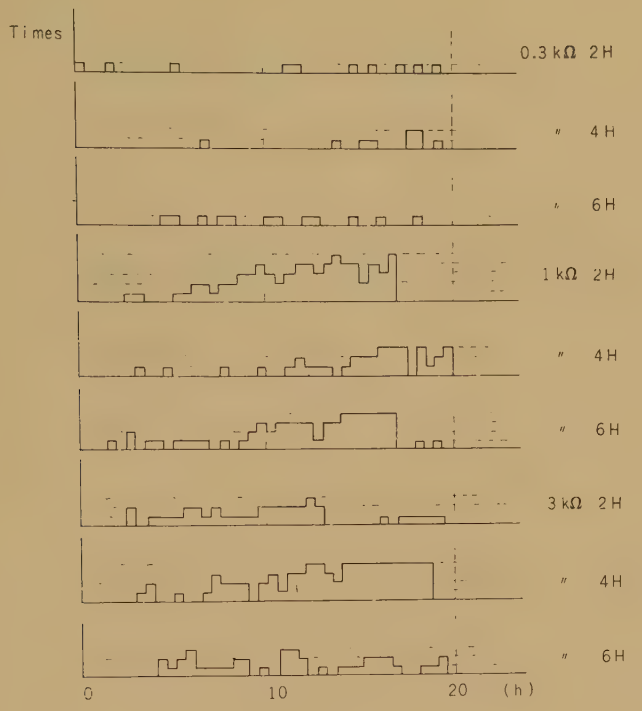

(b) PGS

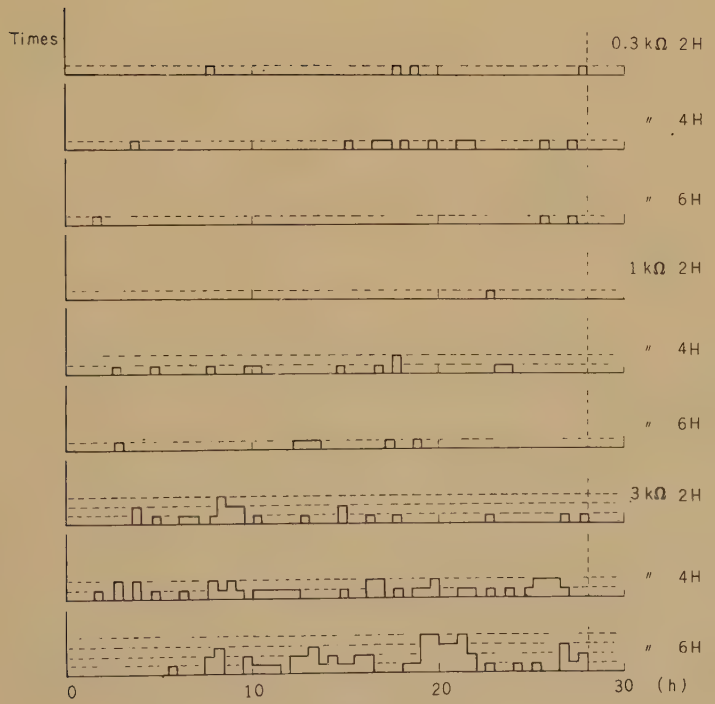

(c) GS

Fig. 7 (b) and (c)—Times of welding.

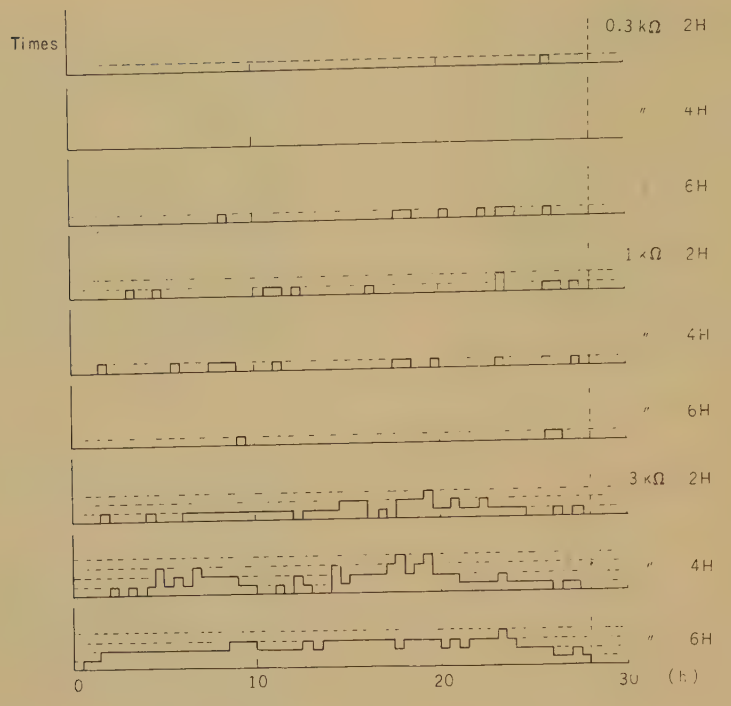

(d) AgPd

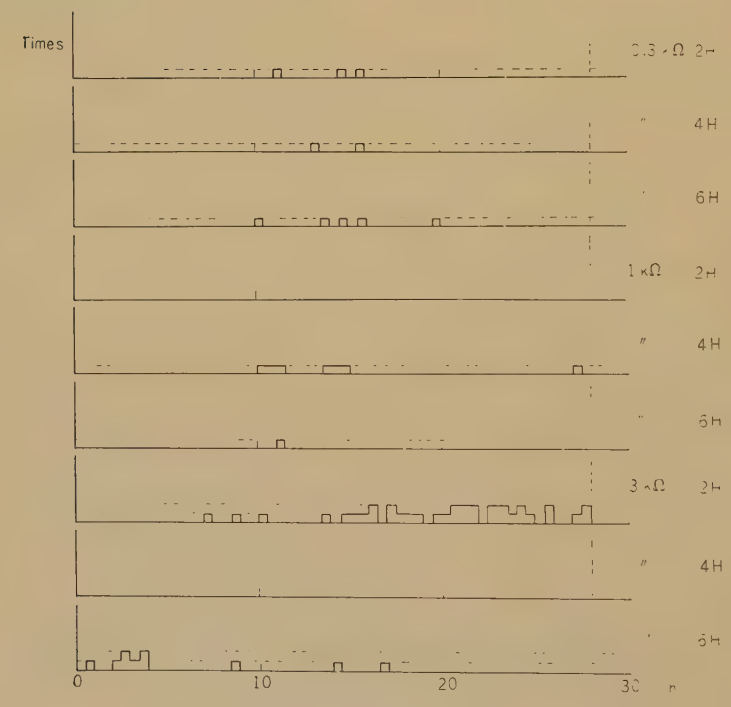

(e) CuPd

Fig. 7 (d) and (e)—Times of welding.

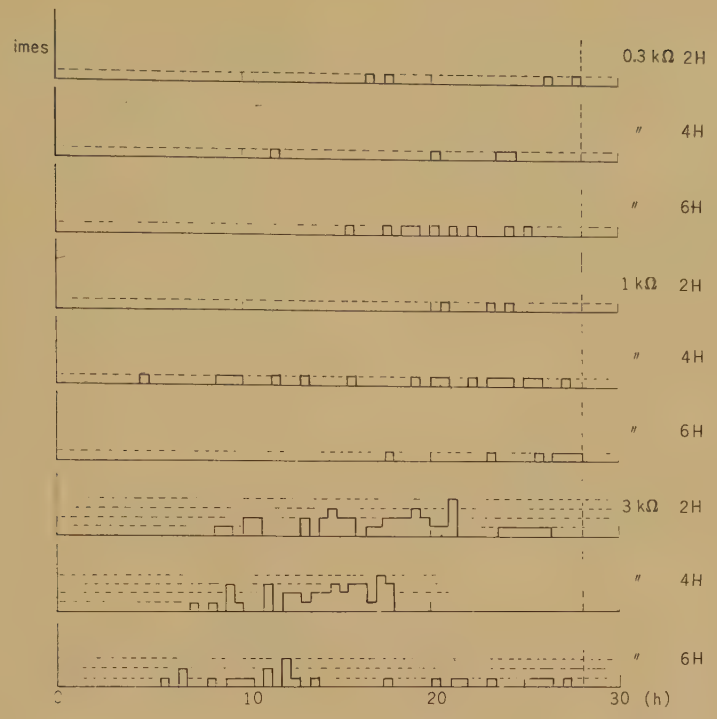

(f) Pt Ir

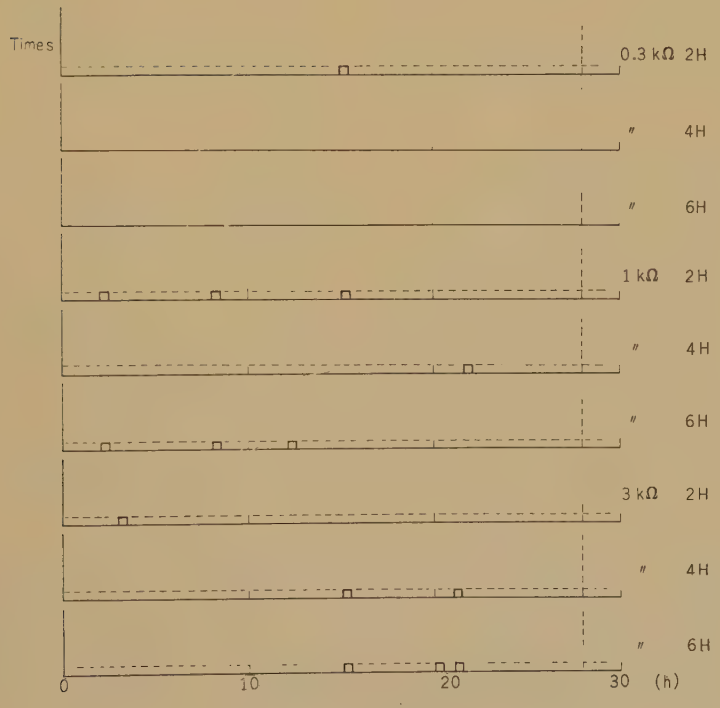

(g) Mo

Flg. 7 (**f**) and (**g**)—Times of welding.

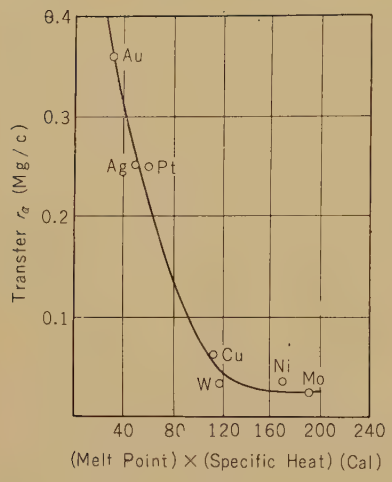

Fig. 8—Relationship between transfar, melting point and specific heat.

Mo contacts were the least prone to weld, and Cu-Pd contacts were second best. Contacts made of the other five kinds of materials were not very satisfactory. The value of the resistor in the spark quench circuit had a definite bearing on the number of welds observed; when this resistor was 3,000 ohms an excessive number of welds took place.

3.6. Relationship between Contact Deterioration and Welding

The test result showed that welding is apt to occur when the contact surfaces become extremely deteriorated. Especially, one slender protrusion was found to be more injurious than a large number of shorter protrusions. Our hypothetical explanation of the mechanism of this process is:

Once a longer slender protrusion is produced, the contact current is forced to concentrate at a very small contact point causing the production of much heat; but radiation is hindered by the sides of the depression in the mating contact, and welding is apt to occur. The bridge made by welding is ruptured by the successive mechanical impulses produced by signal current in the relay winding. The surface at this rupture is flat, but a new slender protrusion will start to grow on this surface.

4. Discussion

4.1. PCT and Bias Distortion

Fluctuation of the values of PCT and of bias distortion was continuous throughout the period of the test, but normal fluctuation of these values results in only a very slight deterioration of transmission quality. However, excessive increase in PCT; e.g., over 95 percent, was a warning of imminent contact welding.

4.2. Unsatisfactory Connection and Welding

Data pertaining to unsatisfactory connections was not sufficient for any meaningful conclusions to be drawn, but the number of faulty connections observed were exceedingly few.

Welding, which is a function of both the contact materials and of the resistance in the spark quench circuit, was not observed for some combinations of contact materials and spark quench resistors. Also, as noted in 3.6, welding is directly related to contact deterioration, especially to the migration of contact material from one electrode to the other.

Professor Ho determine, for contact materials, a relationship between the migration of contact material and the product of the melting point and the specific heat of that alloy. Good agreement with his results was obtained. Mo and Cu-Pd contacts (Professor Ho's value for the migration constant of Pd is 0.1 mg/°C) showed little deterioration and a small number of welds.

4.3. Contact Resistance

Contact resistance was observed to be dependent only on the contact material, and to reach a metastable state after 500,000 to 1,000,000 operations. Therefore, the contacts of relays used in telegraph circuits are thought to be in this state.

Conclusion

The deterioration of contacts of the NTT

Type 21 Polar Relay, whose contact deterioration was thought to be simpler to analyze than those of other types, was tested. From these tests, the following conclusions can be drawn:

a. PCT of all relays in a telegraph circuit fluctuate with time. As long as any of them deviates within a few percent from the preset value, it has a small effect on the transmission quality. Therefore present standard practice of replacing polar relays whose PCT decreases to some definite value e.g. 85 percent should be re-examined. Excessive increase in PCT, however, is a warning of imminent contact welding.
b. Mo contacts do not deteriorate easily.
c. Contact deterioration and contact welding are intimately related.

* * * *

621.375.4.018.78

Harmonic Distortion Factor of Transistors*

Seiichi KAWAGUCHI† and *Minoru HIRAI*†

Starting from expressions (stated in terms of the transistor four-terminal h-parameters and the nonlinear coefficients of h-parameters) for the differential change of gain of a transistor amplifier circuit with a change in signal amplitude, an equation for calculating the second-harmonic distortion factor of the amplifier circuit at low frequencies was derived. Second-harmonic distortion factors for four types of transistors were calculated and measured. Also, variations of the second-harmonic distortion factor, the third-harmonic distortion factor, and gain with changes in bias and with changes in frequency were measured at frequencies up to 660 kc.

Introduction

At the present time a cumbersome method exists for calculating the harmonic distortion factor in low frequencies at which phase rotation is negligible. In the existing method, an equation in the form of the sum of each frequency component of ω (fundamental frequency), 2ω, 3ω, $\cdots\cdots$ is substituted into every current and voltage of input and output of nonlinear four-terminal equation, and then the amplitude of each of these frequency components is obtained.[1],[2] The authors have recently succeeded to obtain the same calculating equation by a new method which is simpler and more practical. In this method, differential coefficient for signal amplitude of circuit amplification is obtained by using four-terminal h-parameters and their nonlinear coefficients.

Subsequently, for the four different types of germanium transistors—alloy type, drift type, alloy diffused type, and grown diffused type—second-harmonic distortion factors at low frequencies were calculated, and second-and third-harmonic distortion factors for fundamental frequencies up to 660 kc were measured.

* MS received by the Electrical Communication Laboratory May 2, 1959. Originally published in the *Electrical Communication Laboratory Technical Journal*, N.T.T., Vol. 8, No. 6, pp. 876-881, 1959.

† Semiconductors Research Section.

1. General Equations of Distortion Factor at Low Frequencies

Now, at low frequency equivalent circuit of transistor amplifier as shown in Fig. 1, between the output current i_2 and the constant current source i_g, suppose that the following relation is formed:

$$i_2=a_1i_g+a_2i_g^2+a_3i_g^3+a_4i_g^4+\cdots\cdots, \quad (1)$$

where a_1, a_2, $\cdots\cdots$ are constants.

If $i_g=I_g\sin\omega t$, Equation (1) bebomes

$$i_2=H_0+H_1\sin\omega t - H_2\cos 2\omega t - H_3\sin 3\omega t+\cdots\cdots, \quad (2)$$

where

$$\left.\begin{aligned} H_0&=\frac{a_2}{2}I_g^2+\frac{3}{8}a_4I_g^4+\cdots\cdots,\\ H_1&=a_1I_g+\frac{3}{4}a_3I_g^3+\cdots\cdots,\\ H_2&=\frac{a_2}{2}I_g^2+\frac{a_4}{2}I_g^4+\cdots\cdots,\\ H_3&=\frac{a_3}{4}I_g^3+\frac{3}{16}a_5I_g^5+\cdots\cdots. \end{aligned}\right\} \quad (3)$$

Then, the second-harmonic distortion factor K_2 and the third-harmonic distortion factor K_3 are as follows:

$$K_2=\left|\frac{H_2}{H_1}\right|=\left|\frac{1}{2}\frac{a_2}{a_1}I_g+\left(\frac{1}{2}\frac{a_4}{a_1}-\frac{3}{8}\frac{a_2a_3}{a_1^2}\right)I_g^3+\cdots\cdots\right|, \quad (4)$$

$$K_3=\left|\frac{H_3}{H_1}\right|=\left|\frac{1}{4}\frac{a_3}{a_1}I_g^2+\frac{3}{16}\left(\frac{a_5}{a_1}-\frac{a_3^2}{a_1^2}\right)I_g^4+\cdots\cdots\right|. \quad (5)$$

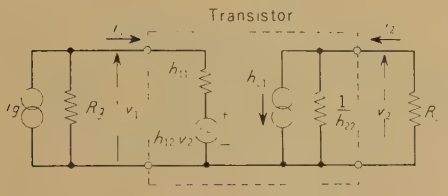

Fig. 1—Fundamental equivalent circuit of transistor amplifier.

2. Calculation Equations ofSecond Harmonic Distortion Factor at Low Frequencies

At low signal levels, H_1 in Equation (3) is approximately

$$H_1=a_1I_g, \quad (6)$$

Equation (4) becomes approximately

$$K_2=\left|\frac{1}{2}\frac{a_2}{a_1}I_g\right|=\left|\frac{1}{2}\frac{a_2}{a_1^2}H_1\right|. \quad (7)$$

Then, if the current gain is $A_i=di_2/di_g$,

$$\left.\begin{aligned}a_1&=\left(\frac{di_2}{di_g}\right)_0=A_{i0},\\ a_2&=\frac{1}{2}\left(\frac{dA_i}{di_g}\right)_0,\end{aligned}\right\} \quad (8)$$

where the sufix "0" shows the value at $i_g=0$.

Now, if A_i is the function of the input current i_1 and the output voltage v_2,

$$K_2=\left|\frac{1}{4A_{i0}^2}\left(\frac{dA_i}{di_g}\right)_0H_1\right|$$

$$=\left|\frac{1}{4A_{i0}^2}\left(\frac{di_1}{di_g}\right)_0\left[\left(\frac{\partial A_i}{\partial i_1}\right)_0+\left(\frac{dv_2}{di_1}\right)_0\left(\frac{\partial A_i}{\partial v_2}\right)_0\right]\cdot H_1\right|. \quad (9)$$

Now, A_i is shown by h-parameters as

$$A_i=\frac{h_{21}R_g}{(R_g+h_{11})(1+h_{22}R_L)-h_{21}h_{12}R_L}. \quad (10)$$

Then

$$K_2=\left|\frac{1}{4h_{21}^2}\frac{di_1}{di_g}\left[\left(1+\frac{h_{11}}{R_g}\right)\times(1+h_{22}R_L)\left(\frac{\partial h_{21}}{\partial i_1}+\frac{dv_2}{di_1}\cdot\frac{\partial h_{21}}{\partial v_2}\right)-\left(1+\frac{h_{11}}{R_g}\right)h_{21}R_L\left(\frac{\partial h_{22}}{\partial i_1}+\frac{dv_2}{di_1}\cdot\frac{\partial h_{22}}{\partial v_2}\right)-(1+h_{22}R_L)\frac{h_{21}}{R_g}\left(\frac{\partial h_{11}}{\partial i_1}+\frac{dv_2}{di_1}\cdot\frac{\partial h_{11}}{\partial v_2}\right)+\frac{R_L}{R_g}h_{21}^2\left(\frac{\partial h_{12}}{\partial i_1}+\frac{dv_2}{di_1}\cdot\frac{\partial h_{12}}{\partial v_2}\right)\right]\cdot H_1\right|, \quad (11)$$

where

$$\frac{di_1}{di_g}=\frac{(1+h_{22}R_L)R_g}{(R_g+h_{11})(1+h_{22}R_L)-h_{21}h_{12}R_L},$$

$$\frac{dv_2}{di_1}=-\frac{h_{21}R_L}{1+h_{22}R_L}.$$

Then, at emitter ground, if h-parameters are the functions of emitter current $i_e=-(i_1+i_2)$ and collector voltage $v_c=v_2$,

$$K_2=\left|\left[u_1\left(\frac{\partial h_{21}}{\partial i_e}+F\frac{\partial h_{21}}{\partial v_c}\right)+u_2\left(\frac{\partial h_{22}}{\partial i_e}+F\frac{\partial h_{22}}{\partial v_c}\right)+u_3\left(\frac{\partial h_{11}}{\partial i_e}+F\frac{\partial h_{11}}{\partial v_c}\right)+u_4\left(\frac{\partial h_{12}}{\partial i_e}+F\frac{\partial h_{12}}{\partial v_c}\right)\right]\cdot H_1\right|, \quad (12)$$

where

$$u_1=\frac{G}{4h_{21}^2}\left(1+\frac{h_{11}}{R_g}\right)(1+h_{22}R_L),$$

Table 1

CALCULATED AND MEASURED VALUES OF SECOND-HARMONIC DISTORTION FACTORS OF FOUR TYPES OF GERMANIUM TRANSISTORS AT 270 C/S, FUNDAMENTAL FREQUENCY (EMITTER GROUND, $T_a=25°$ C)

Name of Tr.		ECL 1204 (19)	2N384 (1)	OC170 (2)	ST27B (2-3)
Maker of Tr.		Electr. Comm. Labor.	RCA Co.	Philips Co.	Nippon Electr. Co.
Type of Tr.		Alloy	Drift	Alloy Diffused	Grown Diffused
$u_1\partial h_{21}/\partial i_e$ (1/A)		4.63	−3.49	−29.4	−32.27
$u_1F\partial h_{21}/\partial v_c$ (〃)		18.82	23.2	9.35	35.2
$u_2\partial h_{22}/\partial i_e$ (〃)		13.4	16.86	3.32	9.63
$u_2F\partial h_{22}/\partial v_c$ (〃)		−1.19	6.13	−0.1	−2.92
$u_3\partial h_{11}/\partial i_e$ (〃)		−8.48	−13.14	−3.66	3.84
$u_3F\partial h_{11}/\partial v_c$ (〃)		−3.28	−4.31	−0.94	−9.8
$u_4\partial h_{12}/\partial i_e$ (〃)		−0.44	−1.41	−0.29	−1.37
$u_4F\partial h_{12}/\partial v_c$ (〃)		0.18	−2.14	0.02	0.59
Sum of Above (〃)		23.64	21.7	−22.7	2.9
K_2 (dB) at Output Level =0 dB	Calculated Value	−31.2	−32	−31.6	−49.5
	Measured Value	−25.5*	−30	−31.1	−36.4

Bias: $V_{CE}=-9.5$ V, $I_E=4$ mA. Source resistance $R_g=3$ kΩ, load resistance $R_L=1.5$ kΩ.
* Only in this case, fundamental frequency=6 kc.

$$u_2=\frac{-G}{4h_{21}^2}\left(1+\frac{h_{11}}{R_g}\right)h_{21}R_L,$$

$$u_3=\frac{-G}{4h_{21}^2}(1+h_{22}R_L)\frac{h_{21}}{R_g},$$

$$u_4=\frac{G}{4h_{21}^2}\frac{R_1}{R_g}h_{21}^2,$$

$$G=\frac{di_e}{di_g}=\frac{-(1+h_{21}+h_{22}R_L)R_g}{(R_g+h_{11})(1+h_{22}R_L)-h_{21}h_{12}R_L},$$

$$F=\frac{dv_c}{di_e}=\frac{h_{21}R_L}{1+h_{21}+h_{22}R_L}. \qquad (13)$$

3. Calculations and Measurements of Second-Harmonic Distortion Factor at Low Frequencies

Concerning the four types of transistors, the values of eight terms in [ ] in Equation (12) were calculated by using not only the values of h-parameters for 270 c/s at $V_{cE}=-9.5$ V and $I_E=4$ mA but the values of partial differential coefficient to i_e and v_c obtained from the tangents of curves dependent on biases centered at above point. Each of the calculated values and their total are shown in Table 1. When $-i_g$ increases, the sign of + and − of these values correspond respectively to the decrease and increase of A_i. In this table, are shown the values of K_2 calculated by Equation (12) and those measured with 720 type wave analyser at $R_g=3$ kΩ, $R_L=1.5$ kΩ, and the output level for fundamental frequency of 270 c/s=0 dB ($H_1=1.153$ mA at $R_L=1.5$ kΩ).

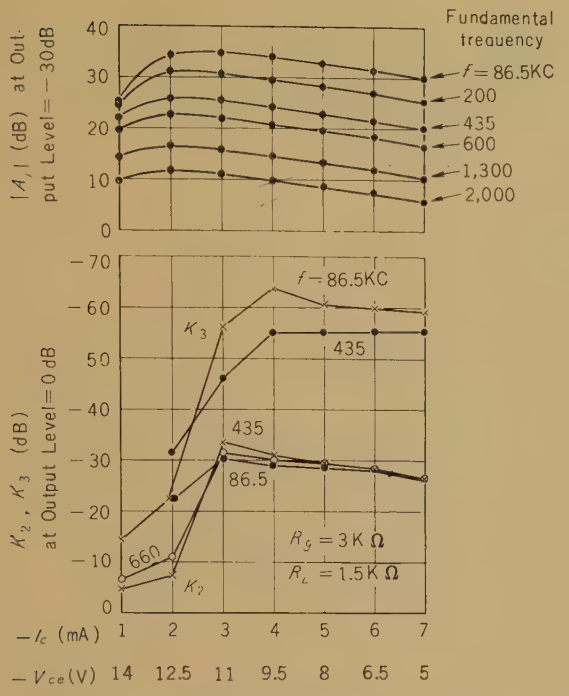

(a) ECL 1204 (21)

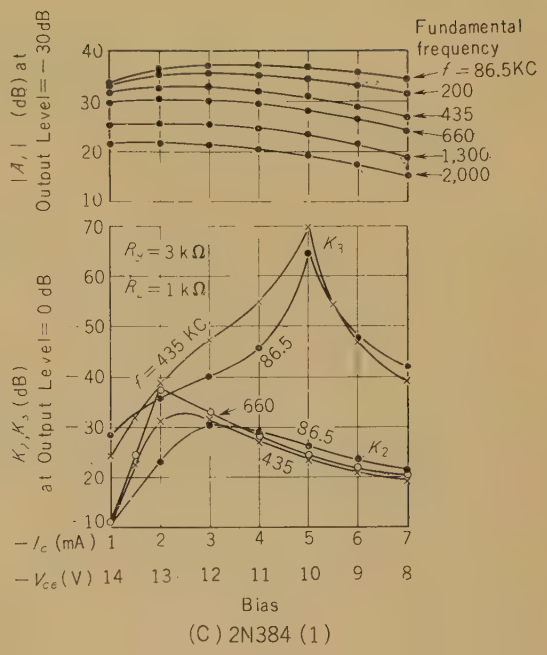

(C) 2N384 (1)

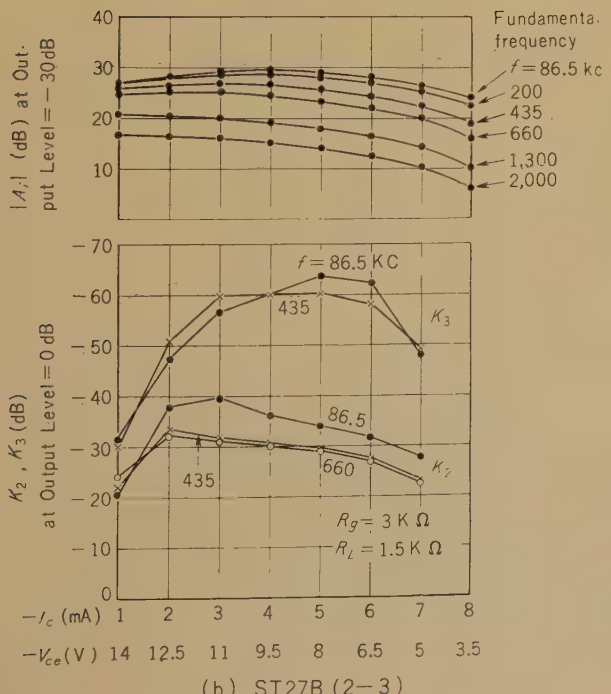

(b) ST27B (2−3)

Fig. 2 (a), (b), and (c)—Variations of A_i, K_2 and K_3 of four types of transistors with biases (emitter ground T_a=25° C).

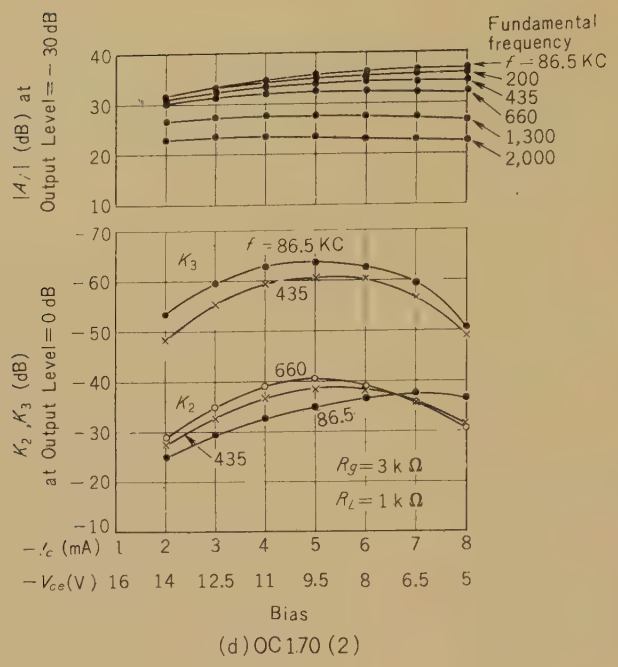

Fig. 2 (d)—Variation of A_i, K_2 and K_3 of four types of transistors with biases (emitter ground T_a=25° C).

4. Variations of Harmonic Distortions with Frequencies and Biases

The values of A_i, K_2, and K_3 of the four transistors are shown in Fig. 2, which were measured by *H*-1 Type Selective Level Meter for several frequency between 86.5 kc and 2 Mc at every point of bias on the load line.

Conclusion

The results of this research are outlined as follow:

(1) A calculating equation of second-harmonic distortion factor of a transistor at low frequencies with *h*-parameters has been obtained by a method simpler and more practical than that known so far.

(2) For the four types of transistors—alloy type, drift type, alloy diffused type, and grown diffused type—relations between second-harmonic distortion factor and bias dependencies of *h*-parameters at low frequencies have been found out and the variations of second- and third-harmonic distortion factors with frequencies and biases have been clarified by the relations between these and current amplification of circuit.

References

(1) Gelli. A. Spescha und Max J. O. Strutt, "Theoretische und Experimentalle Untersuchung der Verzerrungen in Nieder Frequenz-Flächentransistor-Vierpolen," *A.E.Ü.*, Band 11, August 1957, Heft 8, SS. 307–320.

(2) N. I. Meyer, "Nonlinear Distortion in Transistor Amplifier at Low Signal Levels and Low Frequencies," *Proc. I.E.E.*, Pt. C, pp. 208–216. March 1957.

* * * *

621.385.38.032.212.001.6:621.318.57

GCR Discharge Tube (A new grid control cold cathode discharge tube)*

Kiyo-ichi TAKATSU,† *Hideo SHIMURA*,‡ *Tomizo ITO*,† *Toshiharu TODA*,† and *Takeshi HAYASHI*‡

A new type of cold-cathode discharge tube has been developed for use as a relay in telephone switching applications. Five electrodes are mounted in a miniature bulb which is filled to the pressure of 80 mmHg with a mixed gas consisting of Ne+5% A. The principle of operation is similar to that of the hot-cathode thyratron, with the electron cloud from the keep-alive electrodes taking the place of the hot-cathode. The breakdown criterion usually stated for the hot-cathode thyratron must be modified because of the high electron temperature of the electron cloud. Several characteristics of the tube are explained with the aid of breakdown equation. The life of the tube is limited by sputtering; therefore it may be possible to predict the life of the tube for given operating conditions.

Introduction

As a switching element in electronic circuit, discharge tubes have been widely used in recent years. As the equipments become complicated and their controlling procedures have been refined, the severe qualities of the discharge tubes have been required. Especially in telephone exchange, several requirements such as stability, long life, low level control, and cheapness are indispensable.

Hot cathode tubes, e.g. thyratron, are preferable for their stability and low level control, but they are beside the question owing to their heat discipation and short running life.

Cold cathode tubes possess substantially the long life in stand by condition and are free from troubles associated with the supply and discipation of heater power.

They have, however, the disadvantages associated with low speed operation, instability and high level control. These unfavourable characters depend principally on the breakdown mechanism of cold cathode discharge. Even in special trigger tubes which possess keep alive glow, these defects are inevitable. To avoid these troubles, it is necessary to supply ample electrons in discharge gap as in the case of hot cathode discharge tubes. But in usual cold cathode trigger tubes, the supply of ample electrons results in the reduction of forward breakdown voltage and the function of switching is lost.

In this laboratory, it has been attempted for several years to develop an electronic telephone exchange system by means of parametron logical network; in pursuit of this, the group concerned with the research and development of gas discharge devices was required to develop a discharge tube having the excellent characteristics described above, in addition to the requirement of being triggered by a low level signal of 1 Mc which is the output of "parametrons." Commercial trigger tubes are also inferior in this high frequency priming character. The GCR tube was developed to satisfy these requirements. This development is based on the principle of cold cathode thyratron in which the primary electrons due to an auxilliary glow discharge are controlled by a grid and it has been investigated inde-

* MS received by the Electrical Communication Laboratory, Feb. 16, 1959. Originally published in the *Electrical Communication Laboratory Technical Journal*, N.T.T., Vol. 8, No. 5, pp. 506–541, 1959.

† Shindo's Research Section.
‡ Communication Research Section.

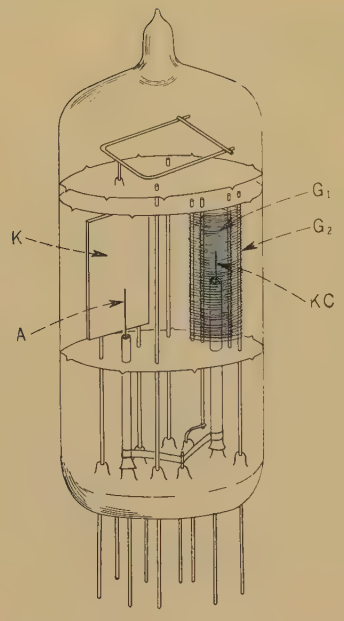

Fig. 1—Electrode configuration of GCR discharge tube and its sketch.

pendently in Bell Telephone Laboratory and Tohoku University (Japan).

1. General Construction

The configurations of electrodes and the sketch of tube are shown in Fig. 1. KC is a rod of 0.3 mm in diameter and G_1, G_2 are spiral grids as usually seen in thermionic vacuum tubes. KC is mounted at the center of the both grids, and feeble glow is kept between KC and G_1. G_2 acts as a control electrode, held at negative potential with respect to G_1. Electrode A is an anode, a rod of 0.6 mm in diameter, and K is a main cathode, a plate of $15 \times 8\ mm^2$. All these electrodes are made of Molybdenum metal and mounted in nine-pin miniature bulb. The tube is filled with Ne+5% A gas at the pressure of 80 mmHg. In discharge tube the leads of electrodes must be covered with glass pipes so as to avoid the spurious discharge, the allocation of electrodes is, therefore, restricted by the situation of stem-pins. The discharge characteristics, accordingly, must be controlled by means of gas pressure and the kind of gases as well

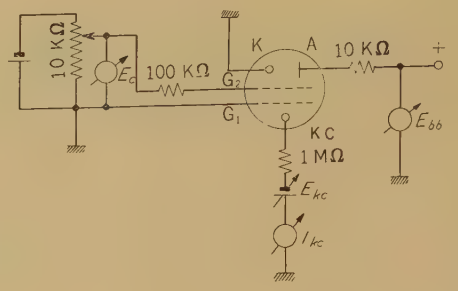

Fig. 2—Measuring circuit of d.c. characteristics.

as the mixing ratio of them.

2. Principle of Operation

The fundamental circuit for operation is given in Fig. 2. Owing to the keep-alive discharge between KC and G_1, the dilute plasma is formed at the space between G_1 and G_2. By the negative potential on G_2, motion of the electron of plasma which has the same space potential as that of G_1 is suppressed in the region limited by G_1 and G_2 by Boltzmann's relation. When the negative potential is gradually reduced, the number of electrons which have sufficient energy to escape into the space between G_2 and A, increase. They are accelerated by the electric field in the space between G_2 and A, and ionize gas molecules. The created positive ions return back to the G_2–G_1 space and reduce the effect of negative potential of G_2. The circulation of these processes and the accumulation of positive space charges take place as in the case of thyratron, and finally lead the tube to conduct. A grid potential to release the critical number of initial electrons which lead the tube to conduct is called critical grid voltage. Once a discharge takes place between anode and grid which is connected to high grid resistance, the discharge gap between anode and main cathode which is directly grounded, brought to conduct, lowering the anode potential to the sustaining potential of the tube so that the discharge between the anode and grid is extinguished. Namely the discharge, triggered in anode-grid space is transferred

Table 1

RATING (GCR-102)

Purpose .....For relay use

Construction .....Cold cathode penta-electrode discharge tube

Base .....*E* 9-1

Pin no.	1	2	3	4	5	6	7	8	9
Electrode	A	IC	IC	G_1	KC	G_2	IC	K	K

Bulb.....Length 70 mm max., diameter 21 mm max.

Rating.....	E_{SH}	E_{SL}	E_{CH}	E_{CL}	E_b	i_K	I_K	I_{KC}
	(V,d.c.)	(V,d.c.)	(V,d.c.)	(V,d.c.)	(V,d.c.)	(mA)	(mA,d.c.)	(μA,d.c.)
	240	150	7	3	107	200	50	50

For the notations, E_{SH}, E_{SL}, E_{CH}, E_{CL}, the text Fig. 3 should be referred.

to anode-catohde space. The time while the anode-grid space is primed is only a few micro-seconds and the current between them is restricted by the high impedance, so that the grid wires are free from destruction due to sputtering.

The priming characteristic curve of GCR 102 is shown in Fig. 3. The broken line indicates the characteristics when the main cathode is floating, so it is called tetrode characteristics. The full line shows the one which is obtained when the main cathode is grounded and it is called pentode characteristics. The operation range is limited by two flat portions, the upper is due to intrinsic breakdown voltage at any deep negative potential on grid, the lower is due to transfer voltage below which the tube fails to transfer the priming discharge to main gap. Table 1 represents the provisional rating of this tube (GCR-102). The rating of the cathode current on the table is only an example and it should be decided substantially from the life prospection chart described in Section 6 for each use.

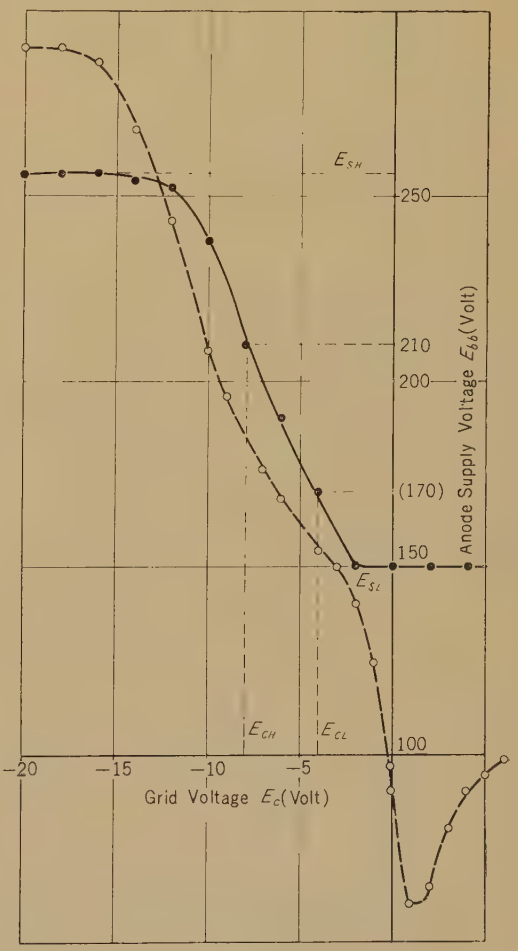

Fig. 3—Priming characteristic curves. Full line represents the pentode characteristics and broken line represents the tetrode characteristics.

3. Some Factors which Influence on Priming Characteristics

The prime mechanism of GCR tube may be considered similar to hot cathode thyratrons.

In the case of thyratrons, the critical grid voltage is usually expressed as follows;

$$E_{cs}=\frac{kT}{e}\log\frac{C_g kT}{I_s e\varepsilon}-\frac{kT}{e}\log N\tau-\frac{E_{bb}}{\mu}, \tag{1}$$

where

E_{cs}: critical grid voltage for prime,
k: Boltzmann's constant,
T: electron temperature,
e: electron charge,
C_g: equivalent capacity between grind and cathode,
I_s: total emission current of cathode,
ε: base of natural longarithums,
$N=(e^{\eta E_{bb}}-1)$: the multiplication factor in anode space,
τ: time to traverse the effective region where the influence of the positive charge to the grid potential considered,
E_{bb}: anode supply voltage,
μ: amplification constant, considered as a vacuum triode.

In Expression (1), the first term is constant and the second term is usually neglected, as the electron temperature of hot cathode is low. Therefore, in the case of thyratrons, the inclination of characteristic curve is determined only by the third term, namely $1/\mu$. However, in the GCR tube the electron cloud trapped in G_1-G_2 space acts as a virtual cathode and its electron temperature is more than ten times higher than that of hot cathode, so the second term of (1) can not be neglected.

As a result of above consideration, the critical voltage of the GCR tube may be expressed as follows, substituting N, τ in Equation (1) with discharge constants.

$$E_{cs}=\frac{kT}{e}\log\frac{C_g kT}{I_s e\varepsilon}-\frac{kT}{e}\log\frac{lp(e^{\eta E_{bb}}-1)}{\kappa E_{bb}}-\frac{E_{bb}}{\mu}, \tag{2}$$

where

l: effective length of linear dimension, where the positive ions effect to the potential of grid,
κ: mobility of positive ion.

The effect of the pressure and the kind of gases as well as mixing ratio of them, will be known from Equation (2), differentiating it with respect to p and η.

$$\frac{\partial E_{cs}}{\partial p}=-\frac{kT}{e}\frac{1}{p}\left\{1-\frac{E}{p}\frac{E_{bb}}{1-\varepsilon^{-\eta E_{bb}}}\frac{\partial\eta}{\partial(E/p)}\right\}>0, \tag{3}$$

$$\frac{\partial E_{cs}}{\partial\eta}=-\frac{kT}{e}\cdot\frac{E_{bb}}{1-\varepsilon^{-\eta E_{bb}}}<0. \tag{4}$$

Equation (3) is valid in the pressure range where E/p is less than 10 V/cm mmHg and this is the case of this tube.

From Equations (2), (3), and (4) the following tendency of the characteristics would be expected.

(i) The pitch or thickness of grid wire determines μ as usual in vacuum tube, and through it, influences on the inclination of the characteristic curve.

(ii) A decrease of pitch or an increase in the thickness of the grid wire steepens the inclination of the characteristic curve.

(iii) An increase of gas pressure steepens the characteristic curve.

(iv) A decrease of the value of η steepens the characteristic curve.

The features of the experimental results are shown in Figs. 4, 5, 6, and 7. Fig. 4, although it is not the case of specified gas, the tendency of the inclination due to gas pressure is the same as expected. Fig. 5 shows the influence of gas mixture, Figs. 6 and 7 show the effect of I_{KC} and the distance of G_1-KC respectively.

4. Dynamic Characters

As previously described, in GCR tube, the ample electrons are released at the instant of starting, so the statistical time lag are excluded. As for the time lag, only the formative time of discharge between grid and anode, and the time necessary to transfer it to a main gap are predominant.

Fig. 8 shows the time lag as a function of pulse height where the effects of the variation of keep-alive current I_{KC} are also indicated. Fig. 9 shows the priming sensitivity

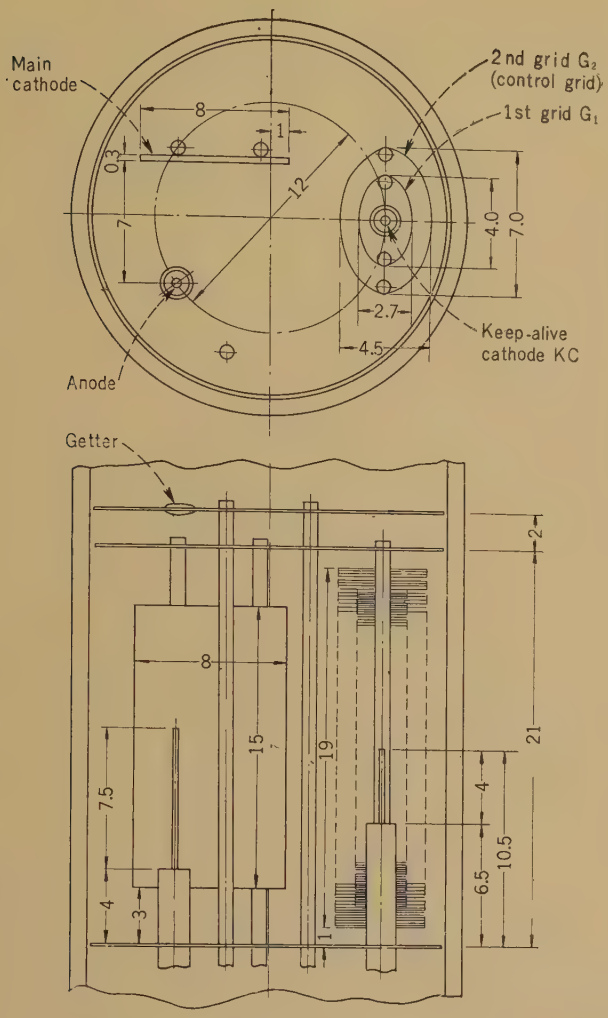

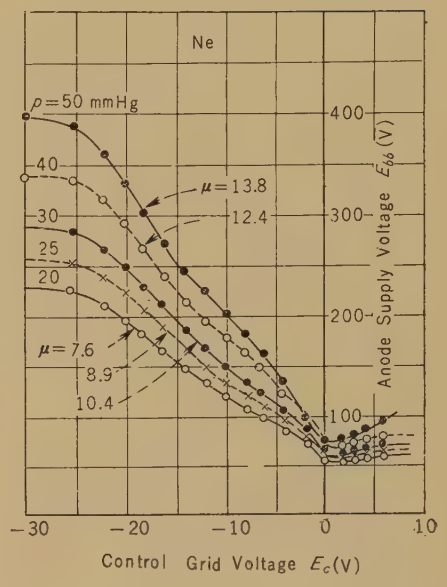

Fig. 4—The influence of filling gas pressure over the priming characteristics. This figure represents the case of pure neon filling. Similar tendency is seen in any kind of gas.

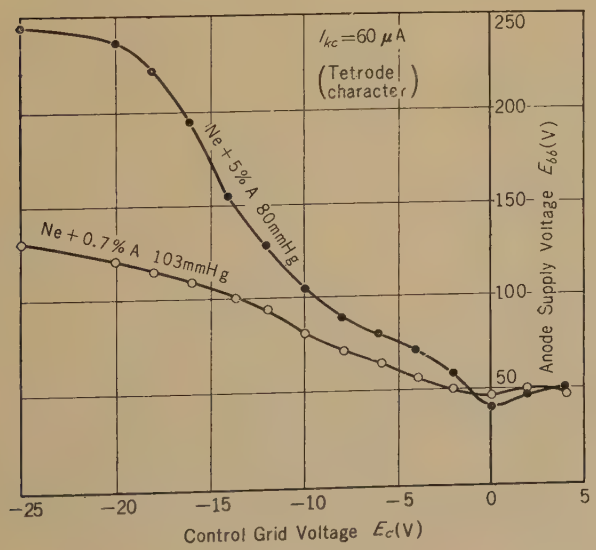

Fig. 5—The influence of percentage contents of argon to neon. This is attributed to the variation of η.

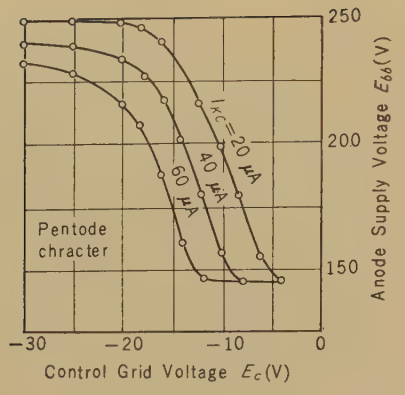

Fig. 6—The effect of keep-alive current I_{KC}.

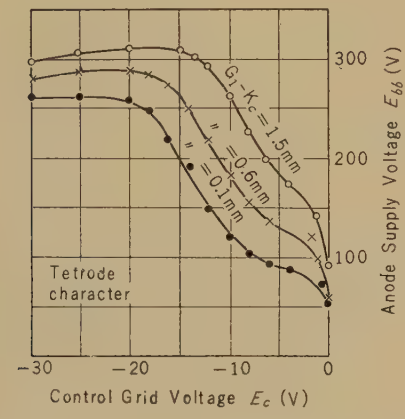

Fig. 7—The effect of the distance between KC and G_1, which is considered equivalent to that of I_{KC}.

which represents the necessary pulse width to prime with respect to grid over voltage Δe_g. The relation of them is expressed by $\tau=k\cdot(\Delta e_g)^{-3/2}$ as in the case of thyratron. The parameter in Fig. 9 is a grid bias voltage, E_{cc}. Fig. 10 shows the frequency characteristics of priming when a priming carrier frequency is keyed at the rate of 10 kc. The shape of the keying waveform is similar to the shape of output signal of parametron logical circuits. In any case the increase of I_{KC} makes priming more sensitive.

To extinguish the discharge, as the control grid acts no role any more, the anode supply voltage must be lowered

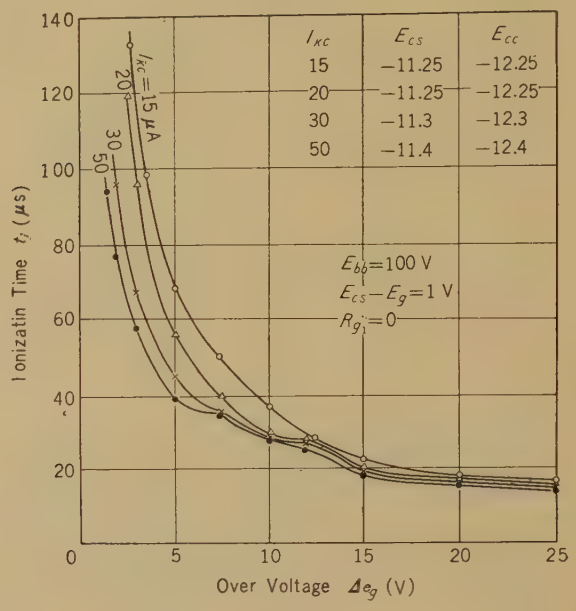

Fig. 8—The time lag of ionization as a function of grid over voltage. The influences of keep-alive current I_{KC} are also shown. The larger the keep-alive current, the shorter the time lag especially in low over voltage region.

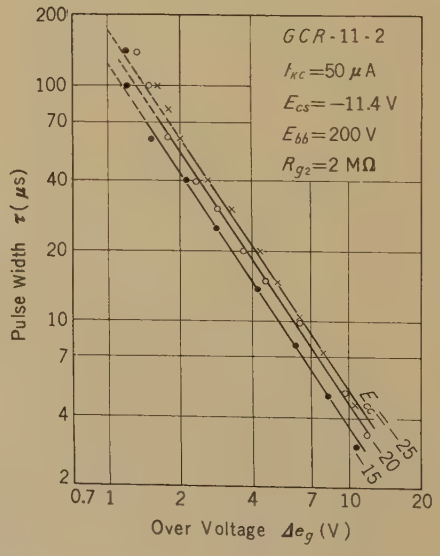

Fig. 9—Priming sensitivity, where the grid bias voltage taken as the parameters. The relation, $(\Delta e_g)^{3/2}\cdot\tau=$const is represented.

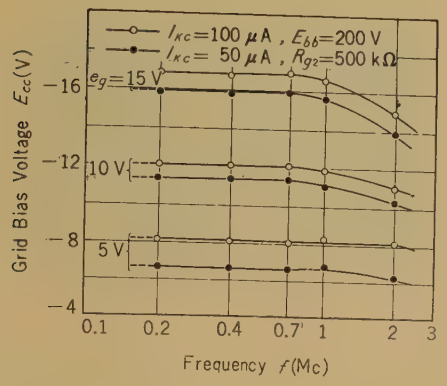

Fig. 10—The effect of the carrier frequency of priming pulse. The carrier frequency is modulated by 10 kc keying signal.

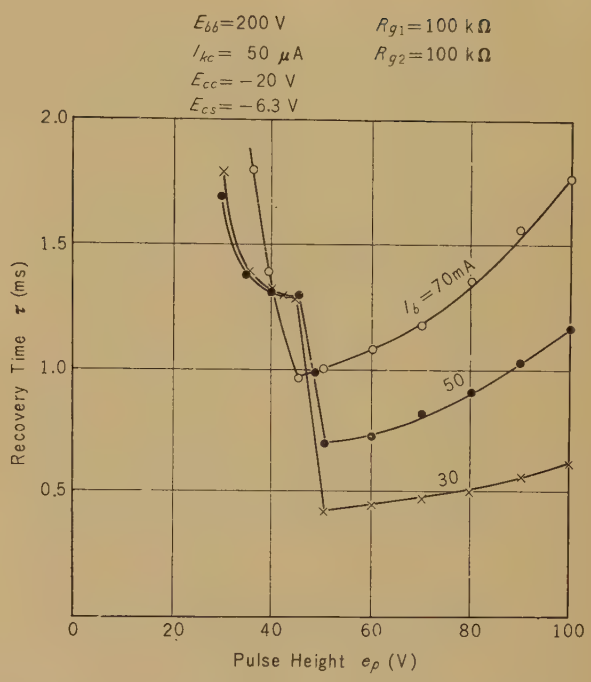

Fig. 11—The recovery time as a function of extinguishing negative pulse on anode. The sharp increase of recovery time near e_p=50 volts is due to residual glow which survive between auxilliary electrodes.

under sustaining voltage or large negative pulse must be applied to anode, as usual in any discharge tube circuits.

The recovery time of this tube is more than one millisecond, owing to the considerably higher pressure of filled gas, which is essential to realize the necessary prime characters. In Fig. 11, the recovery time is shown as a function of negative pulse height, applied on anode. The parameters are the main cathode currents. A sharp increase near e_p=50 V is due to a residual glow which survives between the anode and grid and keep-alive cathode. If the auxilliary electrodes are disconnected, so that the tube is operated as a diode, the recovery time curve represents a smooth V-shaped curve. As the keep-alive current increases, the sharp arising point of Fig. 11 shifts toward the right, namely the curve arises at larger negative pulse. The influences of anode supply voltage E_{bb}, grid bias E_{cc}, and grid resistance on recovery time are small.

5. Life

The life test was performed under the circuit in which the grid voltage was kept at a constant value and a half-rectified voltage was applied on the anode. The tubes under test were divided into four groups according to the load current, 150 mA, 80 mA, 40 mA, 20 mA at average value, each 10 tubes respectively. During operation the priming grid voltage, which is negative under a specified anode voltage at the normal conditions, shifts toward zero, namely the priming sensitivity becomes poor. The variation of grid voltage E_c is proportional to the time of operation as shown in Fig. 12, where ΔE_{CL} and ΔE_{CH} denote the variation of the critical priming voltage E_{cs} under the anode supply voltage of 170 V and 210 V d.c. respectively. Fig. 12 represents the case of working condition at the mean cathode current of 80 mA, but at higher cathode current the increase of E_c is more rapid, tends to saturate. Plotting variation of priming grid voltage E_{CL} and E_{CH} per 1,000 hours with respect to working current, although at 150 mA operation the value is extraporated from linear portion of ΔE-time chart similar to Fig. 12, the relation $\Delta E \propto I^{3.4}$ is obtained as shown in Fig. 13.

This relation is attributed to cathode

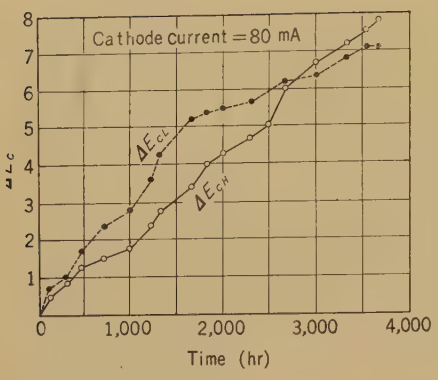

Fig. 12—The variation of priming grid voltage during life test. Cathode current is 80mA at mean value under the anode supply of half rectified voltage.

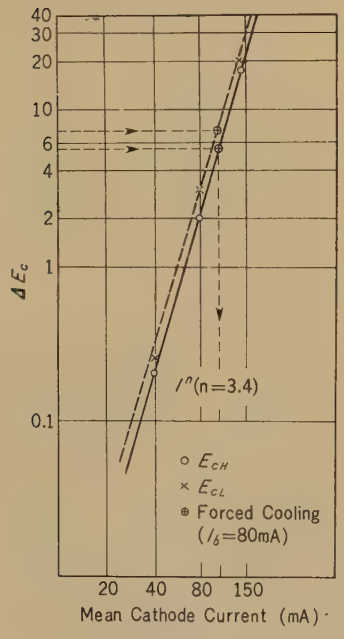

Fig. 13—The relation of the variation of priming critical voltage ΔE_c to the cathode current. ΔE_{CH}, ΔE_{CL} denote the value of ΔE_c, tested under the applied anode voltage of 210 V and 170 V d.c. respectively.

sputtering. The sputtered cathode material deposits on control grid (G_2) wire as well as on the tube wall, mica sheet etc., making

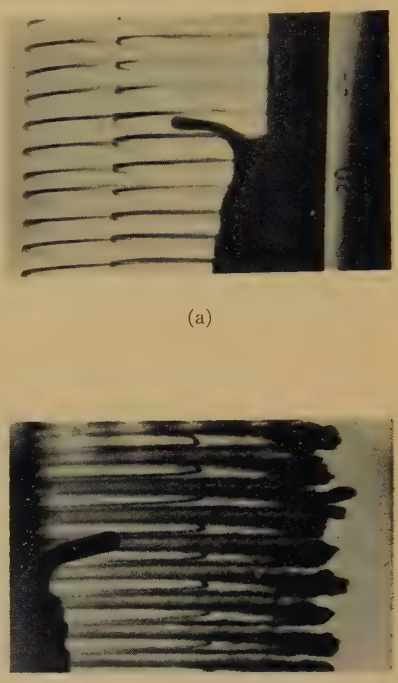

(a)

(b)

Fig. 14—The photographs of grid wire, before life test and after heavy life test. (a) is that of before life test and (b) is that of after 1,120 hours operation under mean cathode current of 150 mA. (The peak value of the current is about 690 mA.) These photographs are the examples of earlier test tubes which have the hook types keep-alive electrode.

the diameter of grid wire gradually thicker.

The extreme example is shown in Fig. 14. (a) is a photograph of the grid before the life test, and (b) is the one after 1,120 hours operations at 150 mA, at that current the rate of sputtering is about 6.5 times of the rate at 80 mA and about 52 times of the rate at 40 mA. It will be seen that the sputtered material from the cathode deposits heavily on the control grid while the inner grid G_1 is free from deposition. The shift of the grid priming voltage E_{cs} is considered proportional to the thickness of the grid wire as shown in Fig. 15. Linearity exists for grid wire diameters of 0.04 to 0.12 mm with a constant pitch of 0.28 mm. On the other hand, the sputtering rate of the

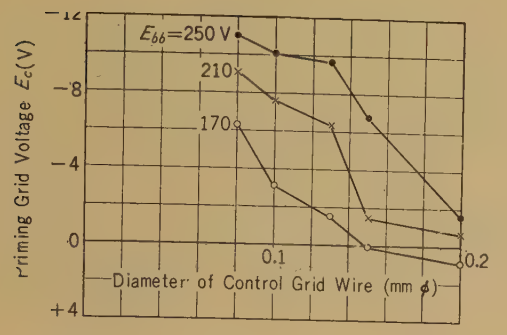

Fig. 15—The variation of priming grid voltage E_{CL} relative to the variation of grid diameter, leaving the grid pitch unchanged. The variation rate is considered about −94 V/mm.

cathode metal is proportional to I^3, of which the precise investigation will be published later, so the combined relation would be cause the result above described.

The extension of this consideration leads to the procedure of forced life test or the possibility of the prospect of the life. Fig. 16 is a life prospect chart obtained from sputter yield data under the specified condition of this discharge tube, concerning the pressure of gas filling, kinds of gases, and cathode material, and from the variation of priming grid voltage relative to the diameter of grid wire shown in Fig. 15.

If the variation of 2 V of ΔE is assumed to be the life end point, the life under continuous operation at cathode current of 60 mA would be 1.8×10^4 hours. At the stand-by condition the tube will be operated in a low duration rate, the apparent life on set will be more longer and may be calculated from the life prospect chart and mean duration factors.

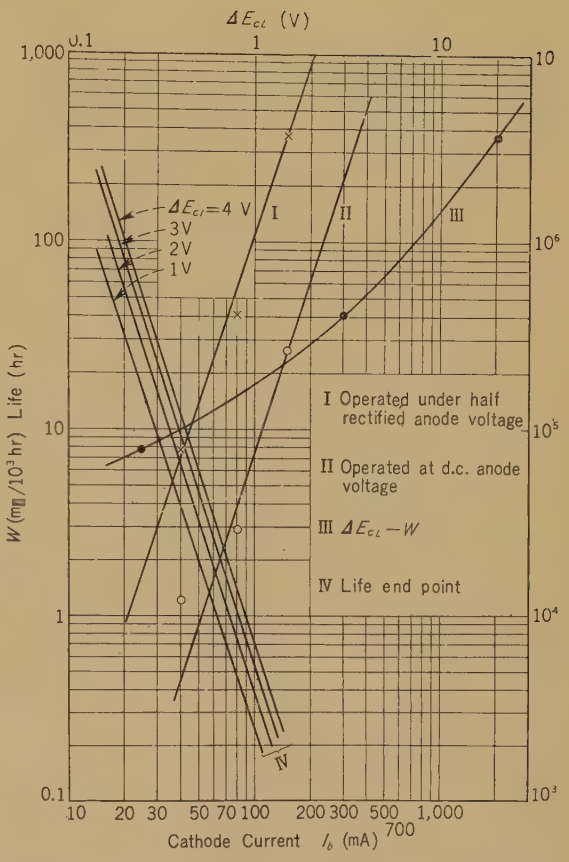

Fig. 16—Life prospect chart. Curves I and II show the sputtered weight of cathode when the tube are operated at remarked current under d.c. anode supply and half rectified alternating voltage on anode respectively. Sputtered weight is measured by the reduction of the weight of cathode. Curve III denotes the relation of the variation of specified grid voltage, E_{CL}, and the sputtered weight of cathode material, which is obtained from the results of Fig. 15 and the experimental results of corresponding reduction of the weight of cathode due to sputtering, for increase of grid diameter due to the deposition of sputtered material. Curve IV is the life prospect curve constructed from Curve II and Curve III.

Acknowledgment

The authors are grateful to Professor Yoshinori Hatta in Tohoku Univ. for his helpful suggestions and to Dr. S. Kobayashi in Nippon Electric Company for the production of this tube in semi-mass-production scale. We also wish to acknowledge to Z. Kiyasu, Associate Director of the Laboratory, for his interest and encouragement. We are also indebt to the member of electron-tube factory in this Laboratory, specially to Mr. Yagasaki, for their unfailing assistance to construct the test tubes, and to the group relating to gas discharge devices for their helpful discussions and assistance.

621.395.61/.62.001.2:621.391.883

Design Requirements of a New Telephone Set from the Standpoint of Transmission Quality*

Zenji YAMAGUCHI†

In a design of a new telephone set, a consideration is given about a problem, what characteristics should be given to the most desirable telephone set from the point of view of transmission quality.

At first, disturbing effects of the distored frequency response and noise in a transmission system are analyzed. Then assuming the objective of the transmission quality which the worst transmission system using the new telephone set should meet, the indispensable considerations are given to each of the transmitter, receiver and the telephone circuit, and the desired responses are finally decided to warrant the required transmission quality.

Further, a deterioration in transmission quality due to a shortening of subscriber line is analysed, and the countermeasures to be taken in the telephone circuit are concretely suggested.

Introduction

When a new telephone set is developed, it is expected (1) to improve service to the subscribers, (2) to expand the service area of subscribers by extension of the subscriber line length, and (3) to minimize the plant cost by adopting smaller gauge of cables due to the new telephone set. But eventually the new telephone set should bring economical advantages to the administration and satisfactory service to the customers. Therefore the basic idea of any new design of telephone set is to create a high quality instrument without increasing the manufacturing cost. Furthermore, a combined use of a new telephone set with the existing one at the transitional stage of practical application, and the fact that a new telephone set should be applicable to the existing telephone network should be given due consideration, consequently, any improvement in quality of new telephone set both on the sending and receiving sides should be balance to the existing set. In this paper, the relationship between the characteristics of the telephone set and its transmission quality are studied, and resultant fundamental data of the design are also presented.

1. General View

1.1. Measure of Transmission Quality

Many studies have been made to quantitatively evaluate transmission quality and several measures have practically been employed; however they all seem to have both advantages and disadvantages and no perfect measure of the assessment exists at the present.

Before a new telephone set is designed, it is necessary to decide what measure should be employed. This measure must satisfy the two requirements; one to be compatible with the existing general conception of transmission quality and the second to be calculable from physical characteristics of the transmission system.

From these considerations the responses of a new telephone are designed to take account of the articulation score mainly, naturalness and loudness subordinately.

* MS received by the ELectrical Communication Laboratory, Oct. 27, 1959. Originally published in the *Electrical Communication Laboratory Technical Journal*, N.T.T., Vol. 9, No. 1, pp. 28–63, 1960.

† Station Apparatus Research Section.

1.2. Objective of the Transmission Quality of a New Telephone Set

Assuming the lower limit of transmission quality to be 80 persent sound articulation, the permissible maximum line loss in the cable connecting the new telephone sets should be 10 dB higher than that obtainable with the No. 4 Telephone Set in present use.

As mentioned later, the articulation score bears no simple relationship with changes in line loss, and often there is much degradation of articulation in short loop rather than in long loop. Therefore, a new telephone set must be so designed as to warrant the prescribed lowest limit of transmission quality under any conditions of cable connection within the permissible maximum loss.

As regards the frequency characteristics of the transmitter and receiver, it is required that the transmission frequency band covers the pass band of a carrier circuit 300–3,400 c/s and that the sensitivity as well as the deviations in frequency response are specified considering attenuation distortion and circuit noise; furthermore a new telephone is to be superior to the No. 4 Telephone Set in its articulation, naturalness, and loudness.

1.3. Transmission Disturbing Elements

Inasmuch as the transmission quality of a new telephone set is analysed with reference to the disturbing elements, it is first necessary to define how to treat these disturbing elements. To define the main factors that affect transmission quality, the following typical conditions will be assumed:

a) Talking level of subscribers: the speech volume measured at a meter distance from the talker's lips corresponds to the free field sound pressure level of 62 dB (re 2×10^{-4} μb).
b) Hearing: normal hearing loss
c) Line:
   Subscriber line—0.32 ϕ, 0.4 ϕ, 0.5 ϕ, 0.65 ϕ mm no loaded cable
   Trunkcable—0.5 ϕ, 0.65 ϕ mm no loaded and loaded cable
   Carrier circuit—SRAEN band pass filter[1]
d) Line noise at end offices:
   Switching equipment noise——8 dB/oct. spectrum, 0.5 mV
   Circuit noise—flat spectrum 1 mV
e) Room noise—Hoth spectrum, sound level 60 dB (A)

2. Fundamental Analysis

2.1. Outline of Calculation Method of Articulation Index

The articulation score is objectively calculated by means of the articulation index which has primary relationship with the articulation score computed from the physical characteristics of the transmission system and the characters of speech and hearing.

The relationship of the articulation index A and the sound articulation s of Japanese language can be expressed as follows:

$$\left.\begin{aligned} &A=-(0.43/p)\log_{10}(1-s) \\ \text{or}\quad &s=1-10^{-pA/0.43} \end{aligned}\right\} \qquad (1)$$

where

p = proficiency factor of the articulation testing crew.

The calculation formula of the articulation index is:

$$A=\int_0^\infty W\cdot D\,df \qquad (2)$$

$$W=\phi(E,\beta_N). \qquad (3)$$

Where D is the contribution factor of articulation index per unit frequency band under the condition of the ideal transmission system and is given by the Fig 1. W is the weighting function when the speech component is disturbed by attenuation distortion and noise, and $1\geq W\geq 0$. Further, W is a function of both the effective sensation level E and the total level β_N of the noise that reaches the ear of the listener. The relationship of these factors can be given by the Fig. 2. The effective sensation level E can be given by the difference in dB between the peak level of the speech and

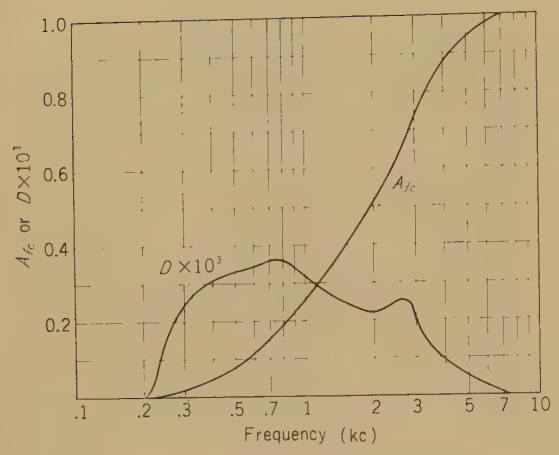

Fig. 1—The articulation index D and its cumulative curve A_{fc} for the Japanese language.

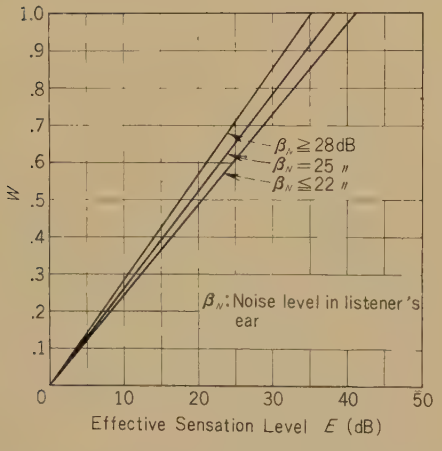

Fig. 2—The relation between the effective sensation level E and weighting function W.

the r.m.s. of the noise reaching the ear of listener.

2.2. The Relationship between the Improvement of the Response of Various Parts of Telephone Set and Articulation Index

As the overall noise level β_N in the actual telephone transmission line is over 28 dB (re 0.0002 μb), the weighting function W and the effective sensation level E have a linear relationship as can be seen in Fig. 2. Therefore only the effective sensation level E and factor D shall be considered to estimate the articulation score. The effective sensation level of the speech component in an ordinary telephone communication can be expressed as follows:

$$E=[B_0+P+R_T-b_T-b_i-b_L-b_R+R_R]-[B_{NS}(+)B_{NG}(+)B_{NL}(+)X], \quad (4)$$

$$\left.\begin{aligned} B_{NS}&=B_{NR}+R_T'-b_{i2}-b_S+R_R \\ B_{NG}&=B_{NR}+R_G \\ B_{NL}&=V_L-b_L'-b_R+R_R \end{aligned}\right\}, \quad (5)$$

where

B_0: long average speech spectrum at one meter from lips in a free field
P: peak factor of speech
B_{NS}: spectrum of side tone noise
B_{NG}: spectrum of leak-in noise
B_{NL}: spectrum of line noise
B_{NR}: spectrum of room noise
V_L: voltage spectrum of the line noise in the receiving end offiice
X: (threshold intensity level of a single frequency)−(critical band expressed in dB)
R_T: response of the transmitter for speech signal
R_T': response of the transmitter for noise signal (Response is not constant with sound level).
R_R: response of the receiver
R_G: response of a leak-in noise
b_T: sending loss of the telephone circuit
b_R: receiving loss of the telephone circuit
b_S: side tone loss of the telephone circuit
b_L: line Loss
b_L': receiving subscriber line loss.
b_{i1}: current supply loss of the transmitting side
b_{i2}: current supply loss of the receiving side
(+): power summation.

Now, the response of the transmitter is

assumed to be raised by α dB, the response of the receiver by β dB, and the side tone loss by γ dB. An increase ΔE in the effective sensation level obtained under these conditions will be examined.

i) In the frequency band where the side tone noise B_{NS} is predominant over other noise, the increase effective sensation level is indicated as follows:

$$\Delta E=\gamma.$$

Therefore, only the amelioration of the side tone loss is effective, whereas the amelioration of the transmitter and or that of the receiver plays no role in the improvement of intelligibility.

ii) In the frequency band where the leak-in noise B_{NG} is predominant over other noise,

$$\Delta E=\alpha+\beta.$$

In this case an amelioration of the transmitter and receiver is effective.

iii) In the frequency band where the line noise B_{NL} is predominant over other noise,

$$\Delta E=\alpha.$$

In this case only the improvement of the response of the transmitter is effective

Inasmuch as the effectiveness of the improvements in various circuits and components of a telephone set is influenced by various kinds of noise, noise characteristics should also be considered simultaneously with the design factors so far taken into account, when the design criteria of the new instrument is specified. Without such consideration it would be impossible to determine transmission quality.

2.3. The Relationship between Changes in the Length of the Subscribers Line and Intelligibility

The response of the telephone transmitter and receiver is basically determined to provide the prescribed transmission quality over the longest expected length of transmission line. Investigation is now conducted to determine the changes in intelligibility when a telephone is used in conjunction with a shortened subscriber line.

i) Effect when the line length is shortened on the sending side:

This situation corresponds to communication from a subscriber near an end office to the most distant from the farthest end office. Indicating the difference from the basic condition with the mark Δ, the difference can be deduced from the relationship (4) and (5):

$$\Delta E=\Delta b_{i_1}+\Delta b_L \qquad (6)$$

thus the shorter the subscriber's line, the greater the intelligibility.

ii) Effect when the line length is shortened on the receiving side:

This corresponds to communication between a talking subscriber most distant from an farthest end office and a listening subscriber near the end office. The changes in the effective sensation level E are:

decrease in the frequency region where B_{NS} is predominant,

increase in the frequency region where B_{NG} is predominant, and

none in the frequency region where B_{NL} is predominant.

In summary, intelligibility undergoes complex changes according to the kinds of the predominant noise.

The interrelationship between the peak level of speech and different kinds of noises in the ordinary telephone communication is illustrated by an example in the Fig. 3. When the subscriber's line is long, the three types of noises remain on approximately the same level, when it is short, however B_{NS} becomes predominant over other noises through the whole effective frequency region. Therefore when the receiving subscriber's line is shortened, the intelligibility progressively decreases.

iii) Effect when the sender's and receiver's line is simultaneously shortened

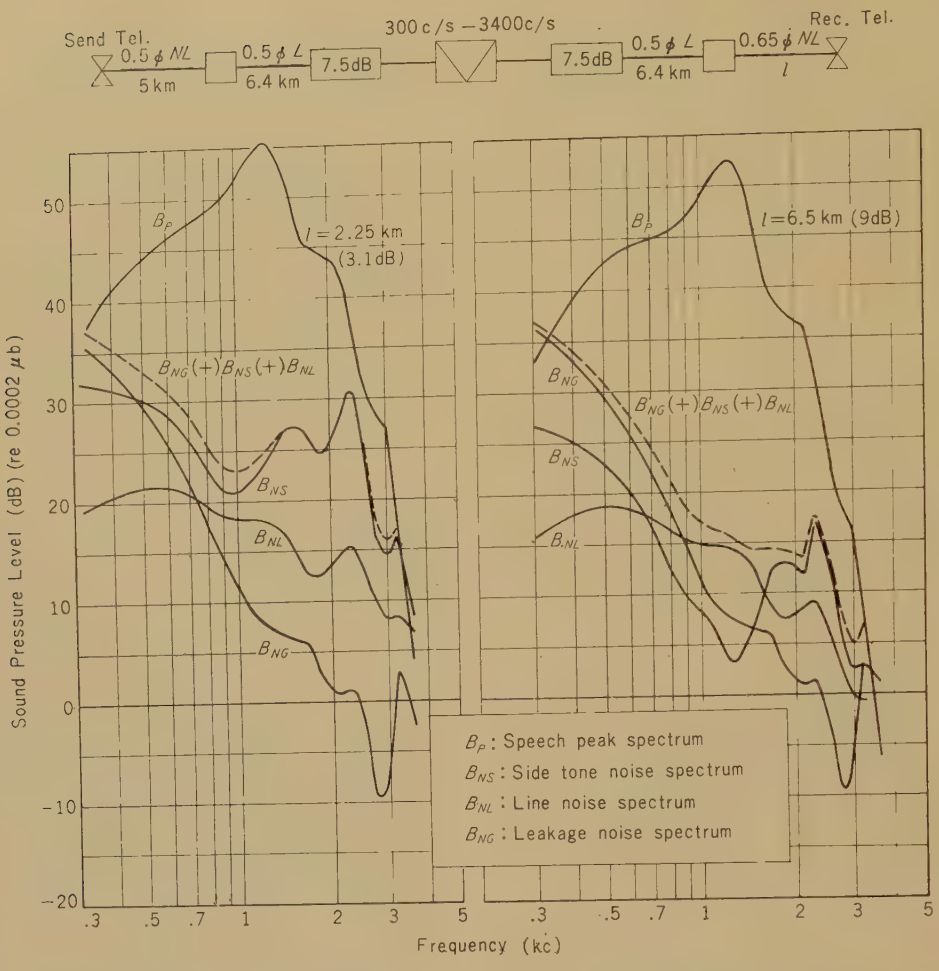

Fig. 3—The speech and noise spectrum in the listener's ear.

This case is a complex of the conditions i) and ii), and assuming the noise B_{NS} to be predominant, the result is:

$$\Delta E=(\Delta b_{L1}+\Delta b_{L2}-\Delta b_S)+(\Delta b_{i1}+\Delta b_{i2}) \qquad (7)$$

and the loss or gain in intelligibility can be determined by the connecting conditions. For example, if the type of line and the changes in distance of both the sender's and receiver's lines be the same, the effective sensation level is increased and the resultant intelligibility is greater.

2.4. The Relationship between the Frequency Characteristic and Transmission Quality

The overall frequency characteristics of telephone transmission system (inclusive of the telephone set) are generally complicated. For analysis typical ideal characteristics of a transmission system were employed and study was conducted to determine the relationship between the types of OTR (orthotelephonic response[2]) and transmission quality.

i) Flat, differential, and integrative frequency characteristics

At first, an articulation test was conducted with respect to three different types of OTR, which were of flat, differential (+6 dB/oct.) and (−6 dB/oct.) characteristics and with reference level at 1,000 c/s, under

several noise conditions. As a result, it is observed that when the high frequency portion, which has larger contribution to articulation index, is emphasized, it is more favorable to the articulation, and the transmission quality measured in articulation decreases in the order of differential-flat-integrative character.

Then, selecting the system gain to provide the same articulation (s=94%), the above-mentioned three types were compared with regards to their naturalness. The naturalness test was carried out by pair-comparison method with the criterion of "Which resembles more the original voice." The data obtained were converted into the psychological naturalness scale according to the Thurston's method of classification. Thus it was observed that the naturalness decreases in the order of flat-integrative-differential characteristics.

ii) Allowable limit of deviations in frequency characteristics

It is favorable to articulation score that the frequency region having a large contribution to articulation index is emphasized, but this impairs naturalness. For this reason, some tests were carried out determine the allowable limit of the frequency character deviation which does not involve too large degradation in naturalness. As the result, it was proposed that from the standpoint of naturalness, the allowable deviation in frequency characteristic of transmission system should be 10 dB at maximum.

2.5. Appraisal Test for Received Volume

The comfortableness of the received volume is one of the contributing factors for evaluating transmission quality. In a psychological test here described, the observers are required to give their opinions of the received volumes by assigning it to one of several specified categories such as follows:

1) Intolerably loud
2) Loud, but tolerable
3) Comfortable
4) Small, but tolerable
5) Too small

In this experiment the Japanese Master Reference System for Telephone Transmission was employed, and the frequency band was limited by means of the low pass filter; 1,500, 3,050, and 9,000 c/s. The line noise (Hoth spectrum; 2, 1, and 0 mV) was introduced at the input of the receiving system of the Reference System. Thus, combining noise and frequency band conditions, the selection probability of each category was investigated for various system gains. Assuming the system gains corresponding to 50 percent value of the appraisal probability as the boundary gain of a categories, the ranges of system gains corresponding each category are given in Fig. 4.

As evident from this graph, the volume criteria are not appreciably affected by the band limitation. However, with an increase of the noise, though the upper limit of the comfortable range remain unchanged, the lower limit rises, eventually making the comfortable range narrower. In this experiment, the long average listening speech level is 62 dB (re 0.0002 μb) for the system gain of 0 dB.

The mark * in Fig. 4 indicates the system gain corresponding to the sound articulation 80 percent. It is evident that the relationship between volume criteria and articulation score is appreciably affected by the pass band region of the transmission system.

3. The Indispensable Considerations in a Design of a New Telephone Set

On the basis of the fundamental analytical data described in the foregoing section, the indispensable considerations shall be given to each of transmitter, receiver and telephone circuit, and to the desirable response to warrant the required transmission quality.

i) Response of the transmitter

A new telephone transmitter is should meet the following conditions.

a) An increase in response makes it possible to extend the transmission line by 5 dB in loss as compared with the existing No. 4 Telephone Transmitter.
b) The response is considered on the basis of sensation level of speech signal at the receiving end office, and sufficient

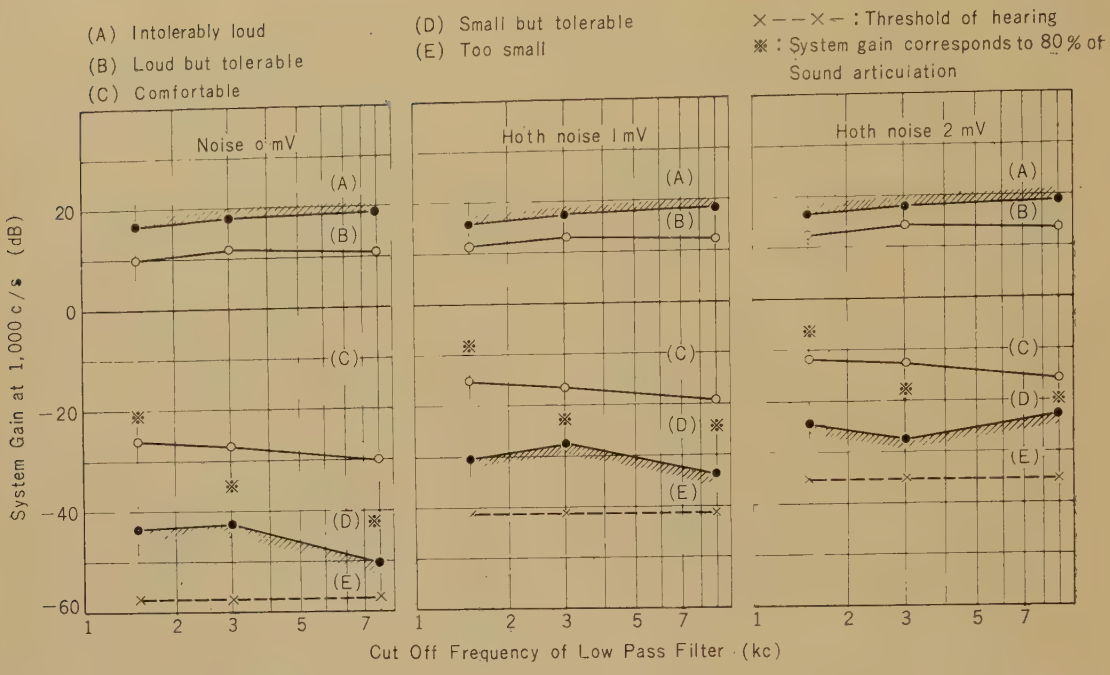

Fig. 4—An appraisal of received speech volume.

to secure an articulation score of 80 percent even for the most distant subscriber.

c) The transmission frequency band should secure at least 300–3,400 c/s.

d) The frequency characteristics is able to compensate the attenuation characteristics of longest subscriber line, but the deviation of the frequency character should not exceed 10 dB.

In Fig. 5 are given the responses of a new telephone transmitter which are supposed to meet the above requirements.

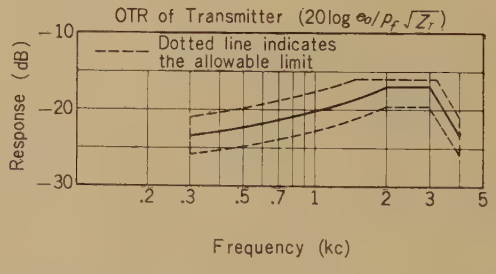

Fig. 5—The desired response for a New Type Transmitter.

ii) Response of the receiver

A new telephone set is required to the following conditions:

a) An increase in response makes it possible to extend the transmission line by 5 dB in loss as compared with the case using the existing No. 4 Telephone Receiver.

b) To improve the leak-out of the speech signal and the leak-in of room noise, the shape of the ear-piece and the acoustic impedance of the receiver is reasonably selected.

c) The OTR of the receiver is flat, lest the resultant OTR of transmitter and receiver should degrade naturalness of speech (cf. (1) d)).

From these consideration, the desirable response of a new telephone receiver is illustrated in Fig. 6.

iii) Telephone circuit

The characteristics of the telephone circuit

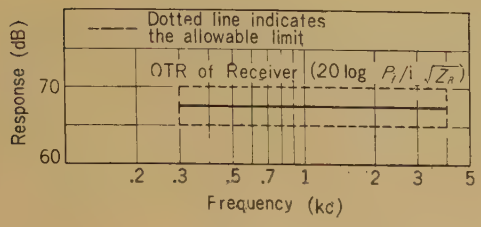

Fig. 6—The desired response for a New Type Receiver.

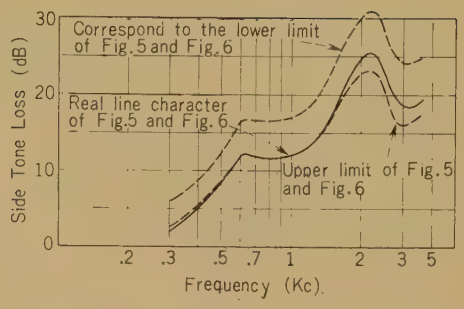

Fig. 7—The desired responses for the side tone loss of a New Type Telephone.

should satisfy the following conditions:

a) The sending and receiving loss of the telephone circuit is minimized as much as possible, particularly in the frequency band from 2,000–3,000 c/s.

b) The side-tone loss is designed for various kinds of line constructions. In the event that a new telephone set is installed near a telephone office and the side-tone loss is insufficient, an adequate measure is taken.

c) The frequency characteristic of the side-tone loss is determined in junction with those of the transmitter and the receiver. From these considerations, in Fig. 7 is given the desirable frequency characteristic of the side-tone loss, which responds to the frequency characteristics of the transmitter and receiver as indicated in Figs. 5 and 6.

4. The Transmission Quality of a New Telephone Set Manufactured on Trial and Treatment for a Short Line Communication

New telephone set have been produced on trial being designed to meet the requirements above described, and also mass production. The response of each component of instrument seems to nearly satisfy the prescribed conditions, and the transmission quality when connected to various lines makes it possible to extend lines by 10 dB in loss as compared with the case using the existing No. 4 Telephone Set. However, when the receiving subscriber's line is shortened, occasionally the lowest limit of the transmission quality can not be satisfied. In this case, the side-tone noise should be considered as the only disturbing noise and the calculation formula can be deduced from the relations (4) and (5) as follows:

$$E=\{(B_0+P-B_{NR})+(R_T'-R_T')\}$$

$$-\{(b_{i1}-b_{i2})+(b_C-b_S)\} \qquad (8)$$

where

$$b_C=b_T+b_L+b_R.$$

The value in the first bracket on the right side being fixed, only the value in the second bracket is to be reduced.

As the second bracket is further analyzed, the equation runs as follows:

$$b_{i1}-b_{i2}+b_C-b_S=(b_{i1}-b_{i2})$$

$$+(b_{T1}-b_{T2})+(b_L-b_{RL}) \qquad (9)$$

where

b_{T1}: sending circuit loss of the telephone set on the sending side

b_{T2}: sending circuit loss of the telephone set on the receiving side

b_{RL}: return loss at the telephone terminals.

As the receiving side is located at a short distance, to reduce the value of Equation (9), the b_{i1}, b_{i2}, b_{RL} of the receiving telephone set should be increaesd.

As one of the practical treatment of the short line communication, the following measures will be suggested:

i) Give an adequate loss to the sending circuit of telephone, and increase thereby the current supply and transmission loss.

ii) Choose the design of the anti-side-tone circuit and try to increase the return loss. In other words, make a better choice of the line impedance, which is the object of the balance.

iii) Make a combined use of above methods, but when this does not satisfy the lower limit of transmission quality there will be no means but to shorten the trunk cable loss under consideration.

Conclusion

The author has tried to lay down the design requirements of a new telephone set considering from the standpoint of transmission quality, and at the same time discussed the treatment of a short line communication with the new telephone set.

Inasmuch as the response of various parts of the telephone set contribute co-jointly to the transmission quality, it is impossible to determine the efficient responses independently. Furthermore, the improvement of the sensitivity of the transmitter and receiver is restricted by the difficulty of realizing high side-tone loss economically. Therefore, the maximum efficiency can only be achieved by a reasonable design, in which all different parts of the telephone set are coordinated in a good balance. On the other hand, an improvement of telephone quality, and a reduction of production cost are not compatible with one another. The solution to this problem would be to compromise them.

It would be undertaken next to make an overall appraisal by taking into consideration the statistical distribution of line loss and the disturbing factors of communication, and to establish a plant standard which will help to develop most effectively the quality of the new telephone set.

References

(1) C.C.I.F. XVIIIth Plenary Assembly, Genoa, 4–12, Oct. 1954, Vol. IV.
(2) L. L. Beranek, *Proc. I.R.E.*, 35, Sept., p. 880, 1947.
(3) S. S. Stevens and J. Volkmann, *Am. J. Psyehol.*, 53, p. 329, 1940.

* * * *

678.742.012:536.41.08+541.64

On Dilatometric Measurements and Crystallization Phenomena in Various Polyethylenes*

Ryuichi NAKANE†

Dilatometric experiments on several samples of polyethylene, including both high pressure polyethylene and low pressure polyethylene, and a calorimetric experiment on a single sample of high pressure polyethylene were performed. From the results of these experiments, especially from that of the volume change with time, it is suggested that the concept of crystallite size distribution is most adequate and natural for the interpretation of our data. Some calculations concerning the relations between the grain size and the melting point are shown. With our concept a new interpretation of the glassy transition and the quenched state is introduced.

Introduction

The dilatometric experiment on polyethylene was reported by Hunter and Oakes,[1] and the specific heat measurement of this polymer by Richards and his school[2] more than ten years ago. Since then only the specific heat measurement of Dole[3] has appeared in well-known journals. It is certain that these measurements have been repeated by many investigators, but it is also supposed that the authority of Richards or of Dole has psychologically blocked the publication of these results. But today the measurements of Richards and of Hunter and Oakes do not seem to be sufficiently precise, and the development on the crystallization kinetics of high polymers has contributed greatly to the research of these thermodynamical phenomena. Besides these, in addition to the usual high pressure polyethylene, a new type of this polymer, the low pressure polyethylene, commercially appeared in recent years, and with this improvement we have wider variety of polyethylene samples. So the present is most opportune for measuring the thermodynamical properties of this polymer, from a new point of view, again.

* MS received by the Electrical Commnnication Laboratory, Nov. 25, 1959.

† High Polymers Research Section.

1. Experiment

1.1. Dilatometric Experiments

Our dilatometric measurements were carried out by using the popular Bekkedahl type mercury-filled dilatometer.[15] This dilatometer was immersed to the neck of its cell position into a silicone oil bath whose temperature could be, if necessary, regulated to the accuracy of 0.02° C with a system consisting of a thermocouple, a potentiometer, a galvanometer and a photoelectric relay.

The samples on which our experiments were carried out were: DYNH, DYGT, and Alathon 10 as typical samples of high pressure polyethylenes; Super Dylan 6200 and 6400 as typical samples of low pressure polyethylenes; and Marlex 50 as a typical sample of medium pressure polyethylenes.

It is usually said that for the dilatometric measurement is necessary a very long time to attain the equilibrium value of volume; but for the sake of measuring speed our experiment was carried out at first by raising the temperature with a constant rate (about 0.3° C per minute), and the volume change with time at one temperature was tested in another run.

Some of the temperature vs. specific volume curves for these samples are shown in Figs. 1, 2, 3, and 4. From these curves the melting points of various samples were

Table 1

MELTING POINTS OF VARIOUS POLYETHYLENE SAMPLES

Sample	T_m (Virginal)	T_m (Annealed)	T_m (Equilibrium Value)	n
DYNH	112.2	113.4	114.7	——
DYGT	——	105.8	105.4	——
Lupolene I	112.0	113.0	114.3	5.40
Alathon 10	112.0	113.0	——	5.26
Super Dylan 6200	128.0	133.0	129.0	6.73
Super Dylan 6400	128.5	133.5	——	——
Marlex 50	133.0	137.0	133.2	7.90

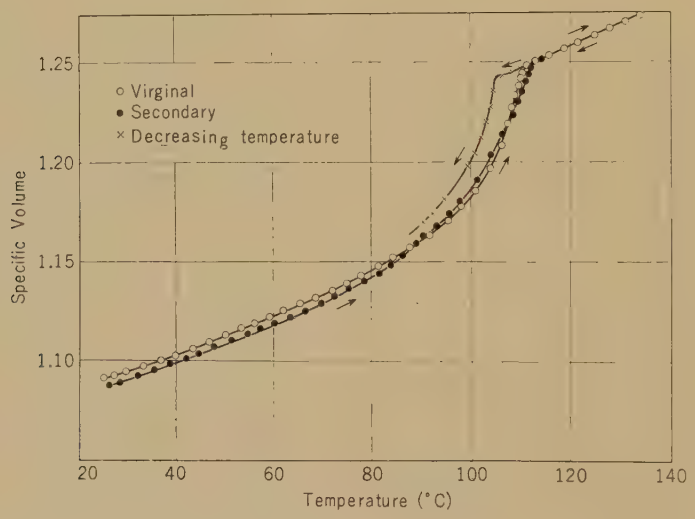

Fig. 1—T vs. V_{sp} curves of Alathon 10.

determined as shown in Table 1. Here the figures labeled as "virginal" are the values determined by the first measurements on pellet-shaped commercial samples, those labeled as "secondary" are of those from the secondary measurements which were carried out after the first experiments and consequently are the values for the samples left cooled or moderately annealed. And those labeled rated as "equilibrium value" are the evaluations from the volume changes with time at several temperatures.

1.2. Volume Change with Time

The specific volume of high pressure polyethylene, when kept at a constant temperature in the melting range of this sample, changed with time in an interesting manner.[17] For example, the result on DYNH at 87.7° C is shown in Fig. 5. During the first 8 hours the volume decreased constantly as if it was converging into a saturation value. Then the whole apparatus was left cooled down to the room

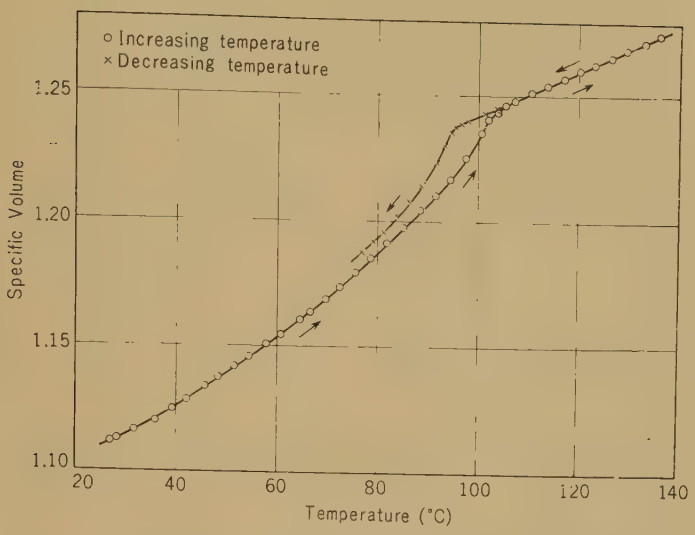

Fig. 2—T vs. V_{sp} curves of DYGT.

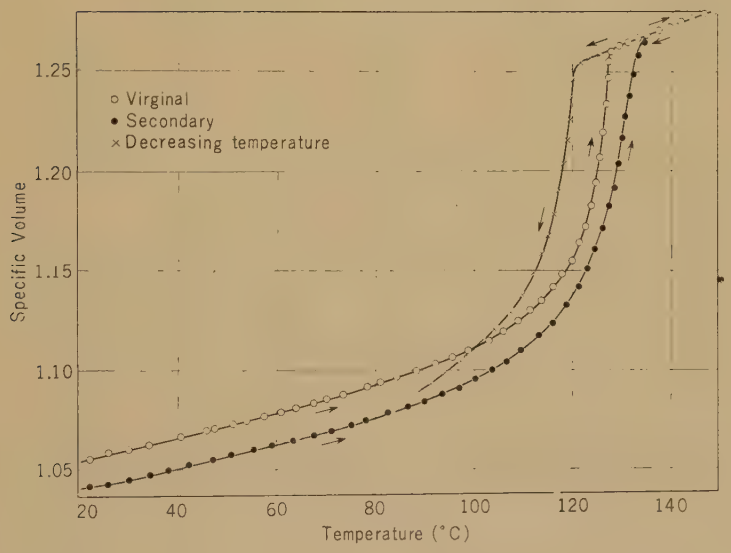

Fig. 3—T vs. V_{sp} curves for Super Dylan 6400.

temperature for the next 16 hours. On the next day, after raising the temperature to just the same temperature as before, a volume change was again observed. In this run a volume change still existed, but it started from about the same value as the end point of the first day's curve and its decreasing rate was much slower than before. Briefly speaking, this curve looks like the direct continuity of the first day's curve. When the third day's experiment was performed, the volume change became almost unobservable and soon became absorbed into the experimental error.

In high pressure polyethylene this tendency continued to exist up to the temperature just below the melting point. For example, when DYNH was kept at 112.1° C, its

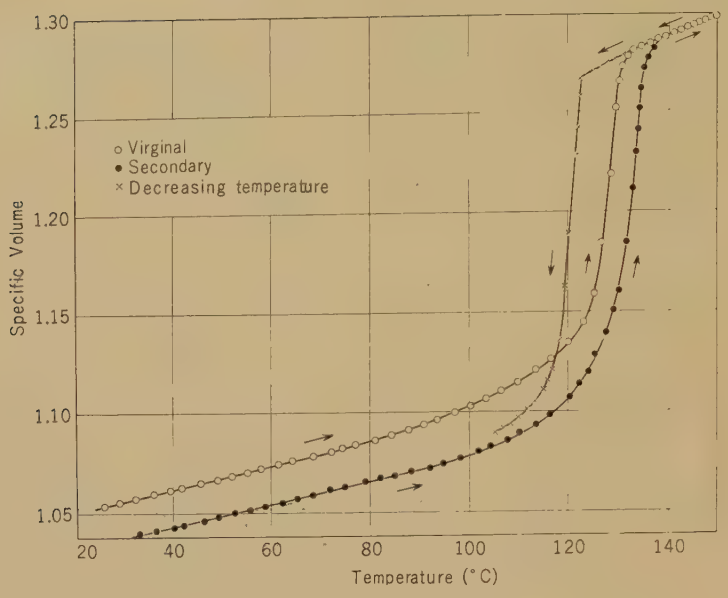

Fig. 4—T vs. V_{sp} curves of Marlex 50.

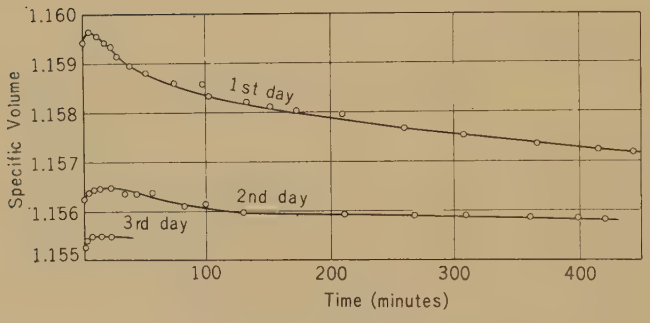

Fig. 5—Change of specific volume with time at constant temperature (DYNH at 87.7° C).

volume change started from the point A in Fig. 6 at the beginning of the experiment and then slowly decreased until it reached the point B, in 4 hours. Meanwhile, the sample which was at first nearly transparent became turbid as the volume decreased. After this heat treatment complete melting did not occur till at 114.7° C. On the other hand, when this sample was directly raised to 113.2° C, its volume completely turned to that of the liquid state. Thus by "pre-melt annealing" the melting point was raised a few degrees.

In low pressure polyethylene the same phenomena were observed when it was kept well below the melting point, e.g. at 115° C. However, at 126° C and higher, the volume did not decrease but increased continuously and convergently with time, and with pre-melt annealing the melting point seemed not to change. This is one of the most notable differences between the dilatometric properties of these two polyethylenes.

Furthermore, it should be noted that this memory phenomenon in the volume change was also observed by us in Kel-F[21] (polychlorotrifloroethylene) and in polypropy-

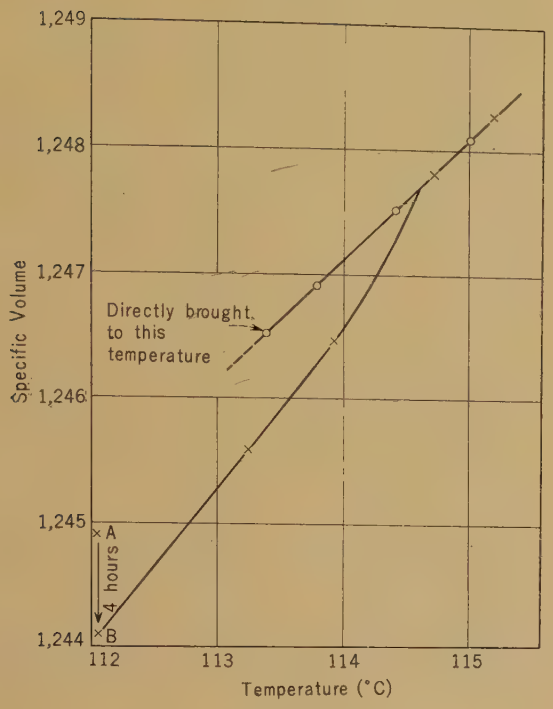

Fig. 6—Effect of pre-melt annealing on DYNH.

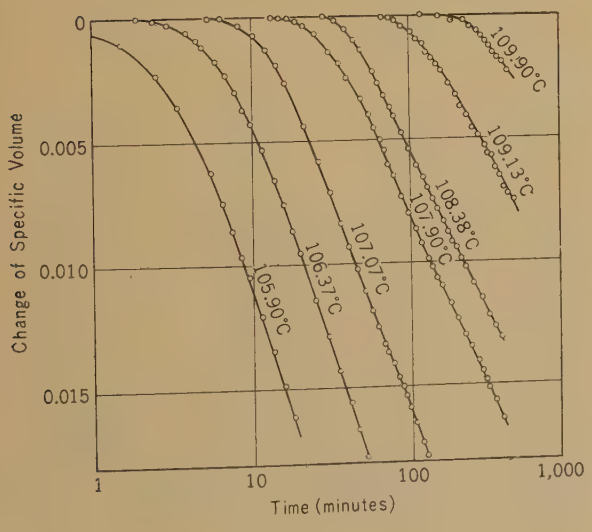

Fig. 7—Crystallization from supercooled state in Alathon 10.

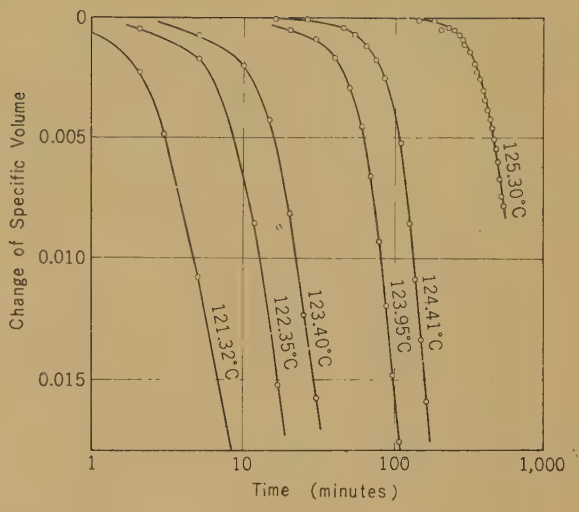

Fig. 8—Crystallization from supercooled state in Super Dylan 6200.

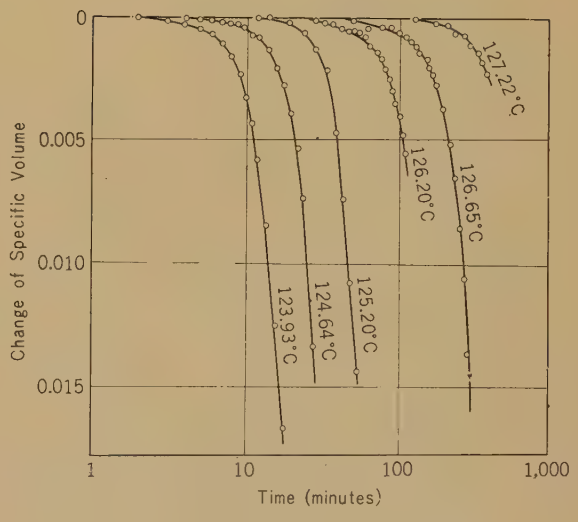

Fig. 9—Crystallization from the supercooled state in Marlex 50.

lene, and is thought to be a general behavior of crystalline polymers. And this phenomenon is a strong support to the concept of the crystallite size distribution as will be discussed below, though it seems to have not been reported.

1.3. Crystallization from the Melted State

Many authors have reported on the crystallization phenomena for various polymers. Especially Manderkern[6],[7] has discussed it in detail completely. We also carried out experiments of this kind on various polyethylenes, and our result will be described briefly.

Our experimental method was a rather conventional one. From about 135° C in the case of high pressure polyethylene or from about 150° C in the case of low pressure polyethylene, the oil bath was cooled as fast as possible down to a temperature a few degrees lower than the melting point. When the required temperature was obtained, the temperature of oil bath was regulated with the aid of a photoelectric relay, and the volume change with time was measured. Figs. 10, 11, and 12 show the results of these experiments. From these curves the the induction periods (the period at which the volume change became noticeable) and their change with temperature was determined.

Strictly speaking, the induction period in the lower temperature region observed by our method was a little too short. For, in this region the crystallinity should have preceded considerably during the period which was spent in lowering the temperature. But if the time necessary to lower the temperature from the melting point was

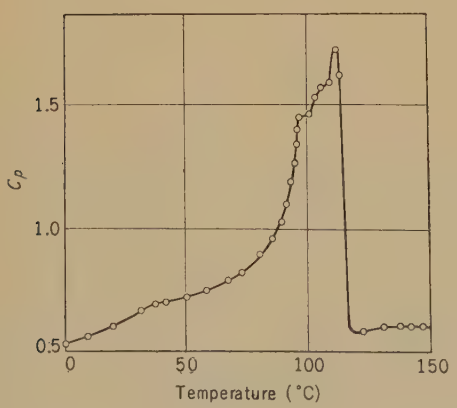

Fig. 10—A example of specific heat data in polyethylene (DYNH).

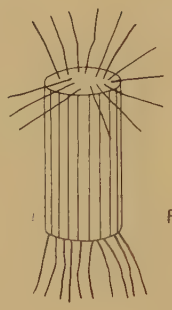

Fig. II (a)—Bundle-like Crystal of Polymer Molecule.

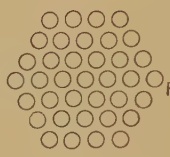

Fig. II (b)—Cross Section of (a), or a Two-dimensional Crystal.

Fig. II (c)—Minimum Two-dimensional Crystal.

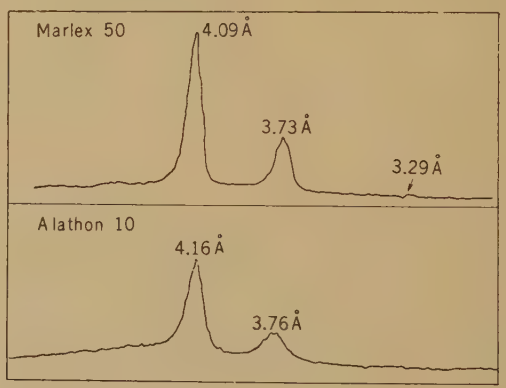

Fig. 12—X-ray diffraction patterns of two polyethylene samples.

short, the error introduced by our method was not thought to be a serious one, for even with a more adequate method the equilibrium of temperature between the dilatometer tube and the oil bath was somewhat doubtful at the beginning of the measurement.

1.4. Specific Heat Measurement

A calorimeter of the vaccum adiabatic type was used in our experiment. Our

calorimeter was not so precise as that of Dole,[3],[5] but more sensitive as a thermocouple of low heat capacity was used in place of Dole's resistance thermometer[3] to measure the temperature of the sample. The time necessary to produce a unit raise in temperature was measured with our newly designed double stopwatch. (Japan Utility Model No. 435413)

Our specific heat measurement was made only for DYNH. The result is shown in Fig. 10. The general behavior was fundamentally the same as that reported by Richards[2] and Dole. The discontinuity of slope at about 30° C might not be essential as it was thought to have resulted from technical faults as the cooling of our adiabatic system from the room temperature to −10° C was not successful. The irregularity at 95° C should be more important as will be discussed below. The shape of this irregularity changed with experimental conditions, but was found in all of our experimental data.

2. Theory of Melting Range

A crystalline polymer usually has a broad melting range. To interpret the existence of this range several theories were suggested since the paper of Frith and Tuckett.[8] But before discussing this problem the answer to a rather primitive question must be presented.

Some may doubt that the coexistence of solid and amorphous phases in a crystalline plymer should not be a true thermodynamical equilibrium, because Gibbs' phase rule requires the appearance of this coexistence only at one temperature, and further that the high inner viscosity of polymer substance prevents the approach to the equilibrium state, and causes the apparent melting range. By examining the introducing way of phase rule, however, it is found that Gibbs' phase rule contains an assumption on the additivity of entropy,

$$\frac{\partial \mu}{\partial n} = -T\frac{\partial^2 S}{\partial n^2} = 0, \qquad (1)$$

implicitly. In the case of usual low molecular substances this additivity always stands, but in polymer substances, so long as the crystallization of a part of one molecular chain is assumed, the division of its volume into two parts means the cutting off of one molecular chain, and the entropy of this chain in the liquid phase changes with this procedure. Therefore this additivity may not be assumed in the general case, and the coexistance of two phases within a proper temperature range is thermodynamically permitted.

The work of Frith and Tuckett[8] is one of the earliest theories that tried to explain this melting range by introducing this non-linear entropy. But their theory contains many faults, one of the greatest being that their calculation gives an excessively narrow melting range. It is readily seen that their theory is fundamentally the same as the interpretation of the variation of melting point with the molecular weight. It is widely known that in an ordinary case the molecular weight affects the melting point very little if the molecular weight is sufficiently high, so it is quite natural that their theory gives an excessively narrow melting range.

Later several authors[9],[10] established their individual theories for this melting range introducing the melting point depression effect by the low molecular weight portions which were originally contained in ordinary synthetic polymer. These theories gave melting ranges of appropriate width if a proper amount of low molecular weight portion was assumed. However, experiments that showed the narrowing of the melting range by removing the low molecular weight portions are scarcely seen. Richards[9] considered the entropy of the side chains and their solvent effect which made the width of the melting range broader, but did not show this effect in a closed form. His consideration is fundamentally the same as the effect of melting point depression by copolymerization which was chiefly treated by Flory.[16] It is an experimental fact that the shape of the T vs. V_{sp} curve varies with kind sample, but it is not expected that by synthesizing perfect linear polyethylene of practically single chain length we shall have an infinitesimally narrow melting

range.

Richards[9] further considered that the gradual melting of polyethylene is partly due to the distribution of the crystalline size. There he referred to the experiment on the mixture of two paraffins, $C_{16}H_{34}$ and $C_{60}H_{122}$.[12] His illustration does not seem to be adequate one, for it contains the same fault as that of the Frith-Tuckett theory explaining only the effect of chain length on the melting point. He did not refer to the effect of surface energy, but other authors considered this effect and showed some calculations. For example, Dole and Smith[4] calculated this depression effect to explain the result of their specific heat measurement on polyethylene terephthalate by introducing an arbitrary amount of surface tension.

We also attempted to calculate this melting point depression effect by adopting a very simple model. According to the generally accepted structure for the polymer crystallite, we imagine a cylindrical crystallite which is constructed with a bundle-like arrangement of molecular chains as shown in Fig. 11. The force which keeps the crystal stable should be the cohesive one acting between the chain elements at the point of contact. Therefore the chain element on the surface of a crystal has some excess energy. A chain that forms a part of this crystallite also runs into the amorphous region, because the chain is thought to be longer than the length of the crystallite. Therefore the surface energy should only exist on the side surface of this cylinder, and on the upper or lower surface of the cylinder there is no excess energy because we find only the continuity of molecular chains here. In this case the problem is reduced to a two dimentional close packed arrangement of chain elements. Assuming that the surface energy is the excess cohesive energy on the surface and is propotional to the exposed surfaces of chain units it is easily seen that the surface energy is equal to the $2/6=1/3$ of the total cohesive energy of the chain units that lie on the side surface. Thus the actual cohesive energy can be written in the form

$$E=E_\infty\left(1-\frac{Sd}{3V}\right), \tag{2}$$

where E_∞ is the cohesive energy of an infinitely large crystal, S the cross section of the cylinder, V its volume, and all linear dimensions are represented by using the length of molecular chain unit in the crystal as the unit of length. From this equation the chemical potential of one chain unit is calculated as follows:

$$\mu=\mu_\infty\left(1-\frac{4}{3d}\right), \tag{3}$$

where d is the diameter of this cylinder, and μ_∞ the chemical potential in an infinitely large crystal. The melting point of this crystal is determined from the equation

$$\mu=T\frac{\partial S_l}{\partial n}, \tag{4}$$

where S_l is the entropy of the liquid phase. Generally $\partial S_l/\partial n$ is not a constant as we discussed above, but the change of melting point by the Frith-Tuckett effect is very small in the usual case and we assumed it was a constant. The highest T_m observed in the experiment is supposed to correspond to the largest grains on which the surface energy effect is negligible, therefore we obtain:

$$\mu_\infty=-T_{\max}\frac{\partial S_l}{\partial n}. \tag{5}$$

Combining (4) and (5) we get the result shown in Table 2, taking T_m as approximately 400° K.

For very small crystallite grains our approximation fails to stand as the ratio of the surface energy to the total cohesive energy cannot be represented in a simple form. In such a case the effect of the surface energy must be calculated directly on the individual aggregation state of chain units. For example, the hexagonal aggregate of 7 units gives the melting point of

$$T_m=\frac{4}{7}T_\infty. \tag{6}$$

Here we considered only the side surface of the crystallite cylinder, but when a molecular chain passes through the upper or

Table 2

MELTING POINT DEPRESSION BY THE SURFACE ENERGY EFFECT, TAKING $T(\text{MAX.}) = 400°$ K

Diameter of Grain	Depression
3	180
10	53
30	18.0
100	5.3
300	1.8
1,000	0.5
Infinite	0.0

lower surface of the crystallite cylinder, its shape must shrink a little to take the form adapting to the crystal lattice, so there may arise some diminution of surface energy. In addition to this, the chain unit on the surface is thought to have a shape a little different from that of those inside, because it does not suffer the compression by the cohesive force from the outer molecules. This effect also reduces the surface energy. Summarizing these factors, the melting point depression is thought to be a little smaller than the result of our calculation.

In the calculations described above, it was assumed that the surface free energy contributing to the melting point depression was equivalent to the excess surface energy. It may be on this central point that our theory suffers criticism. Little is known about the surface tension at the boundary between the liquid and solid phases of the same substance, but in usual theories for the melting phenomena the contribution from the surface tension is generally neglected. If the surface tension of liquid and solid is assumed to be equal, only the excess cohesive energy contributes to the depression of the melting point, and the assumption of our calculations should be appropriate. The surface energy of a solid should not be so mystical as it is generally thought to be, and this may be treated theoretically on some appropriate model.

In spite of these difficulties, it is sufficient at the present stage to know that the smaller crystallite has the lower melting point. With this concept many important results can be introduced as will be discussed below.

3. Discussion

3.1. Appreciation of Dilatometric Data

In Flory's textbook[10] it is written that the measurement of the specific volume near the melting point requires about 24 hours or more to attain an equilibrium value, and more rapidly conducted melting tests usually lead to a fictitiously low melting point. The word "usually" is important, for in some case we have a fictitiously high melting point after such procedure. Our experimental data on DYNH showed the change of melting point from 112.2° C to 114.4° C, and in this case the advice of Flory is right. To conduct the measurement very slowly means to apply the pre-melt annealing thoroughly, and after this heat treatment the melting point shifts upward by several degrees. But in the case of low pressure polyethylene or in the case of low pressure Kel-F the state is a little different. For example, in the case of Marlex 50, with our conventional method we have the melting point of 133.0° C for the virginal sample and 137.5° C for the naturally annealed sample. But from the volume change with time at several fixed temperatures in the melting range, we must conclude that the melting is completed at 133.2° C. So the value 137.5° C which was observed by our temperature raising method is thought to contain some error resulting from the delay in melting. In our experimental equipment the sample itself could be observed through the wall of the glass dilatometer tube and silicone oil, and the sample turned from white to transparent on melting. At about 135° C a part of the sample near the glass wall became transparent, while the center of the dilatometer cell remained white until 137.5° C. This delay in melting could have resulted from

the poor heat conductivity of the polymer sample, or from its high viscosity and the reological delay in the phase change.

A slowly and carefully conducted dilatometry gives the most reliable melting point, of course, but this melting point corresponds to that of the largest crystallite grains accessible. If the melting point of a polymer is thus defined, this method gives the true value.

However, there arises another experimental difficulty. The volume at a given temperature can be determined as a saturation point of volume change with time. But if this saturation is completed, it takes a longer time at the next higher temperature than in the case where it is directly brought to this temperature. So the experiment requires more and more time, and the true equilibrium value becomes to be hardly accessible. Furthermore, if it takes 24 hours, for example, the regulation of temperature during this long interval with sufficient accuracy is not an easy technique; and if the temperature fluctuates, the volume tends to approach the value corresponding to the highest temperature in this fluctuating range.

For these reasons, we find that it is not wise to conduct a dilatometric experiment too slowly every time, because the result obtained by this procedure may not be a valuable one, and therefore, it may be a waste of time and effort. Considering these situations, we determined the T vs. V_{sp} relations with our conventional temperature raising method, and determined only the melting point with the equilibrium method. In this way we obtained an equilibrium value of the melting point and the general shape of the T vs. V_{sp} curve with less effort and less experimental time.

3.2. Variation of Melting Point with Sample Kind

Although high pressure polyethylene and low pressure polyethylene have similar molecular structures, their melting-points differ from each other greatly. The value of 135° C, observed in Marlex 50 agrees well with the value extrapolated from the melting points of low molecular paraffins as indicated by several authors. If there is a slight discrepancy between the value for Marlex 50 and the value for polymethylene[20] as Wunderlich and Dole[5] have pointed out, this may be the result from the molecular chain branchings which are thought to exist even in this polyethylene. And the abnormally low melting point of high pressure polyethylene will be explained by this side chain effect, the smallness of crystallite grains, or the melting point depression effect of the low molecular weight portion.

It is usually said that low pressure polyethylene has a narrower melting range than high pressure polyethylene. This is true, but it should be remembered that this narrowness of the melting range is rather exaggerated by the lowness of the specific volume at room temperature.

3.3 Calculation of Crystallinity

Hunter and Oakes[1] calculated the crystallinity of polyethylene from their dilatometric data. The specific volume at a given temperature is represented as

$$V_{sp}=\theta V_c+(1-\theta)V_a, \qquad (7)$$

where V_c is the specific volume of crystalline phase at this temperature, V_a that of amorphous phase, and θ the degree of crystallinity. Here the evaluation of V_c and V_a is the main problem. Hunter and Oakes used as V_a the value extrapolated from the volume of the melted state, and for V_c used the formula:

$$V_c=1.00+6\cdot10^{-4}(T-10), \qquad (8)$$

following the data on low molecular paraffins.[13]

Our extrapolation from the melted state is

$$V_A=1.2600-9.5\cdot10^{-4}(120-T), \qquad (9)$$

for Marlex 50. But calculating the crystallinity from these values we found a maximum crystallinity at about 80° C. This result is a little unreasonable.

If we assume that the crystallinity is roughly 90% in the low temperature range as calculated by Wunderlich and Dole,[5] the formula

Table 3

CRYSTALLINITY OF ANNEALED MARLEX 50 AT VARIOUS TEMPERATURES

°C	30	40	50	60	70	80	90	100	110	120
%	90.0	90.3	90.9	88.9	90.5	90.0	88.3	85.4	79.5	43.1

$$V_c = 0.9982 + 4.5 \cdot 10^{-4} T, \qquad (10)$$

is obtained, where T is expressed in degrees centigrade. With this formula we obtain a reasonable value of crystallinity at all temperatures as shown in Table 3.* It is noticed that this value of expansion coefficient agrees with the measurement by Seyer, Patterson, and Keays on $C_{34}H_{70}$.[1]

3.4. Interpretation of Volume Change with Time

With our concept of the crystallite size distribution, all of our experimental data are clearly interpreted.

Our experiment on the change of specific volume with time strongly supports our concept, because this phenomenon can only be explained with this concept. As stated above, each crystallite has its own melting point corresponding to its size, and smaller crystallites suffer a larger surface energy effect and so have a lower melting point. When a sample is kept at constant temperature some degrees lower than the melting point, say 87.7° C in our experiment on DYNH, small crystallite grains which have melting points lower than this temperature soon melt away and the volume increases at first. But the larger grains remain unmelted, and they still tend to grow larger to approach the equilibrium state, and the volume decrease proceeds. Meanwhile, the mutual collision of growing grains begins to take place and the feeding amorphous portion tends to be consumed, and the volume decrease becomes gradually slower. If the temperature is lowered after the experiment for several hours, the crystallinity itself increases, but the greater part of this increment is performed by the appearance of small crystallites which have melting points lower than 87.7° C. By raising the temperature again to the same point as before, all these newly appeared crystallites melt away, and the volume comes back almost to the same value as at the end of the preceding experiment, and decreases with gradually diminishing speed as before.

The pre-melt annealing effect in the case of high pressure polyethylene is also easily explained with this concept, Keeping the sample at a temperature just below the melting point, nearly all crystallites melt away and the sample becomes transparent at first. But the largest crystallites remain still unmelted, and begin to grow larger, and as they grow in size to the order of the light wavelength, (or 1/20 of the wavelength is said to be sufficient) the sample becomes turbid gradually. After this heat treatment the melting points of the remaining crystallites rise corresponding to their increase in size, and the melting point of the whole sample rises accordingly.

The same volume decreasing phenomenon for low pressure polyethylene or for Kel-f is also explained in the same way. But in low pressure polyethylene the crystallite size is thought to be much larger than that in high pressure polyethylene. This difference of crystallite size is also seen from the X-ray diffraction patterns shown in Fig. 12. Thus, the melting point depression by the surface energy is much less for low pressure polyethylene than for high pressure polyethylene, and the "pre-melt annealing" affects the melting point rather little. Also the narrower melting range of low pressure polyethylene is explained by this larger

* This formula for the calculation of the crystallinity has been slightly revised from the results of our further experiment in the lower temperature range, which will be published in *Journal of the Physical Society of Japan*, **15**-6 (1960).

crystallite size; because if the distribution of crystallite size is shifted to the larger length side, the smaller the surface energy effect becomes with this shift, and the narrower the distribution of melting point becomes.

In our conventional temperature raising method the secondary measurement always gave a higher melting point than that of the experiment on the virginal sample. The virginal sample was a commercial pellet-shaped sample whose thermal history was unknown, but it is certain that it had sufferred a considerable quenching effect during the manufacturing process. So in the virginal sample the crystallite should not have reached the maximum size obtainable, and this sample gives a lower T_m than the annealed one. But before drawing this conclusion a caution is needed, especially in the case of the low pressure polyethylene. For, in this case the raise of T_m by grain growth and the delay of melting are dependent on each others. In Table 2, it is seen that the T_m for the virginal sample of Super Dylan is 128.0° C, for the annealed sample 133.0° C, and the equilibrium value is 130.0° C. The equilibrium value is thought to be a reliable one, so we adopt it as a standard value. The value of 133.0° C for the annealed sample includes the error caused by the delay of melting, therefore; the value 128.0° C for the virginal sample may also include this error. The imaginary equilibrium value of T_m for a virginal sample is very difficult to measure, but if the amount of delay is assumed to be the same amount in every experiment, i.e. 133° C − 130° C = 3° C, the largest grains in the virginal sample are thought to have the size corresponding to the melting point 128° C − 3° C = 125° C.

3.5. Grain size Distribution and T vs. V_{sp} Curve*

The distribution of the grain size is represented as follows: Let the number of grains that have the number of chain unit between n and $n+\mathrm{d}n$ be $G(n)\mathrm{d}n$. Then the crystallinity of this sample is

$$\frac{1}{N}\int_0^\infty nG(n)\mathrm{d}n, \qquad (11)$$

where N is the total number of the chain units including the amorphous regions. If this sample is kept at a temperature T_1 in the melting range, all crystallites which are smaller than n_1 will melt away, provided the dimention of n_1 corresponds to the melting temperature T_1. Then the grain distribution becomes

$$\frac{1}{N}\int_{n_1}^\infty nQ(n)\mathrm{d}n, \qquad (12)$$

neglecting the further growth of the remaining grains. So it can be roughly said that the shape of T vs. V_{sp} curve tells the grain size distribution in this sample, and the thermal history which this sample experienced in the annealing period is presumed from this. For example, the fact that the virginal sample shows a lower specific volume than the annealed sample at 100° C is interpreted as meaning that this sample has suffered considerable annealing effect at this temperature during the manufacturing process.

3.6. Quenching and Glassy Transition†)

The glassy transition of polyethylene is said to exist at −20° C to −50° C. We have not meatured this, but a new interpretation of the glassy transition is posisble with our present concept. In Table 2 it is seen that a grain having the diameter 3 suffers a melting point depression of 180° C if our general formula is assumed. This corresponds to a melting point of −45° C. Our estimation is of course a very rough one, so it may be said that this value represents the glassy transition point very well. $d=3$ means the two dimensional crystallite grain constructed with an assembly of 7 units, and this is likely to exist in the random distribution of polymer chains. If the generally accepted rule for the second order transition temperature, $T_2=2/3\,T_m$, is as-

* An analogos treatment of the grain size distribution was done by M. G. Gulber and A. J. Kovacs, *J. Polymer Sci.*, **34**, 551 (1959).

† See footnote of page 67.

sumed, the size of the grain corresponding to this temperature is $d=4$. So, according to our concept the glassy point is thought to be the point where the casual arrangement of polymer chains becomes sufficient to crystallize overcoming the surface energy effect. As discussed above, our estimation for the surface energy may be a little too large, so this transition may correspond to the value near $d=3$.

For polyethylene the complete quenching of the amorphous state from the melted state is usually impossible, though quenching to dry-ice temperature remains a possibility. Even so, we can present here a new interpretation of the quenched state. The quenched state is usually considered as a state where all molecular motion of the polymer chain is frozen by shock cooling and further crystallization is prevented. At least at temperatures higher than the glassy transition point of the usual sense, however, the actual freeze-in of all molecular motion is not expected. In addition to this, the change of density of Kel-f with the quenching temperature can not be interpreted with this primitive understandings of the quenched state.

Following our concept, the quenched state is understood as follows. Even in the quenched state there still exists a sufficient number of crystallite grains, all of smaller sizes, and the distribution of the sizes of these grains is determined from their thermal history experienced during the quenching procedure. Between these grains and the amorphous regions there may exist some intermediate regions where the molecular chains suffer some tension as the result of the volume construction with crystallization. So the density in this intermediate region may be even lower than that of the usual amorphous region, and the bulk density of the quenched sample may be comparable with that of the pure amorphous phase though this sample contains many crystallites and gives some amount of X-ray diffraction patterns corresponding to the crystallite phase. If the quenching is done to a temperature lower than the glassy point, the spontaneous aggregate of molecular chains in the melted state becomes crystallite itself as discussed above, and thus this quenching gives the lowest density by leaving as much as possible the richest intermediate regions.

3.7. Irregularity in Apparent Specific Heat

Also, the irregularity in the specific heat of high pressure polyethylene can be interpreted with our concept. The irregularity at 95° C is of the same type and nature as that found by Smith and Dole[4] in polyethylene terephthalate, though they did not give any interpretation of this, except describing that this irregularity varished after pre-melt annealing. We regret we have not realized the varishing of this irregularity in our samples with pre-melt annealing, but it is believed to happen. So this irregularity has a close relation with pre-melt annealing.

Our interpretation of this phenomenon is as follows:

As the temperature rises, the crystallinity decreases, but the speed of grain growth or the rate of volume decrease becomes larger as the inner viscosity of this polymer diminishes and the amorphous portion increases. Therefore, if the temperature is raised at a constant rate, the increase of crystallinity by the grain growth becomes comparable with the decrease of it with the temperature change and the heat generated by crystallization reduces the apparent specific heat.

Such an irregularity should also be found if we plot the expansion coefficient of specific volume against temperature. However, as the heat evolved by crystallization is very large compared with the change of the heat content of the crystalline or the amorphous state at this temperature, and the change of volume by crystallization is comparably small, it is quite reasonable that the irregularity which is clearly found in the specific heat is very small in the expansion coefficient. In spite of this, in the temperature vs. specific volume curves by Hunter and Oakes there exists suggestives disorder of experimental results in this temperature range, and our specific volume data also show some tendency of irregularity in this range.

The melting points determined from the specific heat measurement has the same

nature as that determined from rapid dilatometry. Whether it is higher or lower than the equilibrium value of the melting point is wholly governed by the nature of the sample on which these experiments are carried out.

3.8. Crystallization Penomena from the Melted State

The crystallization of a polymer from its melted state was discussed by Manderkern [6],[7] in detail. He assumed the spontaneous appearance of crystalline nuclei and calculated the temperature dependence of their rate of growth; and had good agreement between his theory and experiment.

Even so, there remains some doubt about the correctness of his theory. As we discussed in another paper,[18] the crystallization phenomena in polyethylene, at least in the case of Marlex 50, seem to be performed by spherulite growth only. This means that the crystallization starts from a few germinal nuclei in the centers of the spherulites and spreads spherically with some mechanism. It is quite doubtful if Manderkern's theory can be applied to such a case. In the case of polychlorotrifloroethylene, comparing the measurement of Yamada[19] on the rate of spherulite growth with our measurement on the density with heat treatment,[21] it is roughly estimated that the induction period of density change corresponds to the period where the diameter of spherulite becomes about 30 microns. The diameter of spherulite increased linearly with time from the start and no trace of induction period was found in this growth phenomenon. So if the density change is proportional only to the volume occupied by the spherulites, this change must be proportional to t^3, neglecting the overlapping of spherulites. Assuming the essential feature of crystallization is the same as in the case of polyethylene, the change of specific volume with time must also conform to this rule. If a more rapid change is observed, more intricate crystallization mechanism must be assumed.

Here we must remember that the spherulite observed under a microscope and the crystalline portion of the polymer solid that contributes to the density change are not identical. To be observed under a microscope the grain must have a diameter of at least that of the wavelength of light, or about 0.5 micron. On the other hand, the single crystal of polyethylene is said to be not larger than several hundred Angstrom units. Thus a spherulite must be an aggregate of such single crystals, perhaps of comparatively larger sizes, all having the ordered crystalline directions; for if they have random directions, the whole sample should be perfectly transparent optically. In addition to this, it is quite probable that at least a part of crystallization is performed by the ultramicroscopic crystallites which cannot be observed optically. So it is entirely possible that even after the spherulite growth has been practically completed there still exists an increase of crystallinity. Such a possibility must be examined by performing the experiments of volume contraction and spherulite growth under exactly identical conditions. The usual hot stage of a microscope has not sufficient temperature precision to make such experiments possible, and we must wait for the improvement of experimental instruments.

Further discussion of the crystallization phenomena must be developed with a more complex model, in consideration of both the visible spherulites and the univisible small crystallites. But much must be known about the structure of the spherulite and that of crystalline region experimentally, and our research will be carried out in these directions where possible.

The temperature dependence of the induction period is represented in the usual form:

$$\tau \propto (T_m - T)^{-n}. \qquad (13)$$

Calculating this n from our experimental data we get the result shown in the last colomn of Table 1. It is noticed that the sample having the higher melting point has the higher n value. Namely, taking the temperature at which the induction period has a certain value, say 5 minutes, as T', we find that the sample having the higher T_m gives the larger $(T_m - T')$ value and higher n value. It is clear from our experi-

ment that some factor corresponding to the chain length or other individual characters of the molecule must be considered.

Conclusion

The crystallinity of a polymer solid has usually been described by a single parameter, the degree of crystallinity. This parameter is defined conventionally by individual experimental values. For example, the dilatometric measurement. The nuclear magnetic resonance, the X-ray diffraction, the specific heat, and the optical turbidity all give different definitions of crystallinity. So it is quite natural that these measurements should each give different values of crystallinity. But as we discussed above in detail, not only the crystallinity but also the distribution of the grain size affects the various properties of the polymer solid. This distribution is chiefly determined by the thermal history of the samples, and many phenomena which were hitherto vaguely attributed to the thermal history must be explained with this concept of grain size distribution. Also there must be many phenomena to which our concept is applicable.

But a precise measurement of this distribution is not an easy one, because by most methods we only find the mean size of these grains; and here the similar difficulties met in the measurement of the molecular weight distribution will arise. Furthermore, the grain distribution usually changes during the measuring period if it is carried out at a high temperature.

As it is, it is sufficient for today to remember the existence of this distribution and refer to it as a powerful aid for the interpretation of some phenomena which are hard to understand with the usual single crystallinity model. For example, the measurment of the melting enthalpy of a polymer from the melting point depression by copolymerization is somewhat dangerous, as Smith and Dole have pointed out, because the maximum grain size may diminish with copolymerization.

The size of a crystallite is chiefly governed by its thermal history, but a more important factor is the nature of the sample. By the branching of molecular chains the growth of the crystallite may be interrupted, and so it is quite reasonable that low pressure polyethylene which is said to have less chain branching seems to have larger grain sizes than high pressure polyethylene.

References

(1) E. Hunter and W. G. Oakes, "The Effect of Temperature on the Density of Polythene," *Trans. Faraday Soc.*, **41**, p. 49 (1945).

(2) H. C. Raine, R. B. Richard, and H. Ryder, "The Heat Capacity, Heat of Solution and Crystallinity Polyethylene," *ibid.*, **41**, p. 59 (1945).

(3) M. Dole *et al.*, "Specific Heat of Synthetic High Polymers," I, *J. Chem. Phys.*, **20**, p. 781 (1952).

(4) C. W. Smith and M. Dole, "Specific Heat of Synthetic High Polymers," VII, *J. Polymer Sci.*, **20**, p. 37 (1956).

(5) B. Wunderlich and M. Dole, "Specific Heat of Synthetic High Polymers," VIII, *ibid.*, **24**, p. 201 (1957).

(6) L. Manderkern, F. A. Quinn Jr., and R. J. Flory, "Crystallization Kinetics in High Polymers," I, *J. Appl. Phys.*, **25**, p. 830 (1954).

(7) L. Manderkern, "Crystallization of Flexible Polymer Molecules," *Chem. Rev.*, **56**, p. 903 (1956).

(8) E. M. Frith and R. F. Tuckett, "The Melting of Crystalline Polymers," *Trans. Faraday Soc.*, **40**, p. 251 (1944).

(9) R. B. Richards, "The Melting of Polythene," *ibid.*, **41**, p. 127 (1945).

(10) R. F. Flory, "Thermodynamic of Crystallization in High Polymers," IV, *J. Chem. Phys.*, **17**, p. 223 (1949).

(11) R. J. Flory, *Principles of Polymer Chemistry*, p. 567 (1945).

(12) W. E. Garner, K. Van Bibber, and A. M. King, "The Melting Points and Heat of Crystallization of the Normal Long-chain Hydrocarbons," *J. Chem. Soc.*, p. 1533 (1931).

(13) C. W. Bunn, "The Crystal Structure of Longchain Normal Paraffin Hydrocarbons," *Trans, Faraday Soc.*, **35**, p. 482 (1939).

(14) C. W. Bunn and T. C. Alcock, "The Texture of Polyethene," *ibid.*, **41**, p. 317 (1945).

(15) N. Bekkedahl, "Volume Dilatometry," *J. Research N.B.S.*, **43**, p. 145 (1949).

(16) R. J. Flory, "Theory of Crystallization in Copolymers," *Trans. Faraday Soc.*, **51**, p. 848 (1955).

(17) R. Nakane, "Memory Phenomenon in the Volume Change of Crystalline Polymer," *J.*

Polymer Sci., **31**, p. 244 (1958).
(18) R. Nakane, "Spherulite Growth of High Density Polyethylene," *ibid.*, **28**, p. 456 (1958).
(19) Private Comm. From N. Yamada.
(20) L. Manderkern *et al.*, "The Melting Transition of Polymethylene," *J. Am. Chem. Soc.*, **75**, p. 4093 (1953).
(21) R. Nakane, "On the Dilatometry and Crystallization of Polychlorotrifloroethylene," *Reports of the E.C.L.*, **6**, 9, p. 341 (1958).

* * * *

678. 7. 047:621. 395. 6
53. 6:159. 937. 51

A Study of colors for Molded Telephone Handsets*

Yumio SUGIHARA†

There are very few types of pigments suitable for the rigid polyvinyl chroride used for molded telephone handsets. Therefore tests were limited to three colored pigments; (red, yellow, and blue) chosen for high heat and light stability, plus black and white pigments for toning.

The range of color matching feasible with these pigments was determined using the CIE chromacity diagram and the Munsell color system.

Experimental colored plastic samples were produced and tested for fading with a carbon arc type tester, and were found to have excellent light stability.

Introdnction

The remarkable development of the plastics and the paint industries has resulted in a floot of colors in our daily life. This trend is being intensified by the progress of industrial design and the increase in the concern for color conditioning. It is in response to this popular demand that it has been decided to produce not only the familiar black telephones but also colored telephones.

The use of rigid polyvinyl chloride as the material for telephone handsets is now being studied. However the colored producton of rigid polyvinyl chloride castings mold is not common; this is probably because there are very few types of pigments which can withstand the severe conditions of the molding process. In this research three pigments (red, yellow, and blue) together with black and white, were selected as the minimum number necessary for color matching; and the range of color matching possible was determined using the C.I.E. chromacity diagram. By selecting three highly stable pigments at the start it is reasonable to expect that all colors made by this system will be highly stable, and experiments have shown that the colors are indeed stable.

After an investigation of the colors used in Japan for telephones and similar instruments, together with studies of the rules of color harmony; fifteen suitable colors were selected from within the range of colors that could be produced by the methods and with the materials discussed above.

1. Selection of Pigments for Use in Rigid Polyvinyl Chloride

It is not common to color rigid polyvinyl chloride which is to be injection molded, probabily because the temperature necessary for molding is so high and the flow of the material is so poor that it is difficult to obtain pigments which can endure such conditions.

In the present study it has been decided to use the minimum number of colors essential for color matching: namely, red, yellow, blue, black, and white. Accordingly, the following five pigments were selected:

(1) Cadmium red (inorganic pigment)
(2) Cadmium yellow (inorganic pigment)
(3) Phthalocyanine blue (organic pigment)
(4) Titanium dioxide (inorgnaic pigment)
(5) Carbon black.

* MS received by the Electrical Communication Laboratory, Oct. 30, 1959. Originally published in the *Electrical Communication Laboratory Technical Journal*, N.T.T., Vol. 8, No. 12, pp. 1550–1561, 1959.

† Plastics Application Research Section.

All of the above pigments can endure temperatures higher than 180° C which are necessary for the injection molding of rigid polyvinylchloride, and have light stability sufficiently strong to be used for telephones. Also, in selecting these pigments special attention has been paid to their dispersion properties and to their stability against the separated hydrochloric acid produced during the molding of the handsets.

2. The Colorants of Rigid Polyvinyl Choloride

Cadmium red and cadmium yellow are inorganic pigments that have a wide hue range from red to yellow, and consist of CdS·CdSe and CdS respectively. Since their mass production has become feasible, it has also become possible to obtain uniform shades of colors from them. Their tinctorial power, which is usually lacking in inorganic pigments, is fairly strong and their dispersion is sufficient. Although they are disintegrated by strong hydrochloric acid, the experiments discerned no harmful effect on them by the weak hydrochloric acid produced in the process of injection molding of rigid polyvinyl chloride.

Phthalocyanine blue is widely recognized as an organic pigment of superior light and heat stability.

3. Color Matching

In the color matching of plastics, the colors of the compounds before and after molding usually look quite different. Therefore, the color matching of plastics is far more difficult than the matching of ordinary coating materials, the progress and the results of which can be visually assured.

During this research, various colored samples of rigid polyvinyl chloride have been produced with the ratios of the pigments systematically determined before production. Also, the change of color caused by varied ratios of pigments has been indicated numerically on the C.I.E. chromacity diagram and in the Munsell color system, and the range of colors possible with the five pigments has been determined.

The colored test samples were produced so as to match the conditions of actual injection molding as closely as possible. Use of a larger proportion of pigments has a bad effect on the flow and on the dispersion of the material at the time of injection molding. Therefore, the maximum ratio by weight of the organic pigments (red, yellow, and white) was fixed at two percent of the weight of the plastic; and the ratio of the weight of the inorganic pigments (blue and black) at 0.5 and 0.3 percent respectively.

Table 1

THE RATIO BY WEIGHT OF THE INGREDIENTS OF COLORED RIGID PVC

Components	Ratio by Weight
PVC (NIKA Vinyl S800)	100
Tribase (tribasic lead sulfate)	5
Diphos (dibasic phosphite)	2
Stearate Lead	1
Pigments	Less than 2

Table 1 shows the ratio of the ingredients of the colored rigid polyvinyl chloride by weight.

Table 2 indicates the ratio of the pigments in the twenty-one test samples, made according to the ratios shown in Table 1. Table 2 also indicates the C.I.E. trichromatic coordinates and the O.S.A. Munsell notations for the twenty-one test samples.

The conversion from the C.I.E. trichromatic coordinates to the O.S.A. Munsell notation was done according to the recommendation of the O.S.A. in 1943.

In Figs. 1 and 2, the trichromatic coordinates of each test sample are plotted on the C.I.E. chromaticity diagram. Each of the lines converging toward the center indicates the locus of the change of the chromaticity resulting from mixing a primary color pigment with white or black. The area within the lines which connect the primary colors is the range of feasible color matching among the three primary colors,

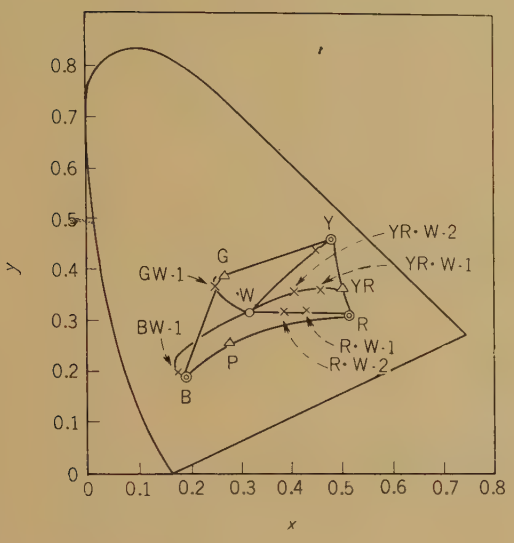

Fig. 1—The locus of chromaticity resulting from mixing the primary pigments with titanium dioxide in fixed amounts.

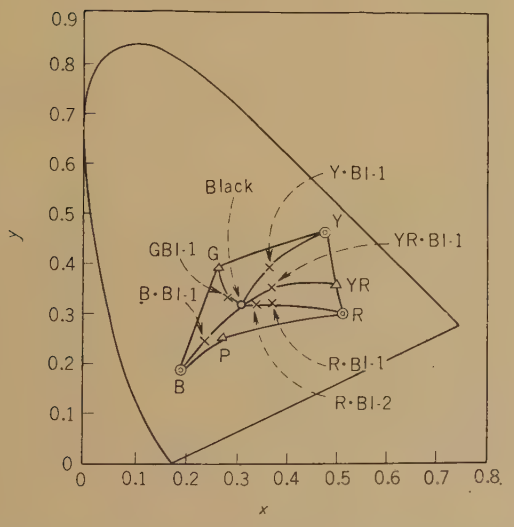

Fig. 2—The locus of chromaticity resulting from mixing the primary pigments with carbon black in fixed amounts.

namely, red (cadmium red), yellow (cadmium yellow), and blue (phthalocyanine blue), and white (titanium dioxide) or black (carbon black).

Figs. 3 through 7 show the relationship of the brightness (value) and the saturation (chroma) of the colors using the O.S.A. Munsell system for each hue. The area enclosed by the solid line and the neutral color axis in each figure indicates the range of chromaticity resulting from the mixture of each of the primary colors (red, orange, yellow, green, and blue) and black or white. The solid body that is obtainable by jointing the solid lines of such hues is the color solid which represents the entire range of coloring possible by such a method.

4. Light Stability Tests

A test was performed in order to examine the light stability of the materials made by the colormatching method described above. The most simple method is to use sunlight, but it has the following weak points: The required testing period is long, and the evaluation of the results of the test tend to become vague owing to changes in the weather. Therefore an ultraviolet ray projecting machine of the carbon arc type with the same specifications as those of the "Fade 0 Meter" of the Atlas Company was used. The fading effect caused by this machine has been proven to have a close correlation with the effect of actual sunlight. Its effect is said to be from 1 to 1.5 times as strong as that of the average annual sunlight. Twelve colors of test samples were chosen from among the twenty one. At the same time, seven colors of NTT Type No. 4 Telephones made of the urea molding materials presently used, and thirty-two colors of telephones made of rigid polyvinyl molding materials by outside makers were also tested. In the tests, a fixed amount of ultraviolet rays were applied to each test sample, and the spectral reflectance was measured by a recording spectrophotometer after the lapse of twenty hours, sixty hours, a hundred and forty hours, and three hundred hours. Thus, the degree of discoloration was compared against the original colors.

Table

RATIO OF THE PIGMENTS OF COLORED RIGID PVC

Test Materials	Ratio of Pigments
R (Red)	Cadmium red (2)
RW-1	Cadmium red (1) Titanium dioxide (1)
RW-2	Cadmium red (0.5) Titanium dioxide (1.5)
RB1-1	Cadmium red (1.5) Carbon black (0.075)
RB1-2	Cadmium red (1) Carbon black (0.15)
YR (Orange)	Cadmium red (1) Cadmium yellow (1)
YR.W-1	Cadmium red (0.5) Titanium dioxide (1) Cadmium yellow (0.5)
YR.W-2	Cadmium red (0.25) Titanium dioxide (1.5) Cadmium yellow (0.25)
YR.B1-1	Cadmium red (0.5) Carbon black (0.15) Cadmium yellow (0.5)
Y (Yellow)	Cadmium yellow (2)
Y.W-1	Cadmium yellow (1) Titanium dioxide (1)
Y.B1-1	Cadminm yellow (1) Carbon black (0.15)
G (Green)	Cadmium yellow (1) Phthalocyanine blue (1)
G.W-1	Cadmium yellow (0.5) Titanium dioxide (1) Phthalocyanine blue (0.125)
GB-1	Cadmium yellow (0.5) Carbon black (0.15) Phthalocyanine blue (0.125)
B (Blue)	Phthalocyanine blue (0.5)
B.W-1	Phthalocyanine blue (0.25) Titanium dioxide (1)
B.B1-1	Phthalocyanine blue (0.25) Carbon black (0.15)
P (Purple)	Cadmium red (1) Phthalocyanine blue (0.25)
W.B1-1 (Gray)	Titanium dioxide (1.5) Carbon black (0.075)
W.B1-2	Titanium dioxide (1) Carbon bleck (0.15)

In order to ascertain the stability to sunlight the Japanese Industrial Standard (JIS) standard blue scale was exposed at the same time. After the completion of the total exposure of three hundred hours, the change in the test materials was examined.

Among the twelve test samples, two of the gray colors showed very slight fading, but no change in the other colors could be discerned by the unaided eye. The seventh grade dyed cloth of the blue scale showed complete discoloration. Therefore, it can be safely said that all the test materials have light stability greater than that of the seventh grade.

Of the seven colors of NTT No. 4 Telephones, pink showed a conspicuous degree of fading, while ivory and wine red showed

2

AND THE CORRESPONDING COLORIMETRIC VALUES

C.I.E. Values			O.S.A. Munsell Values	N.B.S. Units
x	y	Y (%)		
0.507	0.309	10.83	4.0R 3.8/10.5	2.0
0.423	0.311	20.50	4.0R 5.1/ 8.0	3.0
0.383	0.317	30.96	2.5R 6.0/ 5.8	2.2
0.369	0.318	5.28	4.0R 2.7/ 3.0	2.2
0.342	0.311	4.45	3.5R 2.4/ 3.0	
0.491	0.359	17.66	9.5R 4.8/ 9.0	1.6
0.455	0.357	25.28	10.0R 5.6/ 8.4	
0.404	0.360	34.33	3.0YR 6.4/ 5.1	
0.369	0.353	6.61	8.0YR 3.0/ 1.8	
0.476	0.458	56.50	2.0Y 7.9/12.7	
0.447	0.446	67.65	3.0Y 8.5/10.1	2.1
0.367	0.394	10.13	6.0Y 3.0/ 3.0	
0.264	0.384	10.58	6.0G 3.8/ 5.3	2.8
0.251	0.363	18.05	9.0G 4.8/ 6.3	
0.284	0.335	4.76	10.0G 2.5/ 1.1	
0.192	0.186	8.35	4.0PB 3.4/ 7.5	2.0
0.178	0.200	17.03	1.0PB 4.7/10.6	1.8
0.227	0.256	4.26	4.0PB 2.5/ 5.0	
0.263	0.271	5.83	4.0PB 2.8/ 2.3	3.2
0.313	0.310	18.75	N 4.9	3.2
0.302	0.303	9.13	N 3.5	4.0

a lesser degree of fading. The other colors were stable.

Almost all the colors of the rigid polyvinyl chloride telephones that were produced by outside makers began to fade after twenty hours, and after a lapse of 140 hours, they showed a tremendous degree of discoloration, as well as the phenomena of chalking and cracking.

If we indicate in United States National Bureau of Standards (N.B.S.) units the degree of discoloration vs. the hours of the application of ultraviolet rays to the test samples, the degree of discoloration can be estimated in terms of man's ability to perceive the difference of colors. Therefore, by converting the trichromatic coordinates and the reflectance of the samples before

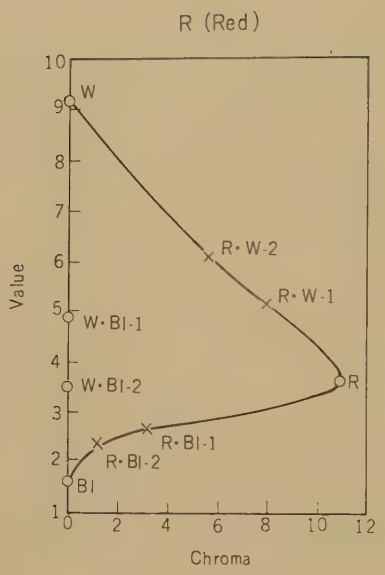

Fig. 3—The range of feasible color matching resulting from the mixture of primary red and black or white.

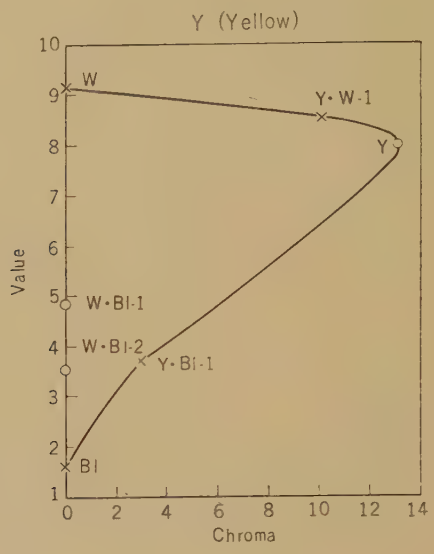

Fig. 5—The range of feasible color matching resulting from the mixture of primary yellow and black or white.

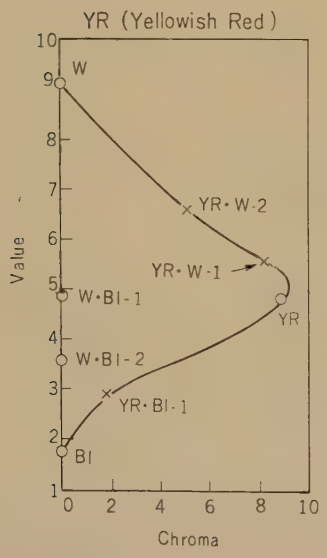

Fig. 4—The range of feasible color matching resulting from the mixture of primary orange and black or white.

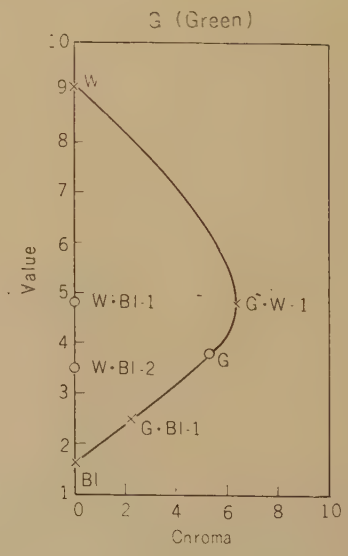

Fig. 6—The range of feasible color matching resulting from the mixture of primary green and black or white.

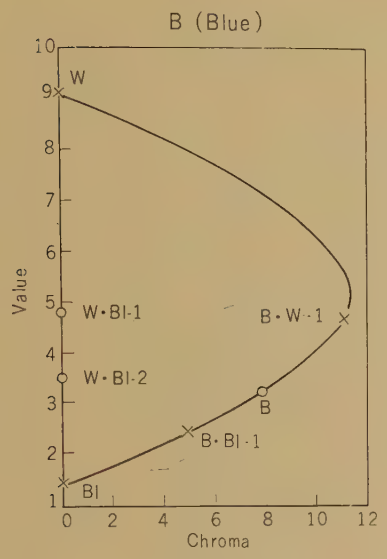

Fig. 7—The range of feasible color matching resulting from the mixture of primary blue and black or white.

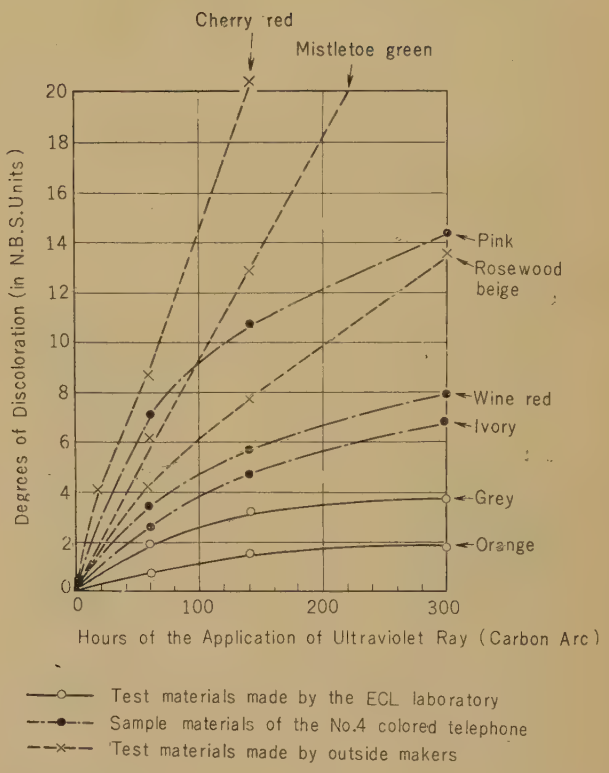

Fig. 8—Degree of discoloration as a function of hours of application of ultraviolet rays.

and after the test (x, y, and Y of Table 2 respectively) to V_x-V_y, V_z-V_y, and V_Y of the chromatic coodinates of A. Q. Adams' uniform chromaticity scale diagram, and by calculating the color differences from Equation (1), the change in color in N.B.S. units can be obtained.

$$\Delta E=40\{[\Delta(V_x-V_y)]^2+(0.23\Delta V_y)^2 + [0.4\Delta(V_z-V_y)]^2\}^{1/2}. \quad (1)$$

Table 2 shows the change of color in N.B.S. units of the twelve samples after the application of ultraviolet rays for three hundred hours.

Fig. 8 shows the relationship between the hours of exposure of the test samples and their discoloration in N.B.S. units. The gray and the yellowish red (orange) colors showed the most and the least discoloration in N.B.S. units; while of the seven colors of the NTT telephone set the pink, the ivory, and the wine red colors showed measurable discoloration. Those colors of outside makers' samples which showed the smallest amount of discoloration are also included in Fig. 8.

5. The Selection of the Colors for Telephone Handsets

Fifteen colors suitable for telephone handsets were selected. Using the Munsell Book of Colors as a standard, the colors used for small electric appliances on display in a Tokyo department stores were investigated. These appliances included small radios, toasters, electric heaters, electric mixers, and interphones; all of which are similar to telephones in shape, size, and texture. The colors recommended by industrial designers and color specialists for plastics products such as interior decorations, and electric instruments; which is included in the fashion color data published annually since 1955 by the Institute of Fashion Colors of Japan were also studied.

In addition, the standard colors for polystyrene, which is extremely useful for

industrial products, were also studied. From this information a study was made of the frequency of appearance of the approximately 350 color found, classified by the three attributes of colors in the Munsell system: i.e., hue, value, and chroma. The results are shown in Figs. 9, 10, and 11.

Let us first look at the frequency of appearance of colors by hue. About fifty percent of the colors examined are warm colors such as red, yellowish red, and yellow; then purplish blue, blue, and green appear in this order by frequency. When we plot the frequency of appearance by value, concentration to medium brightness, 5 and 6, is shown. And for chroma, conservative colors such as 2 and 4 appear most frequently.

As a result of such an analysis, it is possible to grasp the general trends of colors in modern usage. However, such an analysis tends to lack concreteness, for within the reddish colors which appear most frequently, there are light pink, dark wine red, saturated scarlet, etc. It is necessary to examine the individual colors more closely. Therefore the Munsell color solid was divided into ninety blocks, consisting of ten shades of hue (R, YR, Y, GY, G, BG, PB, P, and RP), three degrees of the value (bright: 7–9, medium: 5–6, and dark: 2–4), and three steps of chroma (low saturation: 1–3, medium saturation: 4–6, and high saturation: 7 and above). Then all the colors that had been investigated were placed in the appropriate block according to their respective Munsell notations, and the packing of the various blocks was investigated. Figs. 12 through 21 show the frequency of appearance of colors in the nine blocks that are made by perpendicular division according to the ten shades of hue. The symbol indicates ● colors in fashion, and the symbol × those that are not in fashion. The figures in each block stand for the ratio of the frequency of appearance of the colors within the block to the total.

The observation of the trend of colors according to the blocks, divided by the components of the colors, leads to a very interesting conclusion. For instance, in the red colors, a concentration to the comparatively dark and saturated colors is seen; in

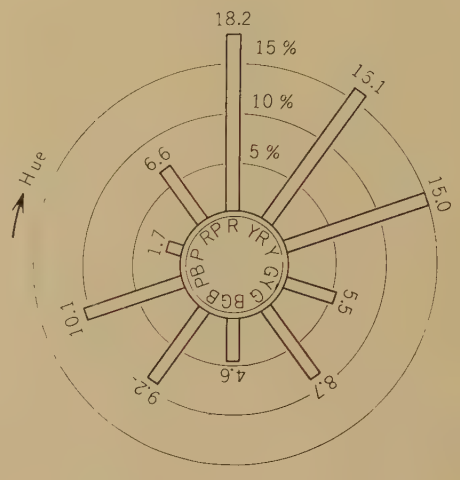

Fig. 9—The frequency of appearance of colors by hue.

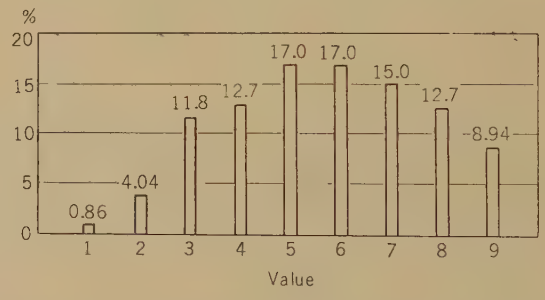

Fig. 10—The frequency of appearance of colors by value.

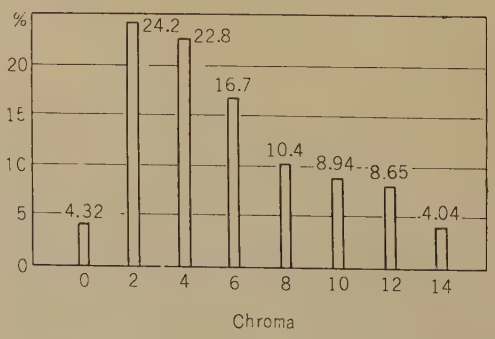

Fig. 11—The frequency of appearance of colors by chroma.

Table 3

COLORS SUITABLE FOR TELEPHONE HANDSETS

Name of Colors Munsell Notation	Color	Name of Colors Munsell Notation	Color	Name of Colors Munsell Notation	Color
Coral 7.5R 5.5/6.0		Wine red 5.0R 4.0/7.0			
Salmon 10.0R 6.5/3.0		Rose beige 2.5YR 5.0/3.0		Blackish brown 2.5YR 2.0/2.0	
Ivory 2.5Y 9.0/3.0		Egg yolk color 10.0YR 7.5/7.0			
Olive green 7.5GY 4.0/2.0		Grass green 7.5GY 6.0/4.0			
Pale green 2.5G 7.0/2.0		Pine leaf 5.0G 4.0/2.0			
Sky blue 2.5PB 5.0/4.0		Navy blue 5.0PB 2.0/3.0		Bluish gray 2.5PB 4.0/2.0	
Silver gray N 6.0					

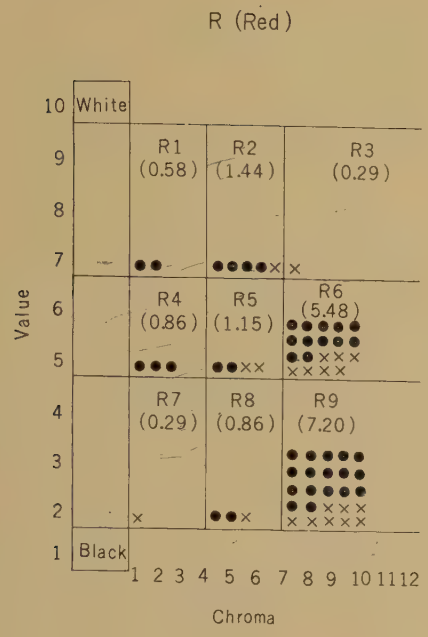

Fig. 12—The frequency of appearance of red by blocks.

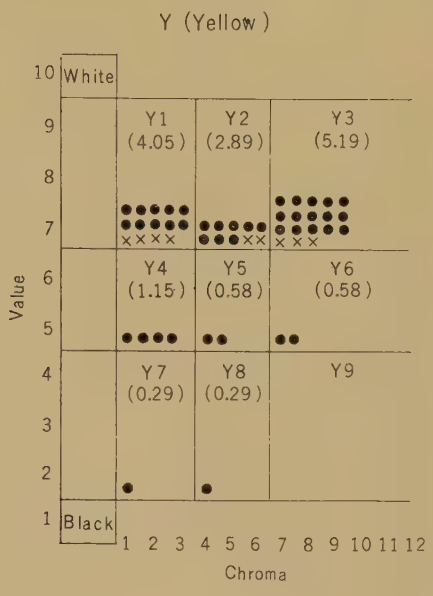

Fig. 14—The frequency of appearance of yellow by blocks.

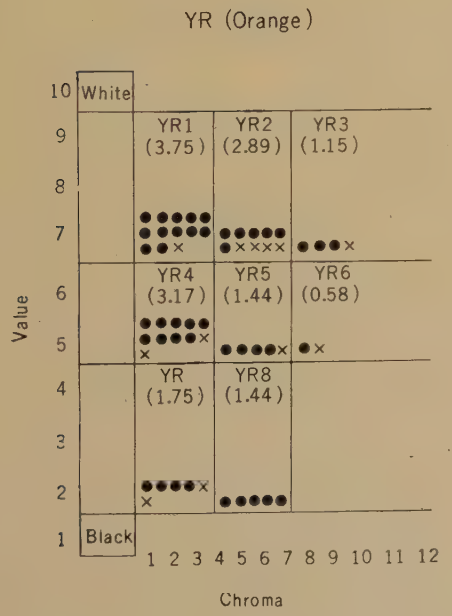

Fig. 13—The frequency of appearance of orange by blocks.

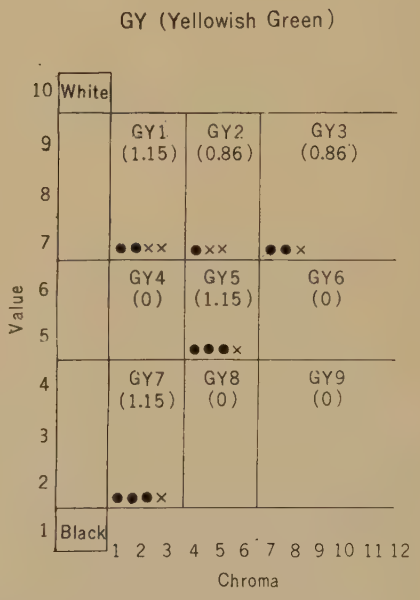

Fig. 15—The frequency of appearance of yellowish green by blocks.

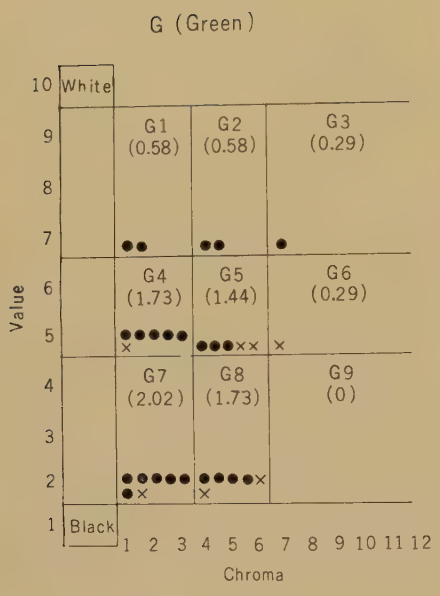

Fig. 16—The frequency of appearance of green by blocks.

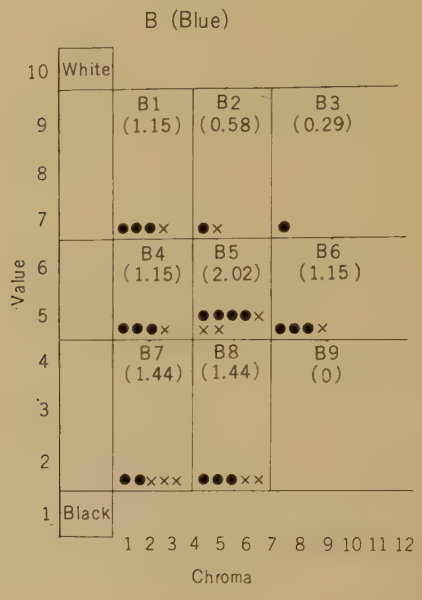

Fig. 18—The frequency of appearance of blue by blocks.

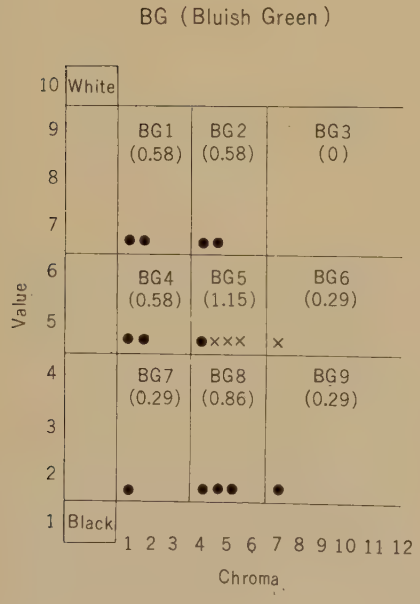

Fig. 17—The frequency of appearance of bluish green by blocks.

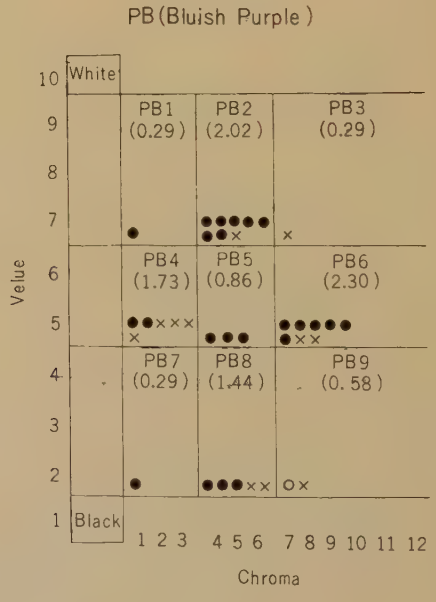

Fig. 19—The frequency of appearance of bluish purple by blocks.

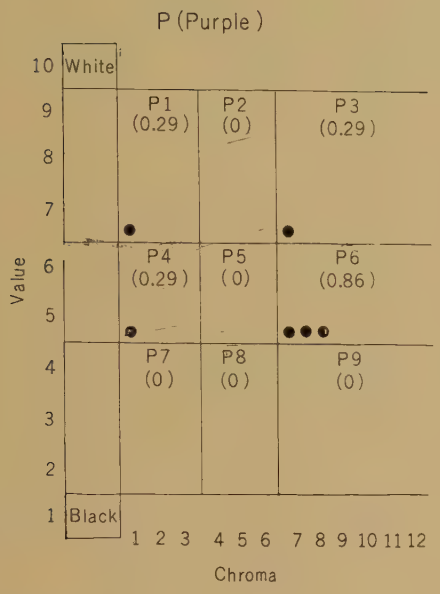

Fig. 20—The frequency of appearance of purple by blocks.

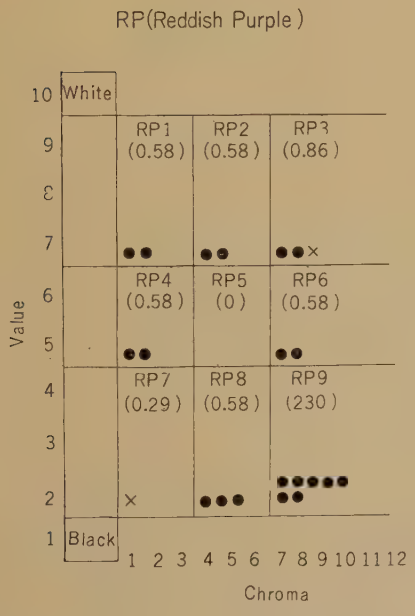

Fig. 21—The frequency of appearance of reddish purple by blocks.

the yellowish red colors, on the contrary, the concentration appears in bright and conservative colors; and in the yellow colors, the concentration is seen to bright colors regardless of chroma. In the hues that range from green to blue, no such distinctive characteristics are seen; but in general, dull colors appear frequently. Using primarily the results of the above investigation, fifteen suitable colors for telephone handsets were selected.

Table 3 shows the names of these colors and their Munsell notations. To determine the colors suitable the representative colors of the blocks having the highest frequency of appearance were chosen, and for these colors the following considerations were studied:

(1) Whether the color can be matched in the process of injection molding of rigid polyvinyl chloride.

(2) Whether it is a stable color not easily tired of.

(3) Whether the color combination with the background of a presupposed place for the telephone set is good.

(4) Whether there is a color that can be used to accent it.

(5) Whether the final choice of colors contains a variety of hues that will meet the variety of human color preference.

All of the above are basic considerations necessary for the problem of color harmony.

Conclusion

There are not many pigments that can be used to color molded rigid polyvinyl chloride because of the limitations caused by the process of its formation into products. Therefore, only three pigments (red, yellow, and blue) plus white and black were selected as the minimum number of pigments essential for color matching. The test results showed an unexpectedly wide range of color matching feasible; except that the purplish colors couldn't be produced. In fact, the test has shown that all the colors required for plastic industrial products can be produced by this method. Its advantage lies not only in the minimization of the kinds of pigments to be managed, but also in that we can expect durability for all the

colors produced. This has been proven by the light stability test described above. The results of this investigation may be applied usefully to other plastics products.

Cadmium red and cadmium yellow are inorganic pigments superior in heat stability and light stability, but are weak in hydrochloric acid. Although no problem seems to have been presented by the small injection molders used in this test, difficulties may be experienced with the larger machines used in real production. This problem of low acid stability should be continuously examined in the future together with the problem of the effect of stabilizers.

Also, further investigation of the problem of poor dispersion of the materials which causes stripes and unevenness in the color of the telephone set is necessary, if one of the reasons for coloring the telephone set is to achieve a beautiful appearance, for this purpose, the adoption of toner color, superior in dispersion, is worth considering; although it should go side by side with considerations of the mechanical strength of rigid polyvinyl chloride.

To select the colors most suitable for colored telephones is not an easy problem, for it is related to the problem of design. The primary criterion of the selection of the fifteen colors presented here is the preferences determined from an objective investigation into recent color preferences, being especially careful not to include the investigators personal preferences. Therefore these colors are not so-called top-mode colors, but are usual colors that have already melted into our daily lives. They may not be strikingly new or rare, but the selection of these colors was, we believe, performed without any major errors.

* * * *

Papers Contributed to Scientific and Technical Journals by the Members of the Laboratory*

Papers Published in Other Publications of the Electrical Communication Laboratory

U.D.C. 538.221:541.451

Magnetic Properties and Ferrimagnetic Resonance in Polycrystalline $3Y_2O_3 \cdot (5-x)Fe_2O_3 \cdot xIn_2O_3$
Yuzo SHICHIJO and *Tomonao MIYADAI*
Kenkyu Zituyoka Hokoku (Electr. Comm. Labor. Techn. Journ.), 8, 11, pp. 1450–1465, 1959

The Ferrimagnetic resonances and the crystal structures of polycrystalline samples of $Y_3Fe_{5-x} \cdot In_xO_{12}$ as a function of x were studied at room temperature. The technical magnetization of YIG($x=0$) was also studied. Interpretation of the results is given.

U.D.C. 621.317.31/.32.029.64.081.4

Measurement of Small Voltage and Power at Radio Frequencies
Nobue INAGE
Kenkyu Zituyoka Hokoku (Electr. Comm. Labor. Techn. Journ.), 8, 11, pp. 1367–1436, 1959

In the proposed method of measurement standard level is accurately established and the subsequent measurements are made relative to this standard level. Precision quantitative studies were conducted to clearly ascertain the accuracy of this method.

U.D.C. 621.395.344:621.318.56

Address Selection of a Reed-Relays Array by an Error-Correcting-Code System
Zen'iti KIYASU and *Hirosi SAWABE*
Kenkyu Zituyoka Hokoku (Electr. Comm. Labor. Techn. Journ.). 8, 11, pp. 1437–1449, 1959

Each relay is threaded with exciting wires for driving currents the direction and sense of which are determined from the theory of an error-correcting code. The relay can select correctly even if one bit of the code is incorrect.

U.D.C. 634.78:495.6]:621.391

Fundamental Qualities in Speech Communication
Yoshiyuki OCHIAI and *Teruo FUKUMURA*
Kenkyu Zituyoka Hokoku (Electr. Comm. Labor. Techn. Journ.), 8, 12, pp. 1469–1549, 1959

Among the various qualities of speech the "Phonemic" and the "vocal" qualities are proposed as the fundamental qualities. Many important observations of these qualities in speech signals are presented, and the confusion phenomena observed are analized in the original scheme.

* Reprint may be available upon your request to the author.

U.D.C. 678.7.047:621.395.6
535.6:159.937.51

A Study of Colors for Molded Telephone Handsets
Yumio SUGIHARA
Kenkyu Zituyoka Hokoku (Electr. Comm. Labor. Techn. Journ.), 8, 12, pp. 1550–1561, 1959

The range of colors obtainable by mixing five pigments and useful for coloring rigid polyvinyl chroride was determined by using the C.I.E. chromacity diagram and the Munsel color system. Fifteen colors especially suitable for molded telephone handsets were selected.

Papers Published in Publications of Scientific and Technical Societies

U.D.C. 531.788+621.527

Nonproportionality in Bayard-Alpert Ionization Gauge and the Ultimate Vacuum Determination of Diffusion Pumps
Yoshihiko MIZUSHIMA and *Zenjiro ODA*
Rev. Sci. Instr., **30**, 11, p. 1037, Nov, 1959

A non-proportionality between ion current and electron current in the Bayard-Alpert ionization gauge was observed. This phenomenon is applied to study an ionization pump-action and the maximum attainable vacuum of diffusion pumps.

U.D.C. 537.57:537.29
621.382:546.289

Field Emission in Germanium
Toshiya HAYASHI
The Journ. Inst. Electr. Comm. Engr. Japan, **42**, 12, p. 1186, Dec. 1959

A phenomenon analogous to the field emission in a vacuum tube that has been found in P- -M and N- -M junctions of Germanium is described in this paper.

U.D.C. 541.138:546.821

Studies on the Anodic Oxcide Film Titanium
Hiroshi CHIBA
Journ, Electrochem. Soc. Japan, **28**, 1, p. 5, Jan. 1960

Anodic oxidation of titanium in alkaline solution was investigated. Oxide films produced at various stages of the anodization process were observed with an electron microscope and by electron diffraction. The relation between the anodic formation and the structure of the films is discussed.

U.D,C, 621.382.2.001.2:537.311.3

The Nonlinear Barrier Capacitance of Silver Bonded Diodes
Shoichi KITA and *Koichi SUGIYAMA*
Journ. Inst. Electr. Comm. Engr. Japan, **42**, 12, p. 1186–1192, Dec. 1959

We measured the impedance variation of the silver bonded diode at 6 KMC. The cut-off frequency of the diode was more than 400 KMC. It was discovered that electrical forming was the most important factor for the characteristic of the diode.

U.D.C. 621.396.11(26)

Distribution of Received Power in an Oversea Propagation within Line-of-Sight
Kazuo MORITA
Journ. Inst. Electr. Comm. Engr. Japan, **42**, 10, p. 929, Oct. 1959

The results of a calculation of the distribution function of received power (combining two stationary waves and random components) and measurements of the distribution function of received power are presented. The agreement between experiment and calculation is good.

U.D.C. 621.396.65.029.64:621.391.812.3

Fading of Microwave Relay Links
Kazuo MORITA
Journ. Inst. Electr. Comm. Engr. Japan, **42**, 10, p. 923, Oct. 1959

This paper describes the results of statistical studies of fading and of the fluctuation of thermal noise in microwave relay links. Also, the results are considered from the view point of Applying then to practical designs.

U.D.C. 621.915-523.8

TUKEN-1 Numerically Controlled Two-Axis Milling Machine
Ken IWABUCHI and *Akira KAWAMATA*
Journ. Inst. Electr. Comm. Engr. Japan, **42**, 11, p.1096-1102, Nov. 1959

The block diagram of the experimental model of this system is described, and the operation of the main elements of the controller are described briefly.

* * * *

CONTENTS